

Hubble Tension or Distance Ladder Crisis?

Leandros Perivolaropoulos^{1,*}

¹*Department of Physics, University of Ioannina, GR-45110, Ioannina, Greece**

(Dated: September 4, 2024)

We present an up-to-date compilation of published Hubble constant (H_0) measurements that are independent of the CMB sound horizon scale. This compilation is split in two distinct groups: A. Distance Ladder Measurements sample comprising of 20 recent measurements, primarily from the past four years, utilizing various rung 2 calibrators and rung 3 cosmic distance indicators. B. One-Step Measurements sample including 33 measurements of H_0 that are independent of both the CMB sound horizon scale and the distance ladder approach. These 33 measurements are derived from diverse probes such as Cosmic Chronometers, gamma-ray attenuation, strong lensing, megamasers etc. Statistical analysis reveals a significant distinction between the two samples. The distance ladder-based sample yields a best fit $H_0 = 72.8 \pm 0.5 \text{ km s}^{-1} \text{ Mpc}^{-1}$ with $\chi^2/dof = 0.51$ indicating some correlations. The one-step measurements result in $H_0 = 69.0 \pm 0.48 \text{ km s}^{-1} \text{ Mpc}^{-1}$ with $\chi^2/dof = 1.37$ indicating some internal tension. If two outlier measurements are removed (TDCOSMO.I-2019 known to have systematics and MCP-2020) the best fit of the one step sample reduces to $H_0 = 68.3 \pm 0.5 \text{ km s}^{-1} \text{ Mpc}^{-1}$ with $\chi^2/dof = 0.95$, fully self-consistent and consistent with sound horizon based measurements. A Kolmogorov-Smirnov test yields a p-value of 0.0001 suggesting that the two samples are fundamentally distinct, with a probability of less than 0.01% that they are drawn from the same underlying distribution. These findings suggest that the core of the Hubble tension lies not between early and late-time measurements, but between distance ladder measurements and all other H_0 determinations. This discrepancy points to either a systematic effect influencing all distance ladder measurements or a fundamental physics anomaly affecting at least one rung of the distance ladder.

I. INTRODUCTION

The Hubble constant (H_0) serves as a fundamental metric for quantifying the rate at which the Universe is expanding. Accurate determination of H_0 is essential for elucidating the Universe's age, composition, and ultimate fate. Despite remarkable progress in observational astrophysics and cosmology, a notable and persistent discrepancy, commonly referred to as the "Hubble tension"[1–13], remains between the H_0 values deduced between different cosmological probes. It is common perception that measurements of H_0 that use the sound horizon at recombination as a standard ruler distance calibrator (early time measurements) lead to a different (lower) value of $H_0 = 67.4 \pm 0.5 \text{ km/s/Mpc}$ [14] than most other measurements which favor a value consistent with the latest SH0ES measurement favoring an elevated H_0 value of $73.04 \pm 1.04 \text{ km/s/Mpc}$ [15]. It is therefore believed by a large sector of the scientific community that an adjustment of the prerecombination physics in such a way that the recombination sound horizon becomes smaller, could lead to a larger measured value of H_0 and thus to consistency between the early time sound horizon based measurements and all other measurements of H_0 [16–35]. This approach is faced by a wide range of challenges[36–41]. It is based on the following assumption: *Most measurements of H_0 that are not based on the Cosmic Microwave Background (CMB) sound horizon as a standard ruler favor a higher value of H_0 consistent*

with the SH0ES measurement which is the most precise local measurement of H_0 .

This assumption is perceived to be correct because the most precise local measurements of H_0 are indeed fully consistent with the SH0ES measurement. These measurements which are highly precise but not necessarily accurate, are based on *distance ladder methods*.

A crucial assumption of distance ladder methods is that both the astrophysical environment and the physical laws[42–44] are consistent among the three rungs used in the distance ladder implementation. Thus, in the context of testing this assumption, the following questions arise:

- What are the observational probes that can lead to measurement of H_0 through a one step process that are independent of both the sound horizon scale and of the distance ladder rung approach?
- Is there a trend for the values of H_0 favored by these probes and if yes, is the favored range of H_0 more consistent with sound horizon based measurements or with distance ladder based measurements of H_0 ?
- Are the distance ladder based measurements of H_0 consistent with each other and with the latest SH0ES measurement?

The main goal of the present analysis is to address these questions using an extensive up-to-date compilation of recent measurements of H_0 (most published during the past 5 years with emphasis in the last 3 years) which are independent of the sound horizon scale and include both distance ladder measurements and one step

* leandros@uoi.gr

measurements that involve no rungs. We thus split the measurements of H_0 that are independent of the sound horizon scale in two groups: 1. Distance ladder based measurements 2. One step measurements that involve direct distance or $H(z)$ probes and are independent of the recombination sound horizon scale. We then test the statistical properties of the H_0 measurements in each group in order to address the above questions. This is the first time that such a statistical meta-analysis is attempted since previous corresponding studies have not separated the two groups of measurements and have also included many early outdated measurements[45–48].

The structure of this paper is the following: In the next section we review the methods for measuring H_0 and classify them into sound horizon based methods, distance ladder methods that require calibrators and rung structure and one step methods that are free from local astrophysics and local calibrators. In section III we present our extensive compilation of the currently available H_0 measurements in each one of the later two groups (distance ladder and one step measurements independent of sound horizon). We also present the statistical properties of the two groups and their consistency with each other and with the H_0 measurements based on the CMB sound horizon scale standard ruler. Finally in section IV we summarize our main results and their implications. We also discuss possible future extensions of the current analysis.

II. METHODS FOR THE MEASUREMENT OF H_0

Methods for the measurement of H_0 may be classified in three broad classes: Methods that use the CMB sound horizon standard ruler as a distance calibrator, distance ladder methods and one step methods independent of the sound horizon scale input. In this section we briefly review the main representative methods of each of these three classes which are used in the present analysis.

II.1. CMB Sound Horizon Standard Ruler Methods

The CMB provides a powerful standard ruler in cosmology—the sound horizon at recombination. This standard ruler is pivotal for inferring the Hubble constant, H_0 , through observations of the CMB power spectrum’s acoustic peaks and the imprint of baryon acoustic oscillations (BAO) in the distribution of galaxies.

II.1.1. Sound Horizon at Recombination

The sound horizon at recombination, r_s , represents the maximum distance that acoustic waves could have traveled in the primordial photon-baryon fluid by the time

of recombination[49, 50]. This scale is imprinted as the characteristic angular scale of fluctuations observed in the CMB power spectrum. Mathematically, it is expressed as:

$$r_s = \int_{z_{\text{rec}}}^{\infty} \frac{c_s(z)}{H(z)} dz, \quad (2.1)$$

where $c_s(z)$ is the sound speed in the photon-baryon fluid, $H(z)$ is the Hubble parameter as a function of redshift, and z_{rec} is the redshift at recombination. The sound speed c_s is lower than the speed of light due to the inertia of baryons, which are coupled to photons by Thomson scattering until recombination.

In the standard Λ CDM model, the sound speed can be approximated as:

$$c_s(z) = \frac{c}{\sqrt{3(1 + R(z))}}, \quad (2.2)$$

where $R(z)$ is the ratio of the baryon to photon momentum density[51]:

$$R(z) = \frac{3\rho_b}{4\rho_\gamma} = \frac{3\Omega_b}{4\Omega_\gamma}(1 + z)^{-1}. \quad (2.3)$$

Using the latest Planck 2018[14] results for the Λ CDM model, which give $\Omega_b h^2 = 0.02237$ and $\Omega_m h^2 = 0.1430$, and assuming $z_{\text{rec}} \approx 1090$, the calculated value of r_s is approximately:

$$r_s \approx 147.09 \pm 0.26 \text{ Mpc}. \quad (2.4)$$

This value of r_s is crucial in determining H_0 from CMB and BAO measurements.

The sound horizon can be modified by changing the physics before recombination. Some proposed modifications include:

1. Early Dark Energy (EDE)[16–22, 52, 53]: Introducing a new component of dark energy that is significant before recombination can increase the expansion rate, reducing the time available for sound waves to propagate and thus decreasing r_s .

2. Modified Neutrino Physics[33–35]: Changing the number of effective neutrino species or their interactions can alter the expansion history and the sound speed, affecting r_s .

3. Varying Fundamental Constants[54]: Allowing fundamental constants like the fine-structure constant to vary over time can change the recombination history and thus r_s .

4. Non-standard Recombination[55, 56]: Modifications to the recombination process itself, such as energy injection from dark matter annihilation, can change z_{rec} and consequently r_s .

5. Modified Gravity[23–32, 57]: Alterations to general relativity in the early universe can change the expansion history and thus r_s .

These modifications aim to reduce r_s , which would allow for a higher H_0 value from CMB and BAO measurements, potentially alleviating the Hubble tension. However, each of these proposals faces challenges in maintaining consistency with other cosmological observations and often requires fine-tuning[36–41].

II.1.2. Measuring H_0 from the CMB

The angular scale of the first acoustic peak in the CMB power spectrum, θ_s , is inversely proportional to the sound horizon at the surface of last scattering[14, 58–60]:

$$\theta_s = \frac{r_s}{D_A(z_{\text{rec}})}, \quad (2.5)$$

where $D_A(z_{\text{rec}})$ is the angular diameter distance to the surface of last scattering. In the context of the standard Λ CDM model, the angular diameter distance is related to the Hubble constant H_0 through the following equation:

$$D_A(z_{\text{rec}}) = \frac{c}{H_0(1+z_{\text{rec}})} \int_0^{z_{\text{rec}}} \frac{dz'}{\sqrt{\Omega_m(1+z')^3 + \Omega_\Lambda}}, \quad (2.6)$$

where c is the speed of light, z_{rec} is the redshift of recombination, Ω_m is the matter density parameter, and Ω_Λ is the cosmological constant density parameter.

Precise measurements of θ_s from CMB experiments like Planck, combined with this model for D_A that depends on H_0 and other cosmological parameters, allow for the inference of the Hubble constant. However, it's important to note that H_0 is degenerate with r_s in this measurement.

This degeneracy arises because the CMB primarily constrains the combination $r_s H_0$ rather than either parameter individually. To see this, we can rewrite the equation (2.5) for θ_s as:

$$\theta_s = \frac{r_s H_0}{c(1+z_{\text{rec}})} \left(\int_0^{z_{\text{rec}}} \frac{dz'}{\sqrt{\Omega_m(1+z')^3 + \Omega_\Lambda}} \right)^{-1} \quad (2.7)$$

In this form, it's clear that a larger r_s could be compensated by a smaller H_0 , or vice versa, while still producing the same observed θ_s . This degeneracy means that additional cosmological probes or assumptions about the early universe are needed to break the degeneracy and determine H_0 uniquely from CMB data. In the context of Λ CDM r_s is calculated as described in the previous subsection. However, in the context of modified cosmological models r_s will vary as the expansion history before recombination $H(z)$ changes (see equation (2.1)).

II.1.3. Connecting BAO and the CMB

Building on the CMB measurements discussed in the previous subsection, Baryon Acoustic Oscillations (BAO) provide an independent confirmation of the sound horizon scale[61–64]. The BAO feature serves as a standard ruler in the late-time universe, manifesting as a peak in the correlation function of galaxies. This peak corresponds to the same comoving scale r_s imprinted in the CMB.

The BAO measurements typically constrain the combination of the sound horizon and a distance scale. For example, in terms of the volume-averaged distance $D_V(z)$, we have:

$$\frac{D_V(z)}{r_s} = \frac{1}{r_s} \left[(1+z)^2 D_A^2(z) \frac{cz}{H(z)} \right]^{1/3}, \quad (2.8)$$

where z is the redshift of the galaxy survey. The left-hand side of this equation is what BAO surveys directly constrain.

Similar to the CMB case, we can see that r_s and H_0 are degenerate in BAO measurements. To illustrate this, let's consider how H_0 enters into $D_V(z)$:

$$D_V(z) = \left[(1+z)^2 \left(\frac{c}{H_0} \int_0^z \frac{dz'}{E(z')} \right)^2 \frac{cz}{H_0 E(z)} \right]^{1/3}, \quad (2.9)$$

where $E(z) = H(z)/H_0$ is the normalized Hubble parameter.

Now, we can rewrite the BAO constraint as:

$$\frac{D_V(z)}{r_s} = \frac{c}{r_s H_0} \left[(1+z)^2 \left(\int_0^z \frac{dz'}{E(z')} \right)^2 \frac{z}{E(z)} \right]^{1/3} \quad (2.10)$$

In this form, we can see that BAO measurements primarily constrain the combination $r_s H_0$, similar to what we saw with CMB measurements. A larger r_s could be compensated by a smaller H_0 , or vice versa, while still satisfying the BAO constraint.

This degeneracy between r_s and H_0 in both CMB and BAO measurements highlights why these early-universe probes, while precise, cannot uniquely determine H_0 without additional assumptions or complementary data. It also underscores the importance of late-time, direct measurements of H_0 that don't rely on the sound horizon scale, as these can potentially break the degeneracy and help resolve the Hubble tension.

These methods, grounded in the physics of the early universe, provide robust constraints on cosmological parameters but are sensitive to assumptions about the cosmological model, primarily the composition and evolution of the universe's energy density. As such, they are crucial in exploring and potentially resolving tensions in the measured values of H_0 observations.

In addition to $D_V(z)$, BAO measurements can also constrain the comoving distance $D_M(z)$. The comoving distance is related to the angular diameter distance by $D_M(z) = (1+z)D_A(z)$. In terms of H_0 , D_M can be expressed as:

$$D_M(z) = \frac{c}{H_0} \int_0^z \frac{dz'}{E(z')} \quad (2.11)$$

where $E(z) = H(z)/H_0$ as before. BAO surveys often measure the combination $r_s/D_M(z)$, which again demonstrates the degeneracy between r_s and H_0 :

$$\frac{r_s}{D_M(z)} = \frac{r_s H_0}{c} \left(\int_0^z \frac{dz'}{E(z')} \right)^{-1} \quad (2.12)$$

This formulation clearly shows that BAO measurements of D_M , like those of D_V , primarily constrain the product $r_s H_0$ rather than either parameter individually.

It's important to note that while we've been discussing the sound horizon at recombination (r_s), BAO measurements are actually sensitive to a slightly different scale: the sound horizon at the drag epoch (r_d). The drag epoch occurs when baryons decouple from photons, which happens slightly later than recombination. The drag scale r_d is defined as the comoving distance a sound wave can travel from the beginning of the universe until the drag epoch:

$$r_d = \int_0^{t_d} \frac{c_s(t)}{\sqrt{3}(1+z(t))} dt, \quad (2.13)$$

where t_d is the time of the drag epoch and $c_s(t)$ is the sound speed in the photon-baryon fluid. The drag scale r_d is typically about 2% larger than r_s . This distinction is crucial because it's the baryons, not the photons, that seed the matter distribution we observe in galaxy surveys. Therefore, the BAO feature in the galaxy distribution corresponds to r_d rather than r_s . However, the two scales are very closely related, and the degeneracy with H_0 applies equally to both. In precise analyses, it's important to use r_d for BAO calculations, while r_s remains the relevant scale for CMB analyses.

II.2. Distance Ladder Approaches

The distance ladder approach[15, 65–67] in cosmology is a methodical technique used to determine cosmological distances across the universe, spanning from nearby stars to distant galaxies. This method is structured into three sequential "rungs," each building upon the accuracy of the previous to extend further into the cosmos.

II.2.1. First Rung: Calibration of Local Distance Indicators

The primary objective of the first rung in the cosmic distance ladder is to calibrate nearby distance indicators, specifically Cepheid variables[68, 69], Tip of the Red Giant Branch (TRGB) stars[70, 71], Mira variables[72, 73] and J-region Asymptotic Giant Branch (JAGB) stars[74]. This calibration process involves determining the precise calibration parameters for each indicator using direct geometric distance measurements.

II.2.1.1. Cepheid Variables and Their Calibration Cepheid variables are a class of pulsating stars that play a crucial role in the cosmic distance ladder. Named after the prototype star δ Cephei, these stars are yellow supergiants that undergo regular variations in their brightness. The key to their importance in astronomy lies in the tight relationship between their pulsation period and luminosity, first discovered by Henrietta Swan Leavitt in 1908 [75].

Cepheids pulsate due to a mechanism known as the kappa mechanism, where ionization zones in the star's atmosphere drive periodic expansions and contractions. This pulsation leads to regular changes in the star's brightness and temperature, with periods typically ranging from a few days to months.

The Period-Luminosity (PL) relation, also known as the Leavitt Law, states that the intrinsic luminosity of a Cepheid is directly related to its pulsation period. This relationship allows astronomers to use Cepheids as "standard candles" for measuring cosmic distances. However, modern calibrations have refined this relationship to include metallicity effects, leading to the Period-Luminosity-Metallicity (PLZ) relation:

$$M_\lambda = a_\lambda \log P + b_\lambda + c_\lambda [\text{Fe}/\text{H}] + d_\lambda \quad (2.14)$$

where:

- M_λ is the absolute magnitude in wavelength band λ
- P is the pulsation period in days
- The symbol $[\text{Fe}/\text{H}]$ represents the metallicity of the star. Fe/H represents the logarithm of the ratio of iron to hydrogen abundance in a star, compared to the same ratio in the Sun. It's expressed mathematically as:

$$[\text{Fe}/\text{H}] = \log_{10} \left(\frac{N_{\text{Fe}}}{N_{\text{H}}} \right)_{\text{star}} - \log_{10} \left(\frac{N_{\text{Fe}}}{N_{\text{H}}} \right)_{\text{Sun}} \quad (2.15)$$

Where N_{Fe} and N_{H} are the number densities of iron and hydrogen atoms respectively.

- a_λ , b_λ , c_λ , and d_λ are calibration parameters

The calibration of this relation is crucial for accurate distance measurements. Modern calibrations (e.g., [15, 76]) utilize a multi-pronged approach:

1. **Parallax Measurements:** The European Space Agency’s Gaia mission has provided precise parallax measurements for Galactic Cepheids [77], allowing direct distance determinations for nearby Cepheids.
2. **Anchor Galaxies:** Geometric distances to nearby galaxies hosting Cepheids provide additional calibration points. Key examples include:
 - NGC 4258, with a precise maser-based distance
 - The Large Magellanic Cloud (LMC), with distances determined from eclipsing binary systems
3. **Multi-wavelength Observations:** Cepheids are observed across multiple wavelength bands to constrain extinction and metallicity effects. Common bands include:
 - Optical: B (445 nm), V (551 nm), R (658 nm), I (806 nm)
 - Near-infrared: J (1.25 μm), H (1.65 μm), K (2.17 μm)
 - Space-based: HST WFC3 F160W (1.60 μm)

Near-infrared bands are particularly valuable as they are less affected by extinction and metallicity variations.

4. **Period Range:** Calibrations typically focus on fundamental mode Cepheids with periods between 3 and 100 days to ensure consistency and reliability.

The calibration process involves simultaneously fitting data from these various sources, accounting for systematic effects such as crowding, metallicity gradients, and extinction. Advanced statistical techniques, including Bayesian hierarchical models, are often employed to handle the complex interdependencies in the data [15].

By refining the PLZ relation through these meticulous calibrations, astronomers can use Cepheid variables to measure distances to galaxies up to about 40 Mpc, providing a crucial rung in the cosmic distance ladder and playing a vital role in the determination of the Hubble constant.

II.2.1.2. The Tip of the Red Giant Branch (TRGB) Method and Its Calibration The Tip of the Red Giant Branch (TRGB) method is a powerful technique for measuring extragalactic distances, complementing the Cepheid variable approach in the cosmic distance ladder. This method utilizes the predictable maximum luminosity of red giant stars in their final evolutionary stages.

Red giant stars are evolved low- to intermediate-mass stars that have exhausted the hydrogen in their cores. As these stars ascend the red giant branch, they reach a maximum luminosity just before the onset of helium fusion in their cores. This maximum luminosity, corresponding to the brightest red giant stars, creates a sharp

cut-off in the luminosity function of the red giant population, which is easily identifiable in color-magnitude diagrams [78].

The TRGB method was first proposed as a distance indicator by Baade in the 1940s [79], but it wasn’t until the 1990s that it was developed into a precise tool for extragalactic distance measurements [80]. The key advantage of the TRGB method is that it relies on old, low-mass stars present in all galaxy types, unlike Cepheid variables which are only found in star-forming regions.

The calibration of the TRGB method focuses on determining the absolute magnitude of the TRGB, primarily in the I-band (~ 800 nm). The I-band is preferred because the TRGB magnitude is nearly constant for old, metal-poor populations in this wavelength range. The calibration can be expressed as:

$$M_I^{\text{TRGB}} = a[\text{Fe}/\text{H}] + b \quad (2.16)$$

where M_I^{TRGB} is the absolute magnitude of the TRGB in the I-band, $[\text{Fe}/\text{H}]$ is the metallicity, and a and b are calibration parameters [81, 82].

The calibration process involves several key components:

1. **Photometric Systems:** While the I-band is most commonly used, observations in multiple bands (e.g., V, R, J, H, K) help constrain extinction and metallicity effects. The Hubble Space Telescope’s ACS F814W filter is often used for space-based observations.
2. **Metallicity Corrections:** The dependence on metallicity, represented by the $a[\text{Fe}/\text{H}]$ term, is crucial for accurate calibration, especially for metal-rich populations [83].
3. **Anchor Galaxies:** Similar to Cepheid calibration, the TRGB method uses anchor galaxies with independently measured distances. Common anchors include:
 - The Large Magellanic Cloud (LMC)
 - NGC 4258 (with maser-based distance)
 - Milky Way globular clusters with precise parallax measurements
4. **Detection Algorithms:** Sophisticated edge-detection algorithms are employed to precisely locate the TRGB in color-magnitude diagrams [84].
5. **Population Effects:** Careful consideration of the stellar population characteristics, including age and metallicity distribution, is necessary for accurate calibration [85].

Recent calibrations of the TRGB method have achieved precisions comparable to or even exceeding those of Cepheid-based measurements. For instance,

Freedman *et al.* [81] reported a calibration of $M_I^{\text{TRGB}} = -4.05 \pm 0.02$ (stat) ± 0.039 (sys) mag, while Li and Beaton [82] provided an updated calibration incorporating the latest Gaia data.

The TRGB method can be applied to distances up to about 20 Mpc, making it a valuable tool for calibrating secondary distance indicators like Type Ia supernovae. Its independence from Cepheid-based measurements provides an important cross-check in the cosmic distance ladder and in determinations of the Hubble constant.

II.2.1.3. Mira Variables and Their Calibration Mira variables, named after the prototype star Mira (o Ceti), are a class of long-period variable stars that play an increasingly important role in the cosmic distance ladder. These stars are cool, highly evolved stars on the asymptotic giant branch (AGB) of the Hertzsprung-Russell diagram, characteristically old (> 1 Gyr) and of low to intermediate mass ($0.8\text{--}8 M_{\odot}$) [86].

Mira variables undergo large-amplitude pulsations with periods typically ranging from 100 to 1000 days, causing their brightness to vary by several magnitudes. These pulsations are believed to be driven by a combination of changes in opacity and convection in the stellar envelope [87].

The potential of Mira variables as distance indicators was recognized in the early 20th century, with initial period-luminosity relationships established by Gerasimovič (1928) and Spine (1948) [88, 89]. However, it wasn't until the advent of near-infrared astronomy in the 1980s that their full potential as standard candles began to be realized [72].

The calibration of Mira variables for distance measurement primarily relies on their Period-Luminosity (PL) relation, which is most commonly expressed in the near-infrared K-band ($\sim 2.2 \mu\text{m}$):

$$M_K = a \log P + b \quad (2.17)$$

where M_K is the absolute magnitude in the K-band, P is the pulsation period in days, and a and b are calibration parameters [90, 91].

The calibration process for Mira variables involves several key aspects:

1. **Wavelength Selection:** While the K-band is most commonly used due to its reduced sensitivity to metallicity and circumstellar dust, observations in multiple infrared bands (e.g., J at $1.25 \mu\text{m}$, H at $1.65 \mu\text{m}$, L' at $3.8 \mu\text{m}$) are often employed to constrain extinction and chemical composition effects [92].
2. **Period Determination:** Accurate period determination requires long-term monitoring, typically over several years, to account for cycle-to-cycle variations and potential period changes [93].
3. **Chemical Composition:** Mira variables are categorized into oxygen-rich (O-rich) and carbon-rich

(C-rich) types based on their surface chemistry. These types follow slightly different PL relations, necessitating careful classification [94].

4. **Anchor Galaxies:** Calibration of the PL relation relies on Mira variables in well-studied environments with independent distance measurements. Key calibrators include:
 - The Large and Small Magellanic Clouds
 - Galactic Miras with parallax measurements from Hipparcos and Gaia
 - Miras in Galactic globular clusters
5. **Metallicity Effects:** While less pronounced than for Cepheids, metallicity can affect the PL relation. Some calibrations include a metallicity term, especially for applications in diverse galactic environments [90].
6. **Pulsation Mode:** Miras are believed to pulsate primarily in the fundamental mode, but overtone pulsators exist. Proper mode identification is crucial for accurate calibration [87].

Recent calibrations have demonstrated the power of Mira variables as distance indicators. For instance, Huang [91] provided an updated calibration incorporating the latest Gaia data, achieving precisions competitive with other primary distance indicators. Whitelock *et al.* [90] reported a K-band PL relation with a slope of $a \approx -3.51$ and an intrinsic scatter of ~ 0.13 mag for O-rich Miras in the LMC.

Mira variables offer several advantages as distance indicators:

- They are brighter than Cepheids in the infrared, potentially extending the reach of primary distance measurements.
- They are present in all types of galaxies, including early-type galaxies lacking young Cepheid populations.
- Their long periods make them less susceptible to aliasing in sparsely sampled datasets.

As observational techniques and calibrations continue to improve, Mira variables are becoming an increasingly valuable tool in the cosmic distance ladder, complementing and cross-checking other methods in the ongoing effort to refine measurements of the Hubble constant and other cosmological parameters.

II.2.1.4. J-region Asymptotic Giant Branch (JAGB) Stars and Their Calibration as Distance Indicators J-region Asymptotic Giant Branch (JAGB) stars have emerged as a promising new standard candle for the cosmic distance ladder, offering a complementary approach to established methods such as Cepheid variables and the Tip of the Red Giant Branch (TRGB) [67, 74, 95]. These

stars represent a specific subset of carbon-rich Asymptotic Giant Branch (AGB) stars, characterized by their location in color-magnitude diagrams and their near-constant luminosity in the near-infrared J-band.

JAGB stars are evolved, low- to intermediate-mass stars (typically $1.5\text{--}4 M_{\odot}$) in the thermally pulsing AGB phase. During this stage, these stars undergo periodic helium shell flashes, leading to the dredge-up of carbon-rich material to the stellar surface. This process results in a transformation from oxygen-rich to carbon-rich composition when the C/O ratio exceeds unity [96].

The key property that makes JAGB stars valuable as distance indicators is the observed constancy of their luminosity in the J-band (centered at $\sim 1.25 \mu\text{m}$). This phenomenon is attributed to a combination of factors:

- The core mass-luminosity relation for AGB stars
- Temperature regulation due to molecular opacity effects in carbon-rich atmospheres
- The specific characteristics of the J-band, which is less affected by molecular absorption than other near-infrared bands

The potential of carbon stars as distance indicators was recognized as early as the 1980s [97], but it was the work of Weinberg and Nikolaev in 2001 that first identified the distinct "J" region in color-magnitude diagrams of the Large Magellanic Cloud (LMC) [98]. However, it wasn't until the comprehensive study by Madore and Freedman [74] that JAGB stars were formally proposed and developed as a new standard candle for extragalactic distances.

The calibration of JAGB stars as distance indicators is based on the empirical finding that their absolute magnitude in the J-band is approximately constant:

$$M_J = \text{constant} \quad (2.18)$$

where M_J is the absolute magnitude in the J-band. The calibration process involves several key steps:

1. **Photometric System:** While the J-band ($1.25 \mu\text{m}$) is the primary calibration band, observations in multiple near-infrared bands (e.g., J, H at $1.65 \mu\text{m}$, and K_s at $2.15 \mu\text{m}$) are typically used to isolate the JAGB population through color selection.
2. **Color Selection:** JAGB stars are identified using color cuts, typically in the (J- K_s) vs. K_s color-magnitude diagram. The exact color range may vary slightly between studies but generally falls within $1.4 \lesssim (J - K_s) \lesssim 2.0$ [74].
3. **Luminosity Function:** The JAGB luminosity function in the J-band is analyzed to determine the characteristic magnitude, often using techniques such as Gaussian fitting or edge detection algorithms.

4. **Anchor Galaxies:** Similar to other distance indicators, JAGB calibration relies on observations in galaxies with well-established distances. Primary calibrators include:
 - The Large and Small Magellanic Clouds
 - M31 (Andromeda) and M33
 - Galaxies with maser distances (e.g., NGC 4258)

5. **Metallicity Effects:** While the J-band magnitude of JAGB stars appears to be less sensitive to metallicity than other indicators, potential metallicity effects are still an active area of research [95].

6. **Population Effects:** The presence and characteristics of JAGB stars depend on the age and star formation history of the stellar population, necessitating careful consideration in diverse galactic environments.

Recent calibrations have demonstrated the promise of the JAGB method. For instance, Freedman *et al.* [67], Madore and Freedman [74] reported an absolute J-band magnitude of $M_J = -6.22 \pm 0.04$ mag for JAGB stars based on observations in the LMC, with a typical dispersion of ~ 0.23 mag for individual stars.

The JAGB method offers several advantages as a distance indicator:

- **Extended reach:** JAGB stars are typically ~ 1 magnitude brighter than the TRGB in the near-infrared, potentially extending the range of primary distance measurements.
- **Single-epoch observations:** Unlike variable stars, JAGB stars can be detected and measured with a single near-infrared observation.
- **Ease of identification:** They are readily identifiable by their distinctive colors and magnitudes in near-infrared color-magnitude diagrams.
- **Reduced extinction:** Near-infrared observations are less affected by dust extinction compared to optical wavelengths.
- **Abundance in various galaxy types:** JAGB stars are present in all galaxies with intermediate-age stellar populations, including early-type galaxies where Cepheids are absent.
- **Independent cross-check:** Their use provides an additional, independent method to verify distances obtained through other techniques.

The JAGB method has been successfully applied to measure distances to nearby galaxies and galaxy groups, including the M81 group [74] and the Leo I group [95]. As observational techniques and calibrations continue to improve, JAGB stars are poised to play an increasingly

important role in the cosmic distance ladder, contributing to the ongoing refinement of the Hubble constant and other cosmological parameters.

II.2.2. Second Rung: Calibration of Type Ia Supernovae

The primary objective of the second rung is to calibrate Type Ia Supernovae (SnIa) using the local distance indicators calibrated in the first rung. This calibration is crucial for extending distance measurements to cosmological scales. The calibration of SnIa involves determining their standardized absolute magnitude, which is typically expressed in the B-band, M_B^{SN} . The process includes:

1. Identifying host galaxies containing both SnIa and calibrated distance indicators (primarily Cepheids or TRGB).

2. Measuring distances to these galaxies using the calibrated indicators from the first rung.

3. Standardizing SN Ia luminosities using the Tripp relation [99]:

$$m_B^{\text{corr}} = m_B + \alpha x_1 - \beta c \quad (2.19)$$

where m_B^{corr} is the corrected B-band magnitude, m_B is the observed peak magnitude, x_1 is a stretch parameter, c is a color parameter, and α and β are nuisance parameters to be determined.

4. Determining the fiducial absolute magnitude M_B^{SN} by combining data from multiple calibrator SnIa:

$$M_B^{\text{SN}} = m_B^{\text{corr}} - \mu_{\text{cal}} \quad (2.20)$$

where μ_{cal} is the distance modulus determined from the calibrated first-rung indicators.

The goal of this second rung is to precisely determine M_B^{SN} , α , and β , which together allow SnIa to be used as standardizable candles for cosmological distance measurements.

The accuracy of the SN Ia calibration is critical for the determination of the Hubble constant. Recent analyses, such as the SH0ES project [15], have focused on refining this calibration to achieve percent-level precision in H_0 measurements. However, a fundamental assumption underlying this calibration process warrants careful consideration:

A crucial premise in the cosmic distance ladder methodology is that the calibration parameters remain constant across all rungs. This assumption implies that the physics governing the behavior of distance indicators (Cepheids, TRGB, SnIa) does not change significantly from local to cosmological scales. This assumption could be violated [76, 100] under several scenarios:

- **Environmental Changes:** Systematic differences in the environments of distance indicators between rungs (e.g., dust properties, metallicity gradients) could affect their observed properties.

- **Evolutionary Effects:** Changes in stellar populations or galaxy properties over cosmic time might alter the characteristics of distance indicators.

- **Fundamental Physics Transitions:** A change in fundamental physics at some distance or time in the recent cosmological past could affect the behavior of distance indicators.

II.2.2.1. Distances, Redshifts, and Past Times of Each Rung: To contextualize these considerations, it's important to understand the typical distances, redshifts, and corresponding past times associated with each rung:

1. First Rung (Local Calibrators):

- Distances: ~ 10 pc to ~ 10 Mpc
- Redshifts: $z \lesssim 0.002$
- Past time: $\sim 0 - 30$ Myr ago
- Examples: Milky Way Cepheids, LMC, NGC 4258

2. Second Rung (SnIa Calibration):

- Distances: ~ 10 Mpc to ~ 40 Mpc
- Redshifts: $0.002 \lesssim z \lesssim 0.01$
- Past time: $\sim 30 - 130$ Myr ago
- Examples: Galaxies hosting both Cepheids/TRGB/Miras/JAGB and SnIa

3. Third Rung (Hubble Flow SnIa):

- Distances: $\gtrsim 40$ Mpc
- Redshifts: $0.01 \lesssim z \lesssim 0.15$
- Past time: ~ 130 Myr - 1.8 Gyr ago
- Note: Upper limit chosen to minimize cosmic acceleration effects

The transition between these rungs spans several orders of magnitude in distance and covers a significant portion of recent cosmic history (~ 1.8 Gyr). This range extends from the present day to when the Universe was about 87% of its current age. The past time estimates are based on a standard Λ CDM cosmology with $H_0 \approx 70$ km s $^{-1}$ Mpc $^{-1}$ and $\Omega_m \approx 0.3$.

This temporal span underscores the importance of validating the assumption of calibration consistency across these scales. Over this time, subtle changes in stellar populations, galactic environments, and even potentially in fundamental physics could occur, potentially affecting our distance indicators.

Potential violations of the calibration consistency assumption across these timescales could introduce systematic biases in H_0 measurements. Therefore, it is crucial to carefully consider and test for any time-dependent effects that might influence our distance indicators and ultimately our determination of the Hubble constant.

II.2.3. Third Rung: Extending to Cosmological Scales

The third rung of the cosmic distance ladder extends measurements to cosmological scales, primarily utilizing Type Ia supernovae (SnIa) as standardizable candles. While the calibration process of SnIa using Cepheids has been discussed in previous subsections, here we describe how these calibrated SnIa are employed to determine the Hubble constant.

II.2.3.1. Cosmographic Expansion Approach The determination of H_0 from SnIa data involves a cosmographic expansion of the Hubble parameter $H(z)$. This expansion is typically carried out to first order [101, 102]:

$$H(z) = H_0[1 + (1 + q_0)z + \mathcal{O}(z^2)] \quad (2.21)$$

where q_0 is the deceleration parameter. The luminosity distance d_L can then be expressed as:

$$d_L(z) = \frac{c}{H_0} \left[z + \frac{1}{2}(1 - q_0)z^2 + \mathcal{O}(z^3) \right] \quad (2.22)$$

For low redshifts ($z \lesssim 0.1$), we can use this cosmographic expansion approach to measure H_0 using SnIa as standardizable candles. This method minimizes the dependence on specific cosmological models while still capturing the essence of cosmic expansion [66, 103].

II.2.3.2. Distance Modulus and Fitting Procedure We start with the distance modulus equation:

$$m_{\text{th}}(z) = M_B + 5 \log_{10} \left[\frac{d_L(z)}{\text{Mpc}} \right] + 25 \quad (2.23)$$

where $m_{\text{th}}(z)$ is the theoretical apparent magnitude, M_B is the absolute magnitude, and $d_L(z)$ is the luminosity distance. Using equation (2.22) in (2.23), we obtain:

$$m_{\text{th}}(z) = M_B + 5 \log_{10} \left(cz \left[1 + \frac{1}{2}(1 - q_0)z \right] \right) + 5 \log_{10} \left(\frac{c/H_0}{1 \text{ Mpc}} \right) + 25 \quad (2.24)$$

where the observables are m_{th} and z , and the parameters are fit from SnIa data.

To break the degeneracy between M_B and H_0 , we use local measurements ($z < 0.01$, typically within 40 Mpc) of M_B using relative distance indicators like Cepheid variables or the Tip of the Red Giant Branch (TRGB) [104]. We then assume this locally calibrated M_B applies to the SnIa in the Hubble flow ($0.01 < z < 0.15$).

The fitting procedure involves minimizing:

$$\chi^2(H_0, q_0) = \sum_i \frac{[m_{\text{obs},i} - m_{\text{th}}(z_i; H_0, q_0)]^2}{\sigma_i^2} \quad (2.25)$$

where $m_{\text{obs},i}$ are the observed magnitudes and σ_i are the associated uncertainties.

II.2.3.3. Practical Approaches In practice, two main approaches are employed:

1. **Fixed q_0 Approach:** The deceleration parameter q_0 is fixed to its value derived from a fiducial cosmological model (e.g., Planck 2018 best-fit Λ CDM), and H_0 is determined solely from the SnIa data [103, 105].
2. **Joint Fit Approach:** Both H_0 and q_0 are simultaneously fit using the SnIa data from the third rung [106, 107]. This approach reduces model dependence but may increase statistical uncertainties.

The choice between these approaches can impact the resulting H_0 value and its associated uncertainties, highlighting the importance of careful consideration of the underlying cosmological model assumptions [7].

II.2.3.4. Systematic Uncertainties Several sources of systematic uncertainty must be carefully addressed in this process:

- **SnIa Standardization:** The intrinsic scatter in SnIa absolute magnitudes after standardization contributes to the uncertainty in H_0 [108].
- **Local Calibration:** Uncertainties in the local calibration of M_B using Cepheids or TRGB propagate directly to the H_0 measurement [104, 105].
- **Redshift Cut:** The choice of the upper redshift limit for the Hubble flow sample can affect the results due to increasing cosmological model dependence at higher redshifts [66].
- **Peculiar Velocities:** Corrections for peculiar velocities, especially important at lower redshifts, can introduce uncertainties [109, 110].

Recent analyses have made significant progress in addressing these systematics, leading to more robust H_0 measurements [15, 111]. However, the persistent tension between local H_0 measurements and those inferred from early universe observations underscores the need for continued scrutiny and refinement of these methods [1, 3].

For a recent pedagogical and detailed description of the distance ladder method, including advanced techniques and potential systematic effects, see Ref. [76].

II.2.3.5. Complementary Secondary Indicators While SnIa serve as the primary tool for H_0 determination in the third rung, several other secondary distance indicators provide valuable cross-checks and complementary information:

- **Surface Brightness Fluctuations (SBF):** This method [112] utilizes the statistical properties of pixel-to-pixel variations in galaxy images to estimate distances.
- **L- σ Relation for HII galaxies:** This technique [113] leverages the correlation between HII region luminosity and gas velocity dispersion.

- **Tully-Fisher Relation:** This empirical relation [114–116] between galaxy rotational velocity and luminosity provides an independent distance measure for spiral galaxies.

These complementary methods serve to validate and refine the distance scale established by SnIa, enhancing the robustness of H_0 measurements.

II.3. One Step Methods

One step methods for measuring the Hubble constant, H_0 , provide an alternative to the traditional distance ladder approach [117]. Unlike the multi-tiered distance ladder that relies on a series of interconnected rungs, one step methods seek to estimate cosmological distances directly from a single distance indicator without the need for intermediate calibrators. This section provides an overview of many of these methods, focusing on those that are independent from the sound horizon scale standard ruler and describing their unique advantages and limitations. One step methods are less susceptible to the cumulative errors and biases that can arise from local astrophysical effects, such as variations in metallicity, extinction, or stellar population characteristics. However, it is important to recognize that while one step methods are less dependent on local astrophysics, they generally offer less precision compared to the well-established distance ladder techniques, primarily due to the inherent challenges in measuring cosmological distances directly from singular observations. In the following subsections we discuss the main one step methods in some more detail.

II.3.1. Sunyaev-Zel'dovich Effect

The Sunyaev-Zel'dovich (SZ) effect, first predicted by Rashid Sunyaev and Yakov Zel'dovich in 1969, has emerged as a powerful tool in observational cosmology [118, 119]. This effect, which arises from the interaction between cosmic microwave background (CMB) photons and high-energy electrons in galaxy clusters, provides a method for measuring cosmological distances that is independent of the traditional cosmic distance ladder.

II.3.1.1. Physical Basis The SZ effect is primarily composed of two components:

- **Thermal SZ effect:** The dominant component, resulting from the inverse Compton scattering of CMB photons by hot electrons in the intracluster medium (ICM).
- **Kinetic SZ effect:** A subdominant component caused by the bulk motion of the electron gas relative to the CMB rest frame.

This subsection focuses on the thermal SZ effect due to its greater magnitude and cosmological utility.

II.3.1.2. Mathematical Formulation The thermal SZ effect manifests as a frequency-dependent distortion of the CMB spectrum. The change in the CMB intensity due to the SZ effect is given by:

$$\frac{\Delta I_\nu}{I_0} = y \cdot g(x) \quad (2.26)$$

where:

- $I_0 = \frac{2(k_B T_{\text{CMB}})^3}{(hc)^2}$ is the undistorted CMB intensity
- y is the Comptonization parameter
- $g(x)$ is the spectral function
- $x = \frac{h\nu}{k_B T_{\text{CMB}}}$ is the dimensionless frequency

The Comptonization parameter y represents the integrated electron pressure along the line of sight:

$$y = \int \frac{k_B T_e}{m_e c^2} n_e \sigma_T dl \quad (2.27)$$

where T_e is the electron temperature, n_e is the electron number density, σ_T is the Thomson cross-section, and the integral is along the line of sight.

The spectral function $g(x)$ is given by:

$$g(x) = \frac{x^4 e^x}{(e^x - 1)^2} \left(x \frac{e^x + 1}{e^x - 1} - 4 \right) (1 + \delta_{\text{SZ}}(x, T_e)) \quad (2.28)$$

where $\delta_{\text{SZ}}(x, T_e)$ accounts for relativistic corrections, which become significant for high-temperature clusters ($k_B T_e \gtrsim 10$ keV).

II.3.1.3. Observational Characteristics The SZ effect has several unique properties that make it valuable for cosmological studies [120–123]:

- It is independent of redshift, allowing for the detection of high-redshift clusters.
- The SZ surface brightness is proportional to the integrated pressure of the ICM, providing a direct probe of cluster thermodynamics.
- The effect causes a decrease in CMB intensity at frequencies below ~ 218 GHz and an increase above this frequency, creating a distinctive spectral signature.

II.3.1.4. Application to Cosmology One of the most significant applications of the SZ effect is in measuring the Hubble constant (H_0). This method combines SZ observations with X-ray measurements of galaxy clusters to derive distances. The process involves:

1. SZ observations provide a measure of $\int n_e T_e dl$.
2. X-ray observations provide a measure of $\int n_e^2 \Lambda(T_e) dl$, where $\Lambda(T_e)$ is the X-ray cooling function.

3. Assuming a geometry for the cluster (often a spherical isothermal β -model), these observations can be combined to solve for the angular diameter distance D_A .
4. The Hubble constant is then derived using the relation $H_0 = cz/D_A$ for low-redshift clusters.

II.3.1.5. Recent Results A notable study by Reese et al. [124] used this technique with a sample of 41 galaxy clusters to derive:

$$H_0 = 61 \pm 3 \text{ (stat.)} \pm 18 \text{ (syst.) km s}^{-1} \text{ Mpc}^{-1} \quad (2.29)$$

where the uncertainties are given at 68% confidence. The large systematic uncertainty reflects challenges in modeling cluster geometry and evolution.

II.3.1.6. Future Prospects Ongoing and future SZ surveys, such as those conducted with the Atacama Cosmology Telescope (ACT) and the South Pole Telescope (SPT), promise to significantly improve the precision of SZ-based cosmological measurements. These improvements will come from:

- Larger cluster samples reducing statistical uncertainties
- Better understanding of cluster physics and improved modeling techniques
- Combination with other cosmological probes to break degeneracies and reduce systematic uncertainties

The SZ effect, with its unique redshift-independence and direct probe of cluster physics, continues to be a valuable tool in modern cosmology, complementing other methods in our quest to understand the universe's expansion history and large-scale structure.

II.3.2. Megamasers as Standard Rulers

Megamasers, particularly those associated with water molecules in active galactic nuclei (AGN), have emerged as powerful standard rulers for measuring extragalactic distances [125, 126]. These astrophysical phenomena provide a direct geometric method for determining the Hubble constant, H_0 , independent of the cosmic distance ladder.

II.3.2.1. Physical Basis Water megamasers are typically found in the accretion disks surrounding supermassive black holes in AGN. The 22 GHz ($\lambda = 1.35\text{cm}$) emission line of water results from the $6_{16} \rightarrow 5_{23}$ rotational transition. This maser emission occurs under specific conditions:

- Temperatures of $\sim 300\text{-}1000$ K

- High water molecule densities ($n_{H_2O} \sim 10^8 - 10^{10} \text{ cm}^{-3}$)
- Presence of a pumping mechanism (likely collisional)

The bright, compact nature of these masers, combined with their Keplerian motion in the accretion disk, makes them ideal targets for very long baseline interferometry (VLBI) observations.

II.3.2.2. Observational Technique VLBI observations of megamasers provide two key measurements:

1. Precise spatial positions of individual maser spots
2. Doppler shifts of maser lines, yielding line-of-sight velocities

These observations typically reveal a characteristic pattern in position-velocity space, with systemic masers near the center of the disk and high-velocity masers on the disk's edge, tracing a Keplerian rotation curve.

II.3.2.3. Physical Model and Distance Determination The geometry and dynamics of the maser-emitting accretion disk allow for the application of Kepler's laws of motion. The enclosed mass M (dominated by the central supermassive black hole) can be derived from the rotation speed v and radius r of the maser spots:

$$v^2 = \frac{GM}{r} \quad (2.30)$$

where G is the gravitational constant. VLBI observations provide both v (from Doppler shifts) and the angular separation θ between maser spots.

The distance D to the galaxy can then be calculated using:

$$D = \frac{v}{\theta\omega} \quad (2.31)$$

where ω is the angular velocity of the maser spots. This equation combines the physical size of the disk (derived from equation (2.30)) with its angular size as observed from Earth.

The Hubble constant can then be estimated using:

$$H_0 = \frac{v_H}{D} \quad (2.32)$$

where v_H is the Hubble flow velocity, typically derived from the galaxy's redshift after correcting for peculiar motions.

II.3.2.4. Advantages and Challenges The megamaser method offers several advantages:

- Direct geometric distance measurement
- Independence from the cosmic distance ladder

- High precision (potentially $\sim 3\%$ per galaxy)
- Applicability to galaxies at cosmologically significant distances

However, challenges include:

- Rarity of suitable megamaser systems
- Complexity of accretion disk models (e.g., warping, non-circular motions)
- Need for high-sensitivity VLBI observations

II.3.2.5. Recent Results The Megamaser Cosmology Project (MCP) has been at the forefront of using this technique. A notable example is their study of NGC 5765b, an Sa-b galaxy hosting water megamasers [127]. Key findings include:

- Confirmation of a thin, sub-parsec Keplerian disk
- Evidence for a spiral density wave influencing accretion dynamics
- Angular-diameter distance to NGC 5765b: 126.3 ± 11.6 Mpc
- Hubble constant estimate: $H_0 = 66.0 \pm 6.0$ km s $^{-1}$ Mpc $^{-1}$

This measurement incorporated secular drifts of maser features and a detailed model of the disk's warped structure to refine the H_0 estimate.

II.3.2.6. Future Prospects The megamaser method continues to be refined and applied to new systems. Future developments may include:

- Increased sample size through more sensitive surveys
- Improved modeling of non-Keplerian motions and disk structure
- Combination with other distance measurement techniques to constrain systematic errors

As an independent probe of H_0 , megamasers play a crucial role in addressing the tension between early and late universe measurements of the expansion rate. Their continued study promises to contribute significantly to our understanding of cosmology and the dynamics of galactic nuclei.

II.3.3. Strong Gravitational Lensing Time Delays

Strong gravitational lensing time delays have emerged as a powerful, independent method for measuring the Hubble constant (H_0) [128–133]. This technique leverages the phenomenon of gravitational lensing, where a massive foreground object (typically a galaxy or galaxy cluster) bends light from a background source (often a quasar), creating multiple images. The difference in light travel time between these images provides a direct probe of cosmological distances.

II.3.3.1. Theoretical Foundation The fundamental principle of time-delay cosmography is rooted in general relativity. Light from a background source, when lensed by a foreground mass, travels along different paths with varying lengths and gravitational potentials. This results in the lensed images arriving at the observer at different times. These time delays, when accurately measured, are directly related to the geometry of the Universe and the mass distribution of the lens, thus providing a means to constrain cosmological parameters, particularly H_0 .

The key quantity in time-delay cosmography is the time-delay distance $D_{\Delta t}$, which is a combination of angular diameter distances:

$$D_{\Delta t} \equiv (1 + z_d) \frac{D_d D_s}{D_{ds}}, \quad (2.33)$$

where z_d is the redshift of the deflector (lens), D_d is the angular diameter distance to the deflector, D_s is the angular diameter distance to the source, and D_{ds} is the angular diameter distance from the deflector to the source.

The observed time delay Δt_{AB} between two lensed images A and B is related to the Fermat potential difference $\Delta\phi_{AB}$ by:

$$\Delta t_{AB} = \frac{D_{\Delta t}}{c} \Delta\phi_{AB}, \quad (2.34)$$

where c is the speed of light. The Fermat potential $\phi(\boldsymbol{\theta})$ at a position $\boldsymbol{\theta}$ on the sky is defined as:

$$\phi(\boldsymbol{\theta}) = \frac{(\boldsymbol{\theta} - \boldsymbol{\beta})^2}{2} - \psi(\boldsymbol{\theta}), \quad (2.35)$$

with $\boldsymbol{\beta}$ being the source position and $\psi(\boldsymbol{\theta})$ the lensing potential.

II.3.3.2. Methodology and Challenges The Time-Delay COSMOgraphy (TDCOSMO) collaboration, building upon earlier efforts such as COSMOGRAIL, H0LiCOW, and STRIDES, has refined the methodology for using strong lensing time delays to measure H_0 [130, 131]. Their approach involves:

1. Precise time delay measurements through long-term, high-cadence monitoring of lensed quasars.
2. Advanced lens mass modeling, incorporating both parametric and non-parametric approaches.
3. Rigorous accounting for line-of-sight effects using spectroscopic data and numerical simulations.
4. A comprehensive Bayesian framework for inferring cosmological parameters.

Key challenges in this method include:

- Accurate characterization of the lens mass distribution, including the effects of dark matter.

- Proper accounting for the mass-sheet degeneracy and other potential degeneracies in lens modeling.
- Quantifying and mitigating the impact of line-of-sight structures on the lensing potential.
- Obtaining sufficiently long and well-sampled light curves for precise time delay measurements.

II.3.3.3. Current Results and Implications The landscape of H_0 measurements from time-delay cosmography has evolved significantly in recent years:

- TDCOSMO’s early combined analysis of seven lens systems yielded $H_0 = 74.2 \pm 1.6 \text{ km s}^{-1} \text{ Mpc}^{-1}$ (2.2% precision) [134], aligning with distance ladder results.
- Du et al. (2023) [135] found $H_0 = 71.5_{-3.0}^{+4.4} \text{ km s}^{-1} \text{ Mpc}^{-1}$ using time-delay galaxy lenses combined with gamma-ray bursts.
- Birrer et al. (2020) [130], in a joint analysis of TDCOSMO and SLACS samples, obtained $H_0 = 67.4_{-3.2}^{+4.1} \text{ km s}^{-1} \text{ Mpc}^{-1}$, shifting towards lower values more consistent with Planck results.
- Most recently, TDCOSMO (2024) [136] reported $H_0 = 65_{-14}^{+23} \text{ km s}^{-1} \text{ Mpc}^{-1}$ from time-delay cosmography of WGD 2038-4008, albeit with large uncertainties.

This progression suggests that as methods are refined and datasets expanded, time-delay cosmography and related techniques are increasingly yielding H_0 measurements more in line with Planck CMB-based estimates, rather than supporting the higher values from local distance ladder methods.

II.3.3.4. Future Prospects The future of time-delay cosmography is promising, with several developments on the horizon:

- Upcoming wide-field surveys like the Vera C. Rubin Observatory’s Legacy Survey of Space and Time (LSST) are expected to discover thousands of new lensed quasars, dramatically increasing the sample size.
- Advancements in adaptive optics and space-based imaging will improve the resolution and quality of lens imaging, enhancing mass modeling capabilities.
- Improved spectroscopic follow-up will better constrain line-of-sight effects and lens dynamics.
- Integration with other cosmological probes, such as strongly lensed supernovae and gravitational waves, may provide complementary constraints and help break degeneracies.

As TDCOSMO and other collaborations continue to refine their methodology, expand their lens samples, and explore potential systematic effects, time-delay cosmography is poised to play an increasingly important role in precision cosmology and in addressing the Hubble tension. The method’s strength lies in its direct approach, utilizing fundamental physics without reliance on distance ladder calibrations, making it a valuable complement to other cosmological probes.

II.3.4. Horizon at Matter-Radiation Equality as a Standard Ruler

The horizon at matter-radiation equality presents an alternative standard ruler for cosmological distance measurements, distinct from the widely used sound horizon scale [137–139]. This section elucidates the principles underlying this approach, presents key equations, and discusses recent research findings.

II.3.4.1. Theoretical Foundation The horizon at matter-radiation equality, characterized by the wavenumber k_{eq} , represents the comoving scale entering the horizon when the energy densities of matter and radiation are equal. This scale significantly influences the shape of the matter power spectrum, particularly affecting the turnover point, which is crucial for determining the broadband shape of the linear power spectrum at scales $k \sim k_{\text{eq}}$.

The comoving wavenumber at matter-radiation equality, k_{eq} , is given by:

$$k_{\text{eq}} = \sqrt{2\Omega_m H_0^2 a_{\text{eq}}^{-1}}, \quad (2.36)$$

where Ω_m is the matter density parameter, H_0 is the Hubble constant, and a_{eq} is the scale factor at matter-radiation equality. This can be rewritten in terms of the redshift at matter-radiation equality, z_{eq} , as:

$$k_{\text{eq}} = \sqrt{2\Omega_m H_0^2 (1 + z_{\text{eq}})}. \quad (2.37)$$

The scale k_{eq} sets the peak of the matter power spectrum and is crucial for determining the linear power spectrum’s shape at scales around and larger than k_{eq} .

II.3.4.2. Methodology and Applications Recent studies, such as those by Philcox et al. (2022) [137], Brieden et al. (2022) [138], and D’Amico et al. (2020) [139], have utilized k_{eq} to derive independent constraints on the Hubble constant, H_0 , within a Λ CDM framework. This approach combines measurements from various cosmological probes:

- Galaxy surveys: Providing information on the matter power spectrum shape
- CMB lensing: Offering complementary constraints on matter clustering

- Supernovae: Constraining the expansion history of the Universe

The key advantage of this method is its independence from the sound horizon scale, which is typically used in BAO studies. This independence makes it less sensitive to early universe physics and potential new physics that might affect the pre-recombination era.

II.3.4.3. Recent Results Philcox et al. (2022) [137] combined data from BOSS galaxy power spectra, Planck CMB lensing, and the Pantheon+ supernova compilation to derive an H_0 value of:

$$H_0 = 64.8_{-2.5}^{+2.2} \text{ km s}^{-1}\text{Mpc}^{-1} \quad (68\% \text{ confidence level}). \quad (2.38)$$

This result is consistent with Planck CMB-based estimates and in tension with local distance ladder measurements, providing an independent cross-check on the Hubble tension.

II.3.4.4. Advantages and Limitations The use of the horizon at matter-radiation equality as a standard ruler offers several advantages:

- Independence from early universe physics: Less sensitive to potential new physics affecting the pre-recombination era.
- Complementarity: Provides a check on results from BAO and CMB analyses.
- Robustness: Relies on well-understood physics of the matter-radiation transition.

However, there are also limitations to consider:

- Precision: Currently less precise than BAO measurements.
- Model dependence: Assumes a Λ CDM cosmology.
- Systematic uncertainties: Requires careful modeling of nonlinear effects in galaxy clustering.

II.3.4.5. Future Prospects The potential of this method is likely to grow with forthcoming galaxy surveys such as DESI, Euclid, and the Vera C. Rubin Observatory's LSST. These surveys will provide more precise measurements of the matter power spectrum over a wider range of scales and redshifts, potentially improving constraints on k_{eq} and, consequently, on H_0 .

Furthermore, combining this approach with other probes, such as gravitational lensing and the kinetic Sunyaev-Zel'dovich effect, could break degeneracies and further improve constraints on cosmological parameters.

In conclusion, using the horizon at matter-radiation equality as a standard ruler provides a compelling alternative for cosmological distance measurements. Its robustness against potential new early universe physics makes it a valuable tool for modern cosmology, offering an independent check on the consistency of cosmological

measurements and theories. As observational data improve and analysis techniques are refined, this method is poised to play an increasingly important role in addressing key cosmological questions, including the Hubble tension.

II.3.5. Cosmic Chronometers

Cosmic chronometers offer a novel approach to measure the expansion rate of the Universe, $H(z)$, directly from observational data without relying on the standard cosmological model [140–143]. This method, based on the differential age approach, utilizes the time difference (Δt) between two distinct epochs of the Universe to infer the Hubble parameter. This section outlines the foundational principles, key equations, and practical applications of this method.

II.3.5.1. Theoretical Foundation The cosmic chronometer approach leverages the age of the oldest galaxies at different redshifts to estimate the rate of cosmic expansion. The core assumption is that the most massive, passively evolving galaxies, often termed 'red and dead' galaxies, form their stellar populations early and evolve with minimal subsequent star formation. These galaxies serve as 'chronometers' because their age can be closely associated with the age of the Universe at their formation redshift.

II.3.5.2. Methodology The Hubble parameter, $H(z)$, which quantifies the expansion rate of the Universe, can be directly related to the observable quantities of redshift (z) and time (t) via the differential age method. The fundamental relation is given by:

$$H(z) = -\frac{1}{1+z} \frac{dz}{dt}. \quad (2.39)$$

In practice, this is approximated using finite differences:

$$H(z) \approx -\frac{1}{1+z} \frac{\Delta z}{\Delta t}, \quad (2.40)$$

where Δz is the redshift difference between two galaxy populations, and Δt is the differential age between these populations, estimated from their stellar populations.

II.3.5.3. Implementation and Challenges The implementation of the cosmic chronometer method involves several key steps:

1. Selection of passively evolving galaxies: Identifying massive, early-type galaxies with minimal ongoing star formation.
2. Spectroscopic observations: Obtaining high-quality spectra to determine redshifts and estimate stellar population ages.

3. Age determination: Using stellar population synthesis models to estimate the age of the galaxies based on their spectral features.
4. Differential age calculation: Computing the age difference between galaxy populations at different redshifts.
5. Hubble parameter estimation: Applying Equation (2.40) to calculate $H(z)$ at various redshifts.

This method faces several challenges:

- Accurate age determination: Requires precise stellar population models and high-quality spectroscopic data.
- Sample selection: Ensuring a consistent selection of passively evolving galaxies across cosmic time.
- Systematics: Addressing potential biases in age estimates and selection effects.
- Limited redshift range: Currently restricted to $z \lesssim 2$ due to observational limitations.

II.3.5.4. Illustrative Example Consider two populations of galaxies at redshifts z_1 and z_2 , with $z_2 > z_1$. Spectroscopic studies determine their ages to be t_1 and t_2 respectively. Let $\Delta t = t_2 - t_1 = 1$ Gyr and $\Delta z = z_2 - z_1 = 0.1$. The Hubble parameter at the mean redshift $\bar{z} = (z_1 + z_2)/2$ can be calculated as:

$$H(\bar{z}) = -\frac{1}{1 + \bar{z}} \frac{\Delta z}{\Delta t}. \quad (2.41)$$

Assuming $\bar{z} = 1.5$ and converting units appropriately:

$$H(1.5) \approx -\frac{1}{2.5} \frac{0.1}{1 \text{ Gyr}} \approx 78 \text{ km s}^{-1} \text{ Mpc}^{-1}, \quad (2.42)$$

where the negative sign indicates expansion.

II.3.5.5. Recent Results and Future Prospects Recent studies have applied the cosmic chronometer method to constrain $H(z)$ over a wide redshift range. For instance, Moresco et al. (2016) [143] provided measurements of $H(z)$ up to $z \sim 2$, finding good agreement with Λ CDM predictions but with larger uncertainties at high redshifts.

Future prospects for this method include:

- Improved stellar population models: Enhancing the accuracy of age determinations.
- Larger galaxy samples: Upcoming surveys like DESI and Euclid will provide larger samples of passive galaxies.
- Extended redshift range: Near-infrared spectroscopy may allow measurements at $z > 2$.

- Synergies with other probes: Combining with BAO and SNe Ia data for tighter cosmological constraints.

The cosmic chronometer method offers a unique, model-independent approach to measure the expansion history of the Universe. While it currently provides less precise measurements compared to other probes, its independence from the cosmic distance ladder and standard cosmological assumptions makes it a valuable tool for cross-validating results from other methods and potentially uncovering new physics beyond the standard model.

II.3.6. Standard Sirens and Kilonovae

Standard sirens, a term coined for gravitational waves (GWs) emitted from compact binary mergers, provide a unique method for measuring the Hubble constant, H_0 , directly from the gravitational wave signal without requiring a cosmic distance ladder [144–149]. This section details the principles behind using GWs and their electromagnetic counterparts, kilonovae, as cosmological probes, highlighting their potential to resolve the Hubble tension.

II.3.6.1. Gravitational Waves as Standard Sirens Gravitational waves emitted from mergers of binary neutron stars (BNS) or neutron star-black hole (NS-BH) binaries offer a direct measure of the luminosity distance to the source [144]. The amplitude of the gravitational wave signal is inversely proportional to this distance, and by combining it with the redshift of the host galaxy, H_0 can be directly inferred.

The relationship between the strain amplitude h of the gravitational wave and the luminosity distance D_L is given by the quadrupole formula:

$$h = \frac{4(G\mathcal{M})^{5/3}}{c^4 D_L} (\pi f)^{2/3} \mathcal{F}(\text{angle, orientation}), \quad (2.43)$$

where G is the gravitational constant, c is the speed of light, \mathcal{M} is the chirp mass, f is the frequency of the gravitational wave, and \mathcal{F} is a function of the binary's inclination angle and sky position.

II.3.6.2. Kilonovae as Electromagnetic Counterparts A kilonova (KN) is a thermal electromagnetic emission resulting from the radioactive decay of heavy elements synthesized in the neutron-rich ejecta of a neutron star merger. This emission is quasi-isotropic and can be seen from a wide range of viewing angles, making it an excellent counterpart for observing gravitational wave events. The combined observation of a gravitational wave and a kilonova from the same event provides a powerful tool for cosmology, as it adds an independent measurement of the electromagnetic flux, which aids in breaking degeneracies in the gravitational wave signal.

II.3.6.3. Hubble Constant Measurement The relationship between luminosity distance D_L and redshift z in the local universe is expressed by:

$$v_H = cz = H_0 D_L, \quad (2.44)$$

where v_H is the Hubble flow velocity. For nearby sources where peculiar velocities are significant, this relation is modified to:

$$v_H = cz_{\text{helio}} - v_{\text{pec,LOS}} = H_0 D_L, \quad (2.45)$$

where z_{helio} is the heliocentric redshift and $v_{\text{pec,LOS}}$ is the line-of-sight peculiar velocity.

II.3.6.4. The GW170817 Event The landmark event GW170817, where both gravitational waves and a kilonova [144, 150] were observed, serves as a prime example of this method. The gravitational wave signal provided a measurement of the luminosity distance, while the identification of the host galaxy NGC 4993 led to a redshift measurement. Combining these measurements allowed for an independent estimate of H_0 .

II.3.6.5. Breaking the Inclination Degeneracy The inclination of the binary system affects the amplitude of the gravitational wave signal, introducing a degeneracy between inclination and distance. The kilonova emission, being anisotropic and dependent on the viewing angle, provides additional constraints on the system's orientation. By combining the gravitational wave data with kilonova light curves and spectra, the inclination-distance degeneracy can be partially broken, leading to more precise H_0 measurements.

II.3.6.6. Statistical Approach For events without identified electromagnetic counterparts, a statistical approach can be employed. This method involves cross-correlating the GW-inferred sky localizations with galaxy catalogs to obtain a probabilistic estimate of the host galaxy and its redshift. While less precise than the direct counterpart method, this approach allows for the use of a larger sample of GW events.

II.3.6.7. Current Results and Future Prospects Recent analyses combining multiple GW events have provided competitive constraints on H_0 . For example, the LIGO-Virgo-KAGRA collaboration reported:

$$H_0 = 68_{-7}^{+8} \text{ km s}^{-1} \text{ Mpc}^{-1} \quad (68\% \text{ credible interval}), \quad (2.46)$$

based on a sample of binary black hole mergers and GW170817 [151].

Future prospects for this method are promising:

- Increased event rate: Advanced detectors will observe more BNS and NS-BH mergers, improving statistical precision.

- Improved detector sensitivity: Enhanced strain sensitivity will lead to more precise distance measurements.
- Better kilonova models: Improved theoretical understanding and observations of kilonovae will enhance constraints on system parameters.
- Synergies with other probes: Combining standard siren measurements with other cosmological probes can provide powerful constraints on cosmological parameters.

The combination of gravitational waves as standard sirens and kilonovae offers a promising route to independently measure the Hubble constant. These multimessenger observations not only provide a direct measurement of cosmic distances but also enhance our understanding of the universe's expansion through the precise calibration of H_0 without reliance on traditional distance ladders. As the field of gravitational wave astronomy matures, standard sirens are poised to play a crucial role in resolving the Hubble tension and advancing our understanding of cosmology.

II.3.7. Gamma-Ray Attenuation

Gamma-ray attenuation through interaction with the extragalactic background light (EBL) provides a unique method to study the universe's expansion and to estimate cosmological parameters such as the Hubble constant (H_0) [152–154]. This subsection explores the principle behind gamma-ray attenuation, its theoretical framework, and its application in deriving cosmological parameters.

II.3.7.1. Theoretical Framework High-energy gamma-ray photons emitted by distant astrophysical sources such as blazars and gamma-ray bursts interact with the EBL—comprising photons mainly in the ultraviolet, optical, and infrared wavelengths—resulting in electron-positron pair production [154, 155]. This process attenuates the gamma-ray flux from these sources, and the extent of attenuation depends on the gamma-ray photon energy, the density of the EBL, and the distance the gamma rays have traveled, which is linked to the redshift of the source.

The optical depth τ for gamma rays traveling from a source at redshift z with observed energy E can be described by the equation:

$$\begin{aligned} \tau(E, z) = & \int_0^z \frac{dl}{dz'} dz' \int_{-1}^1 d\mu \frac{1-\mu}{2} \\ & \times \int_{\epsilon_{\text{th}}}^{\infty} d\epsilon n(\epsilon, z') \\ & \times \sigma_{\gamma\gamma}(E(1+z'), \epsilon, \mu) \end{aligned} \quad (2.47)$$

where:

- $\frac{dl}{dz'}$ is the cosmology-dependent line-of-sight element,
- $\mu = \cos \theta$, with θ being the interaction angle,
- ϵ is the energy of the EBL photon,
- ϵ_{th} is the threshold energy for pair production,
- $n(\epsilon, z')$ is the proper number density of EBL photons,
- $\sigma_{\gamma\gamma}$ is the pair production cross-section.

The pair production cross-section $\sigma_{\gamma\gamma}$ is given by:

$$\sigma_{\gamma\gamma}(\beta) = \frac{3\sigma_T}{16}(1 - \beta^2) \left[(3 - \beta^4) \ln \frac{1 + \beta}{1 - \beta} - 2\beta(2 - \beta^2) \right], \quad (2.48)$$

where σ_T is the Thomson cross-section and $\beta = \sqrt{1 - \frac{2m_e^2 c^4}{E\epsilon(1-\mu)}}$ is the velocity of the electron/positron in the center-of-mass frame.

The line-of-sight element is given by:

$$\frac{dl}{dz} = \frac{c}{H_0} \frac{1}{(1+z)\sqrt{\Omega_m(1+z)^3 + \Omega_\Lambda}}, \quad (2.49)$$

where c is the speed of light, H_0 is the Hubble constant, Ω_m is the matter density parameter, and Ω_Λ is the dark energy density parameter.

II.3.7.2. Cosmic Gamma-Ray Horizon (CGRH)

The cosmic gamma-ray horizon (CGRH) defines the energy at which the universe becomes opaque to gamma rays due to EBL attenuation ($\tau = 1$). By measuring the CGRH as a function of redshift, one can directly probe the EBL and thus indirectly measure the expansion rate of the universe. The CGRH is defined implicitly by:

$$\tau(E_{\text{CGRH}}, z) = 1, \quad (2.50)$$

where E_{CGRH} is the energy of the CGRH at redshift z .

II.3.7.3. Application to Cosmology Using improved EBL models from comprehensive galaxy surveys such as CANDELS [156] and gamma-ray attenuation data from telescopes like Fermi-LAT, recent studies [152–154] have derived new optical depths and used these to calculate the CGRH. This approach provides an one-step sound horizon free estimate for H_0 .

The methodology typically involves:

1. Constructing an EBL model based on galaxy survey data.
2. Calculating gamma-ray optical depths using Eq. (2.47).
3. Determining the CGRH from Eq. (2.50).
4. Fitting cosmological parameters to the observed CGRH.

Recent results from this method have yielded[153]:

$$H_0 = 62.4_{-3.9}^{+4.1} \text{ km s}^{-1} \text{ Mpc}^{-1} \quad (\Omega_m = 0.32 \text{ fixed}), \quad (2.51)$$

$$H_0 = 65.1_{-4.9}^{+6.0} \text{ km s}^{-1} \text{ Mpc}^{-1} \quad (\Omega_m = 0.19 \pm 0.08), \quad (2.52)$$

showcasing the utility of this method in cosmology.

II.3.7.4. Strengths and Limitations The gamma-ray attenuation method offers several advantages:

- Independence from traditional distance ladders.
- Probes the universe at high redshifts ($z \sim 1 - 5$).
- Sensitive to the EBL, providing insights into galaxy evolution.
- Offers a crucial cross-check in the era of precision cosmology.

However, it also faces challenges:

- Requires accurate modeling of the EBL.
- Sensitive to assumptions about blazar spectra and their evolution.
- Limited by the current statistics of high-energy gamma-ray observations.

II.3.7.5. Future Prospects The future of this method looks promising with:

- Upcoming gamma-ray telescopes like the Cherenkov Telescope Array (CTA) providing better statistics and higher energy reach.
- Improved EBL models from future galaxy surveys.
- Advancements in our understanding of blazar physics and evolution.

In conclusion, gamma-ray attenuation provides a powerful cosmological tool that leverages high-energy astrophysics to probe the fundamental parameters governing the universe's expansion. As our understanding of the EBL and gamma-ray sources improves, this method is poised to play an increasingly important role in resolving cosmological tensions and advancing our knowledge of the universe.

II.3.8. BAO Measurement of H_0 Independent of Sound Horizon Drag Scale

Baryon Acoustic Oscillations (BAO) have long served as a powerful standard ruler in cosmology. Traditionally, BAO measurements depend on the sound horizon scale at the drag epoch, r_d . However, recent developments have enabled measurements of the Hubble constant (H_0) using BAO data that are independent of r_d , offering new insights into cosmological parameters and potentially resolving tensions in modern cosmology [157–159].

II.3.8.1. Theoretical Framework The key to this approach lies in the BAO observable $\beta_{\perp}(z)$, which represents the ratio of the comoving angular diameter distance to the sound horizon scale:

$$\beta_{\perp}(z) = \frac{D_M(z)}{r_d}, \quad (2.53)$$

where $D_M(z)$ is the comoving angular diameter distance at redshift z . In a flat Λ CDM cosmology, neglecting radiation density at the redshifts of interest, $\beta_{\perp}(z)$ can be expressed as:

$$\beta_{\perp}(z) = \frac{c}{r_d H_0} \int_0^z \frac{dz'}{\sqrt{\Omega_m(1+z')^3 + 1 - \Omega_m}}, \quad (2.54)$$

where c is the speed of light, H_0 is the Hubble constant, and Ω_m is the matter density parameter.

II.3.8.2. Methodology The innovative aspect of this method involves several key steps:

1. Measure $\beta_{\perp}(z)$ at multiple redshifts.
2. Analyze the shape of $\beta_{\perp}(z)$ as a function of redshift.
3. Introduce a prior on $\Omega_m h^2$ from CMB measurements.

Measuring $\beta_{\perp}(z)$ at multiple redshifts allows us to constrain two key parameters: $r_d h$ and Ω_m . This is because the shape of $\beta_{\perp}(z)$ as a function of redshift depends on Ω_m , while its overall normalization is set by $r_d h$, where $h = H_0/(100 \text{ km s}^{-1} \text{ Mpc}^{-1})$.

However, there exists a degeneracy between r_d and h that cannot be broken by BAO measurements alone. To resolve this, an additional constraint is introduced: a prior on $\Omega_m h^2$ from CMB measurements. This prior is particularly useful because it's derived from the overall shape of the CMB power spectrum and is largely independent of assumptions about the sound horizon scale.

With these three pieces of information:

- $\beta_{\perp}(z)$ measurements at multiple redshifts (constraining $r_d h$ and Ω_m)
- The shape of $\beta_{\perp}(z)$ (further constraining Ω_m)
- A prior on $\Omega_m h^2$ from CMB data

There is now sufficient information to solve for three parameters: r_d , Ω_m , and h (or equivalently, H_0).

II.3.8.3. Mathematical Framework The method can be formalized as follows:

1. From BAO measurements, we obtain $\beta_{\perp}(z_i)$ at various redshifts z_i .
2. We fit these measurements to the theoretical model given by Eq. (2.54), which depends on $r_d h$ and Ω_m .

3. We incorporate the CMB prior on $\Omega_m h^2$, which we can write as:

$$\Omega_m h^2 = (\Omega_m h^2)_{\text{CMB}} \pm \sigma_{\Omega_m h^2}, \quad (2.55)$$

where $(\Omega_m h^2)_{\text{CMB}}$ is the central value from CMB measurements and $\sigma_{\Omega_m h^2}$ is its uncertainty.

4. We can then solve for h using:

$$h = \sqrt{\frac{(\Omega_m h^2)_{\text{CMB}}}{\Omega_m}}, \quad (2.56)$$

where Ω_m is determined from the fit to $\beta_{\perp}(z)$.

5. Finally, we can determine r_d using the best-fit value of $r_d h$ and the derived value of h .

II.3.8.4. Results and Implications Using data from the Dark Energy Spectroscopic Instrument (DESI) alongside Planck CMB measurements, this method yields [157]:

$$H_0 = 69.88 \pm 0.93 \text{ km s}^{-1} \text{ Mpc}^{-1}. \quad (2.57)$$

This result is particularly noteworthy as it falls between the lower values typically obtained from CMB analyses and the higher values from local distance ladder measurements, potentially offering a path towards resolving the Hubble tension.

II.3.8.5. Strengths and Limitations The strength of this approach lies in its ability to provide an H_0 estimate that is independent of sound horizon-based calibrations. Key advantages include:

- Independence from early-universe physics assumptions that affect r_d .
- Utilization of well-understood BAO physics.
- Combination of late-time (BAO) and early-time (CMB) information.

However, limitations and potential sources of systematic error should be considered:

- Dependence on the accuracy of BAO measurements across multiple redshifts.
- Reliance on the Λ CDM framework for the $\beta_{\perp}(z)$ model.
- Potential sensitivity to the CMB prior on $\Omega_m h^2$.

II.3.8.6. Future Prospects This methodology not only serves as a consistency check for Λ CDM but also opens up new avenues for understanding early universe physics and potentially resolving cosmological tensions. Future prospects include:

- Improved BAO measurements from upcoming surveys like DESI, Euclid, and the Vera C. Rubin Observatory.

- Refinement of CMB priors from future CMB experiments.
- Extension to models beyond Λ CDM to test for new physics.

In conclusion, this r_d -independent method for measuring H_0 using BAO data represents a significant advance in cosmological analysis. By decoupling the determination of H_0 from assumptions about the sound horizon scale, it provides a valuable new tool for probing both the early and late-time universe, potentially shedding light on the Hubble tension by providing a one step method for measuring H_0 that is independent of the sound horizon scale.

III. STATISTICAL ANALYSIS OF GROUPED H_0 MEASUREMENTS

In this section, we aim to construct a comprehensive compilation of the most available measurements of the Hubble constant (H_0) focusing mainly in the last 5 years. These measurements will be categorized into two distinct groups: those based on the distance ladder and those derived from one-step methods that are independent of the distance ladder. The primary goal is to analyze and compare the statistical properties of each group, focusing on the mean H_0 and its standard deviation. This comparison will help assess the consistency between the two groups and their alignment with the sound horizon-based measurement from the Planck 2018 data. By doing so, we aim to gain insights into the potential sources of the Hubble tension and explore whether discrepancies arise from systematic effects or fundamental differences in measurement techniques.

III.1. Presentation of measurements

In this subsection, we present a detailed overview of the H_0 measurements compiled into two categories: distance ladder-based measurements and one-step, distance ladder-independent measurements. We begin with the distance ladder-based measurements, which rely on multiple calibration steps to estimate cosmic distances.

III.1.1. Distance Ladder-Based Measurements

In this subsection we briefly describe the H_0 measurements of Table I based on distance ladder measurements used in the present analysis

1. Mira Calibrators [160]: In Ref. [160], Mira variables [90, 175] are utilized to calibrate the luminosity of Type Ia supernovae (SnIa) and subsequently measure the Hubble constant (H_0). The analysis involves a year-long observation of O-rich Miras in the galaxy NGC

1559, host to SN Ia 2005df, using the Hubble Space Telescope’s WFC3/IR. Mira variables, identifiable by their Period-Luminosity Relation (PLR) in the near-infrared, are calibrated using the geometric distance to NGC 4258, known from water megamaser measurements, and the Large Magellanic Cloud (LMC) via detached eclipsing binaries. The study reports a distance modulus for NGC 1559 of $\mu_{1559} = 31.41 \pm 0.05$ (statistical) ± 0.06 (systematic) mag, leading to an H_0 measurement of 73.3 ± 4.0 km s⁻¹ Mpc⁻¹ when combined with calibrations from the NGC 4258 megamaser and the LMC. This approach positions Miras not only as a complementary method to Cepheids for calibrating SnIa but also as a potential tool for resolving discrepancies in measurements of H_0 from the early and late Universe, contributing to ongoing discussions about the “Hubble tension.”

2. Tully Fisher + Cepheid + TRGB [161]: In the study by Kourkchi et al. (2020) [161], the Tully-Fisher relation, which correlates the rotational velocity of spiral galaxies with their luminosity, is finely calibrated using both Cepheid variables and the Tip of the Red Giant Branch (TRGB) as part of the Cosmicflows-4 project. This calibration effort is extensive, involving measurements across optical (SDSS u, g, r, i, z) and infrared (WISE W1 and W2) bands for a large sample of spiral galaxies. The study incorporates a subsample of approximately 600 spiral galaxies located in 20 galaxy clusters to refine the Tully-Fisher relation. The calibration process includes determining inclinations through an online graphical interface and utilizing new HI linewidth data primarily from the Arecibo Legacy Fast ALFA Survey. By integrating these calibrations, the study achieves a preliminary determination of the Hubble constant, $H_0 = 76.0 \pm 1.1$ (statistical) ± 2.3 (systematic) km/s/Mpc, offering a crucial stepping stone in resolving discrepancies in the measurement of the universe’s expansion rate. This comprehensive approach underscores the intricate multi-tier calibration necessary in the distance ladder methodology, aiming to reduce the scatter in the Tully-Fisher relation and hence improve the accuracy of distance measurements.

3. SBF + Cepheids + TRGB: In the study by Blakeslee et al. (2021) [162], the Surface Brightness Fluctuations (SBF) method is employed in conjunction with Cepheid variables and the Tip of the Red Giant Branch (TRGB) to calibrate and measure distances to galaxies. Specifically, the SBF technique, which utilizes the variance in brightness between different sections of a galaxy to infer its distance, is applied to infrared observations from the Hubble Space Telescope’s Wide Field Camera 3. This approach is complemented by calibrations using Cepheids and TRGB, which serve as standard candles. These calibrations are refined with the latest parallax data from Gaia EDR3 and direct geometric measurements from masers in galaxies like NGC 4258. Through this multifaceted calibration strategy, the study achieves a highly precise measurement of the Hubble constant, $H_0 = 73.3 \pm 0.7$ (statistical) ± 2.4 (sys-

Index	First Author (Year)	Measured H_0 (km/s/Mpc)	Method
1	Huang (2019) [160]	73.3 ± 4.0	Mira calibrators
2	Kourkchi (2020) [161]	76.0 ± 3.4	Tully Fisher + Cepheid + TRGB
3	Blakeslee (2021) [162]	73.3 ± 3.1	SBF + Cepheids + TRGB
4	Freedman (2021,24) [67, 111]	69.8 ± 2.3	TRGB calibrators
5	Riess (2021) [15]	73.04 ± 1.04	Cepheid (SH0ES)
6	Dhawan (2022) [163]	76.94 ± 6.4	TRGB calibrators
7	Dhawan (2022) [164]	74.82 ± 1.81	BayeSN + Cepheids
8	Dhawan (2022) [164]	70.92 ± 2.63	BayeSN + TRGB
9	Kenworthy (2022) [165]	73.1 ± 2.5	two rung distance ladder
10	Scolnic (2023) [166]	73.22 ± 2.06	TRGB calibrators (SH0ES)
11	Uddin (2023) [167]	71.76 ± 1.32	TRGB + Cepheids with SnIa and SBF (B band)
12	Uddin (2023) [167]	73.22 ± 1.45	TRGB + Cepheids with SnIa and SBF (H Band)
13	de Jaeger (2023) [168]	74.1 ± 8	SnII Weighted mean SCM
14	Huang (2023) [169]	72.37 ± 2.97	Mira calibrators
15	Chavez (2024) [170]	73.1 ± 2.3	$L - \sigma$ HII galaxies
16	Li (2024) [171, 172]	74.7 ± 3.1	JAGB calibrators with SnIa
17	Lee (2024) [95]	68.00 ± 2.7	JAGB calibrators with SnIa
18	Freedman (2024) [67]	72.05 ± 3.6	Cepheid calibrators with SnIa
19	Boubel (2024) [173]	73.3 ± 4.08	Tully Fisher + Cepheid + TRGB
19	Boubel (2024) [173]	73.3 ± 4.08	Tully Fisher + Cepheid + TRGB
20	Said (2024) [174]	76.05 ± 4.90	DESI FP relation + SBF

TABLE I: Distance ladder-dependent measurements of H_0 with corresponding first authors and methods.

tematic) km/s/Mpc. This value is consistent with other high-precision measurements using Cepheids and Type Ia supernovae, reinforcing the robustness of the combined SBF, Cepheid, and TRGB approach within the framework of the cosmic distance ladder.

4. TRGB Calibrators [67, 111] (see also 18.): In the study by Freedman et al. (2021), the Tip of the Red Giant Branch (TRGB) method is utilized to calibrate the Hubble constant (H_0) with a focus on reducing systematic uncertainties inherent in cosmic distance measurements. This paper consolidates various TRGB calibrations, which are demonstrated to be internally consistent at the 1% level, with additional verification from Gaia Early Data Release 3 (EDR3) providing a lower 5% accuracy level due to Gaia’s angular covariance bias. The TRGB-calibrated distance to a sample of Type Ia supernovae from the Carnegie Supernova Project yields an H_0 value of 69.8 ± 0.6 (stat) ± 1.6 (sys) km/s/Mpc. This value aligns closely with Cosmic Microwave Background (CMB) measurements under the standard Λ CDM model, suggesting no significant tension with early universe estimates, thereby indicating that the observed discrepancies in H_0 might stem from unrecognized systematic errors rather than new physics. This study underscores the efficacy of the TRGB method, noted for its straightforward underlying physics and minimal systematic susceptibilities, in refining the local measurement of H_0 .

5. Cepheid (SH0ES) [15]: In the comprehensive study by Riess et al. (2022), the SH0ES team employed Cepheid variables as primary distance calibrators within a refined distance ladder framework to determine the local value of the Hubble constant (H_0). Utilizing the Hubble Space Telescope (HST), they observed Cepheid variables in 42 Type Ia supernova (SN Ia) host galaxies, sig-

nificantly enhancing the sample size and thereby refining the precision of H_0 . These Cepheids were geometrically calibrated using parallaxes from Gaia EDR3, masers in NGC 4258, and detached eclipsing binaries in the Large Magellanic Cloud, ensuring uniform measurement across different systems to mitigate zeropoint errors. The resultant measurement from the Cepheid-SN Ia calibration yielded an H_0 value of 73.04 ± 1.04 km/s/Mpc, incorporating systematic uncertainties and demonstrating a significant tension with the Planck CMB observations under the Λ CDM model. This tension underscores potential discrepancies in cosmological models or the presence of unaccounted systematic errors in distance measurement techniques.

6. TRGB Calibrators [163]: In the study presented by Dhawan et al. (2022), a uniform distance ladder is constructed using Type Ia supernovae (SnIa) observed by the Zwicky Transient Facility (ZTF), with absolute calibration based on the Tip of the Red Giant Branch (TRGB) method. The TRGB calibration leverages the core helium flash luminosity of low-mass stars at the end of the Red Giant Branch, providing a standard candle that is less sensitive to environmental conditions compared to Cepheids. This method enables probing SN Ia host galaxies of all types within a volume-limited sample, thereby minimizing systematic errors related to host-galaxy bias. In their pilot study, Dhawan et al. apply this approach to SN 2021rhu in NGC 7814, using high-cadence ZTF observations and HST data for TRGB distance estimation. The TRGB-calibrated distance to NGC 7814 leads to an H_0 measurement of 76.94 ± 6.4 km/s/Mpc, reflecting significant potential for resolving the Hubble tension if the TRGB calibration can be applied across a broader sample of SnIa, supported by future JWST observations.

7-8. BayeSN + Cepheids or TRGB [164]: In the study by Dhawan et al. (2022), the Hubble constant (H_0) is estimated using a multi-faceted approach combining Bayesian analysis of Type Ia supernovae (SnIa) light curves across optical and near-infrared (NIR) spectrums with the BayeSN model, alongside distance calibrations based on Cepheid variables and the Tip of the Red Giant Branch (TRGB). This hierarchical Bayesian model, BayeSN, integrates data across a wide wavelength range to provide a continuous spectral energy distribution, enhancing the accuracy of distance measurements by utilizing the intrinsic properties of SnIa, which are less scattered in NIR. Two separate calibrations are employed: one using Cepheid distances to 37 host galaxies of 41 SnIa, yielding an estimated $H_0 = 74.82 \pm 0.97$ (stat) ± 0.84 (sys) km/s/Mpc, and another using TRGB distances to 15 host galaxies of 18 SnIa, resulting in $H_0 = 70.92 \pm 1.14$ (stat) ± 1.49 (sys) km/s/Mpc. These estimates underscore the sensitivity of H_0 measurements to the choice of distance ladder rung, with significant differences arising from the methodologies and inherent systematics of the Cepheid and TRGB calibrations. The analysis demonstrates the potential of combining optical and NIR data to refine local measurements of H_0 and thereby address the existing tension between local and early-universe estimates.

9. Kenworthy (2022) [165]: This analysis presents a measurement of the Hubble constant using a two-rung distance ladder consisting of Cepheid variables and redshifts of their host galaxies. The authors report $H_0 = 73.1^{+2.6}_{-2.3}$ km s⁻¹ Mpc⁻¹. The method employs 35 Cepheid host galaxies from the SH0ES team at $z \leq 0.011$, using their distances and redshifts to measure the Hubble flow. To mitigate the significant impact of peculiar velocities at these low redshifts, the analysis incorporates detailed modeling of the local velocity field using two independent reconstructions. The authors implement a hierarchical Bayesian model to account for selection effects, covariances in peculiar velocities, and systematic uncertainties in the Cepheid distances. Multiple analysis variants are considered to assess the impact of different assumptions about sample selection and peculiar velocity corrections. The final result is derived by combining four model variants, yielding a 3.5% precision measurement that is in 2.6σ tension with Planck. While not as precise as the full three-rung SH0ES ladder, this measurement provides an important cross-check that is independent of potential systematic uncertainties in Type Ia supernovae.

10. TRGB Calibrators (SH0ES)[166]: In this analysis, the Tip of the Red Giant Branch (TRGB) method is leveraged within the SH0ES project framework to refine the measurement of the Hubble constant (H_0). The TRGB, a luminous standard candle used for constructing distance ladders, is calibrated using an unsupervised algorithm, Comparative Analysis of TRGBs (CATs), which minimizes variance among multiple halo fields across various host galaxies without reliance on subjective adjustments. This study applies CATs to

an expanded sample of SN Ia hosts standardized to the geometric anchor NGC 4258, alongside the Pantheon+ SN Ia sample. By standardizing the apparent TRGB tips across different hosts using empirical correlations between TRGB measurements and contrast ratios, the study achieves a refined measurement of $H_0 = 73.22 \pm 2.06$ km/s/Mpc. This enhanced approach addresses discrepancies in earlier TRGB studies by incorporating systematic algorithmic adjustments that account for variations in the TRGB measurement process, thus contributing to a more consistent and accurate cosmological distance scale.

11-12. Uddin (2023) [167]: This analysis presents measurements of the Hubble constant using Type Ia supernovae (SnIa) from the Carnegie Supernova Project I and II, calibrated with three independent distance indicators: Cepheid variables, the tip of the red giant branch (TRGB), and surface brightness fluctuations (SBF). The authors report $H_0 = 71.76 \pm 0.58$ (stat) ± 1.19 (sys) km s⁻¹ Mpc⁻¹ from B-band data and $H_0 = 73.22 \pm 0.68$ (stat) ± 1.28 (sys) km s⁻¹ Mpc⁻¹ from H-band data. The analysis employs a Bayesian framework to fit a warped disk model to the SN Ia data, incorporating peculiar velocity corrections and marginalizing over nuisance parameters. Systematic uncertainties are derived by combining results from different calibrators. The methodology critically examines various sources of uncertainty, including sample selection effects, host galaxy properties, and the wavelength dependence of SN Ia standardization. While the precision is comparable to other recent H_0 measurements, the use of multiple calibrators provides insight into systematic differences between distance scales. The authors find that dust may not be the primary driver of the host-mass step in SN Ia luminosities, contrary to some previous studies.

13. SnII + Cepheids + TRGB [168]: In the study by de Jaeger and Galbany (2023) [168], Type II supernovae (SnII) are utilized as distance indicators. The paper employs both the Expanding Photosphere Method (EPM) and the Standard Candle Method (SCM) to derive distance estimates which are then used to calculate the Hubble constant (H_0).

The EPM is a geometric approach that calculates distances by measuring the physical expansion of the supernova's photosphere and comparing it to its apparent brightness, while SCM employs a correlation between the supernova's luminosity at the plateau phase and its photospheric velocity. The SCM method is calibrated using Cepheids and TRGB, providing a link to the cosmic distance ladder. From the EPM, Ref. [168] reports a range of H_0 values, with the latest measurements giving $H_0 = 84.70^{+2.28}_{-2.21}$ km/s/Mpc and $H_0 = 75.57^{+2.04}_{-1.89}$ km/s/Mpc. The SCM, highlighted for its empirical approach, shows values such as $H_0 = 75 \pm 7$ km/s/Mpc and $H_0 = 75.8^{+5.2}_{-4.9}$ km/s/Mpc among others over the years (Table 1.1 of Ref. [168]).

In our analysis, we utilize the weighted mean of the SCM method measurements from Table 1.1 of [168] Thus

we use 74.1 ± 8 . We use the average uncertainty of these measurements to account for their correlation.

14. *Mira Calibrators* [169]: In this analysis, Mira variables are employed to refine measurements of the Hubble constant (H_0), using a method that parallels the Cepheid distance ladder but incorporates Mira variables as an alternative or complementary standard candle. The analysis leverages a comprehensive dataset from the Hubble Space Telescope (HST), consisting of 11 epochs of F110W and 13 epochs of F160W observations, to identify and analyze 211 Mira variables within the galaxy M101. These variables, characterized by periods between 240 and 400 days, are used to establish a Period-Luminosity Relation (PLR), calibrated against geometric distances to the Large Magellanic Cloud (LMC) and the NGC 4258 galaxy, known for its water megamaser measurements. The calibration yields a distance modulus to M101 of $\mu_{M101} = 29.10 \pm 0.06$ mag, aligning closely with values derived from other methods like Cepheids and TRGB. Subsequently, utilizing the calibrated Mira variables and the peak luminosity of Type Ia Supernova SN 2011fe, the study calculates $H_0 = 72.37 \pm 2.97$ km s⁻¹ Mpc⁻¹, a precision of 4.1%. This result not only supports the consistency of Mira variables within the cosmic distance ladder but also corroborates the higher H_0 values observed in the local universe compared to those predicted from early universe measurements, contributing to the ongoing investigation into the "Hubble tension."

15. *L - σ HII Galaxies* [170]: In the study by Chávez et al. (2024), the $L - \sigma$ relation, which correlates the luminosity of Balmer lines with the velocity dispersion in HII galaxies, is employed as a cosmological distance indicator, extending to a redshift $z \approx 7.5$. This method capitalizes on the observation capabilities of the James Webb Space Telescope (JWST) to observe high-redshift HII galaxies, facilitating a comprehensive measurement of the Hubble constant (H_0) across a vast redshift range, covering 95% of the Universe's history. Utilizing a dataset of 231 HII galaxies and extragalactic HII regions, the study applies Bayesian inference to refine cosmological parameters, yielding results for a flat Universe as $h = 0.731 \pm 0.039$, $\Omega_m = 0.302_{-0.069}^{+0.12}$, and $w_0 = -1.01_{-0.29}^{+0.52}$ (statistical uncertainties). These parameters are pivotal for understanding the expansion history of the Universe and are derived from a method that complements traditional distance indicators such as Cepheid variables and Type Ia supernovae within the cosmic distance ladder framework. The calibration of the $L - \sigma$ relation is cross-checked against Cepheid and Type Ia supernova measurements to ensure accuracy and consistency, enhancing the reliability of this method as a robust cross-check against other distance indicators. This approach not only underscores the uniformity of photo-kinematic properties of HII regions across cosmic time but also enhances our understanding of cosmic expansion dynamics, contributing significantly to the ongoing precision cosmology efforts.

16. *JAGB Calibrators (SH0ES)*[171]: The recent analysis of Ref. [171] presents a study of JAGB stars using

JWST NIRCcam photometry in NGC 4258 and 4 hosts of 6 Type Ia supernovae (SN Ia): NGC 1448, NGC 1559, NGC 5584, and NGC 5643. Key findings include:

- JAGB clumps are readily apparent near $1.0 < F150W - F277W < 1.5$ and $m_{F150W} = 22 - 25$ mag
- Various methods for assigning an apparent reference magnitude were tested, including mode, median, sigma-clipped mean, and modeled luminosity function parameter
- Intra-host variations of up to ~ 0.2 mag were found, significantly exceeding statistical uncertainties
- The non-uniform shape of the JAGB luminosity function was observed, similar to that in the LMC and SMC
- Broad agreement was found with distances measured from Cepheids, tip of the red giant branch (TRGB), and Miras
- Different methods for estimating H_0 yielded a range of 71 - 78 km s⁻¹ Mpc⁻¹
- A fiducial result of $H_0 = 74.7 \pm 2.1(\text{stat}) \pm 2.3(\text{sys})$ km s⁻¹ Mpc⁻¹ was obtained

17. *JAGB Calibrators (Freedman)* [95]: While the recent analysis by Li et al. (2024) [171] provides useful insights into the JAGB method using JWST NIRCcam photometry, the more recent analysis by Lee et al. (2024) [95] presents a different approach and findings.

Lee et al. (2024) introduce a novel algorithm to identify the optimal location in a galaxy for applying the JAGB method, aiming to minimize crowding effects. This approach differs from Li et al. (2024), who examined intra-host variations across different regions of the galaxies.

- **Sample Size:** Lee et al. studied seven SN Ia host galaxies, while Li et al. examined NGC 4258 and 4 hosts of 6 SN Ia.
- **Filters:** Lee et al. primarily used F115W (J-band equivalent) and F356W, with F444W for some galaxies. Li et al. used F150W and F277W.
- **Analysis Approach:** Lee et al. employed a blind analysis, adding random offsets to the photometry that were only removed after finalizing the analysis. This blind approach was not mentioned in Li et al.'s study.

III.1.1.1. Photometry and Star Selection Both studies used DOLPHOT for photometry, but with some differences:

- Lee et al. used the warm-start mode in DOLPHOT, extracting photometry from F115W images first and then reducing LW images using the source list from the first run.
- Lee et al. applied specific quality-metric cuts (Table 1 in their paper) to remove non-stellar sources, prioritizing sample purity over completeness.
- Lee et al. calculated deprojected galactocentric radii for each source, using these to separate JAGB stars into 'inner' and 'outer' regions of each galaxy.

III.1.1.2. JAGB Identification and Measurement

The methods for identifying and measuring JAGB stars differ between the two studies:

- Li et al. identified JAGB clumps near $1.0 < F150W - F277W < 1.5$ and $m_{F150W} = 22 - 25$ mag.
- Lee et al. used F115W (J-band) for JAGB magnitude measurements, consistent with the theoretical basis of the JAGB method [74].
- Lee et al. focused on the outer regions of galaxies to minimize crowding and reddening effects, whereas Li et al. examined intra-host variations across different regions.

III.1.1.3. Results and H_0 Measurements The two studies arrived at different H_0 values:

$$H_0(\text{Lee et al.}) = 67.96 \pm 1.85(\text{stat}) \pm 1.90(\text{sys}) \text{ km s}^{-1} \text{ Mpc}^{-1} \quad (3.1)$$

$$H_0(\text{Li et al.}) = 74.7 \pm 2.1(\text{stat}) \pm 2.3(\text{sys}) \text{ km s}^{-1} \text{ Mpc}^{-1} \quad (3.2)$$

These results highlight a significant discrepancy, with Lee et al.'s measurement aligning more closely with CMB-based estimates, while Li et al.'s result is more consistent with Cepheid-based measurements.

18. Freedman (2024) [67] (used also in 4.): This analysis presents measurements of the Hubble constant using three independent methods applied to JWST observations of 10 nearby galaxies hosting Type Ia supernovae: the Tip of the Red Giant Branch (TRGB), J-region Asymptotic Giant Branch (JAGB) stars, and Cepheid variables. The authors find $H_0 = 69.85 \pm 1.75$ (stat) ± 1.54 (sys) $\text{ km s}^{-1} \text{ Mpc}^{-1}$ for TRGB, $H_0 = 67.96 \pm 1.85$ (stat) ± 1.90 (sys) $\text{ km s}^{-1} \text{ Mpc}^{-1}$ for JAGB, and $H_0 = 72.05 \pm 1.86$ (stat) ± 3.10 (sys) $\text{ km s}^{-1} \text{ Mpc}^{-1}$ for Cepheids. Combining these methods and tying to SnIa yields $H_0 = 69.96 \pm 1.05$ (stat) ± 1.12 (sys) $\text{ km s}^{-1} \text{ Mpc}^{-1}$. The analysis employs a consistent calibration using NGC 4258 for all three methods, allowing for a direct comparison. The TRGB and JAGB methods show excellent agreement, while the Cepheid distances

are systematically shorter. The authors critically assess various sources of uncertainty, including the small number of calibrating galaxies, and discuss the implications for the Hubble tension. They conclude that while their results are consistent with Λ CDM predictions, more data are needed to definitively resolve the tension. The study demonstrates the power of JWST for improving local distance measurements but also highlights remaining challenges in achieving 1

19. Boubel (2024) [173]: This analysis presents an improved method for measuring the Hubble constant (H_0) using the Tully-Fisher relation and a peculiar velocity model. The authors apply their technique to the Cosmicflows-4 catalog, simultaneously fitting the Tully-Fisher relation and peculiar velocity field for the full sample. They calibrate the zero-point using galaxies with independent distance measurements from Cepheids, TRGB, and SnIa. For the i -band sample, they find $H_0 = 73.3 \pm 2.1$ (stat) ± 3.5 (sys) $\text{ km s}^{-1} \text{ Mpc}^{-1}$, while the $W1$ -band yields $H_0 = 74.5 \pm 1.2$ (stat) ± 2.6 (sys) $\text{ km s}^{-1} \text{ Mpc}^{-1}$. The method improves upon previous approaches by using the entire dataset to fit the Tully-Fisher relation, incorporating a comprehensive model with curvature and varying intrinsic scatter, and accounting for selection effects and Malmquist bias. However, the authors note that the precision is currently limited by systematic uncertainties in the absolute distance calibrations and the small number of galaxies with such calibrations. They critically assess various sources of uncertainty, including the choice of calibrators, peculiar velocity modeling, and galaxy inclination measurements. While the method shows promise for future large surveys, its full potential awaits resolution of ongoing debates regarding absolute distance scales.

20. Said et al. (2024) [174]: This analysis employed the Fundamental Plane (FP) relation for early-type galaxies in combination with Surface Brightness Fluctuation (SBF) measurements to estimate the Hubble constant. The study utilized data from the Dark Energy Spectroscopic Instrument (DESI) Peculiar Velocity Survey, focusing on a sample of early-type galaxies. The FP relation, which correlates the effective radius, velocity dispersion, and surface brightness of elliptical galaxies, was calibrated using SBF distances to nearby galaxies, particularly the Coma cluster. This approach yielded $H_0 = 76.05 \pm 4.90 \text{ km s}^{-1} \text{ Mpc}^{-1}$. It's important to note that this method is dependent on the cosmic distance ladder and requires local calibration. The reliance on local calibrators, such as SBF measurements of the Coma cluster, means that the resulting H_0 value is sensitive to potential systematic errors in these calibrations. This dependence on local distance indicators places this measurement in the category of distance ladder dependent H_0 determinations, which often yield higher values compared to measurements that are independent of the distance ladder.

III.1.2. One Step Distance Ladder-Independent Measurements

In this subsection we briefly describe the H_0 measurements of Table II based on one step methods, independent of both distance ladder and sound horizon scale used in the present analysis

1. Reese (2003) [124]: This analysis presents a measurement of the Hubble constant H_0 using the Sunyaev-Zel'dovich effect (SZE) combined with X-ray observations of galaxy clusters. The author reports $H_0 \approx 61 \pm 3 \pm 18 \text{ km s}^{-1} \text{ Mpc}^{-1}$ for an $\Omega_m = 0.3$, $\Omega_\Lambda = 0.7$ cosmology, where the uncertainties are statistical and systematic at 68% confidence. The method exploits the different density dependences of the SZE and X-ray emission to determine angular diameter distances to clusters, independent of the cosmic distance ladder. The analysis combines 41 distance determinations to 26 galaxy clusters, using ROSAT X-ray data and modeling clusters as spherical isothermal β models. The author critically discusses systematic uncertainties, including cluster structure, gas clumping, and potential SZE contaminants, which dominate the error budget. While the precision is limited by systematics, the technique's ability to measure distances at high redshifts makes it a promising tool for constraining cosmological parameters. The author notes that improved X-ray observations and larger cluster samples could significantly reduce uncertainties in the future.

2. Kuo 2013 [176]: This analysis utilized the water megamaser technique to measure the angular diameter distance to NGC 6264, a galaxy located at approximately 140 Mpc. This study is notable for being one of the first to apply the megamaser method to a galaxy well into the Hubble flow, where peculiar velocities have a reduced impact on distance measurements. The authors used Very Long Baseline Interferometry (VLBI) observations to map the spatial and velocity distribution of masers in the circumnuclear disk, combined with single-dish monitoring to measure accelerations. By modeling the three-dimensional structure of the maser disk, they derived a Hubble constant of $H_0 = 68 \pm 9 \text{ km s}^{-1} \text{ Mpc}^{-1}$. This result is in tension with a later study by Pesce et al. (2020), which found $H_0 = 73.9 \pm 3.0 \text{ km s}^{-1} \text{ Mpc}^{-1}$ using a larger sample of megamasers. However, the Pesce et al. sample included galaxies at smaller distances, ranging from about 8.5 to 140 Mpc ($z \approx 0.002 - 0.034$), potentially making it more susceptible to biases from peculiar velocities. While the Kuo et al. measurement has larger uncertainties due to the challenges of observing more distant masers, it benefits from reduced systematic errors associated with local flows, making it an important independent check on H_0 measurements derived from nearer galaxies.

3. Gao (2015) [127]: This analysis presents a measurement of the Hubble constant using water maser observations in the megamaser galaxy NGC 5765b. The authors report $H_0 = 66.0 \pm 6.0 \text{ km s}^{-1} \text{ Mpc}^{-1}$. The method,

part of the Megamaser Cosmology Project, employs very long baseline interferometry (VLBI) to map the spatial distribution of masers and single-dish monitoring to measure their accelerations. These data are combined in a Bayesian framework to fit a warped disk model, simultaneously constraining H_0 , the black hole mass, and disk geometry. The analysis uses a Markov chain Monte Carlo approach with multiple strands to explore parameter space. Systematic uncertainties, including acceleration measurement methods and unmodeled spiral structure, are carefully considered. The precision achieved (9.1%) is limited by the acceleration measurements of systemic masers. While not yet competitive with other H_0 probes, this geometric method is independent of the cosmic distance ladder and early universe physics. The authors critically discuss the requirements for good distance measurements using this technique and compare their results to previous megamaser analyses. This work demonstrates the potential of megamaser observations to provide independent constraints on H_0 , which could help resolve the current tension between early and late universe measurements.

4. Millon (2019) and 19. Shajib (2023)[131, 185]: Millon et al. (2019) [131] utilized time-delay cosmography in strong gravitational lensing systems to measure $H_0 = 74.2 \pm 1.6 \text{ km s}^{-1} \text{ Mpc}^{-1}$. By observing the time delays between multiple images of background quasars lensed by foreground galaxies, and modeling the mass distribution of the lensing galaxies, they provided a measurement independent of the sound horizon scale used in CMB observations. However, subsequent analysis has revealed that this measurement was potentially affected by significant systematic uncertainties.

As highlighted by a subsequent analysis of the same collaboration (TDCOSMO) Shajib *et al.* [185], the analysis by Millon *et al.* [131] relied on simple parametric assumptions about the mass profiles of the lensing galaxies, which could potentially bias the H_0 measurement or underestimate the errors. The key systematic issue lies in the mass-sheet degeneracy (MSD), which allows for multiple mass distributions to produce the same lensing observables, leading to a degeneracy in the inferred H_0 value.

To address these systematics, Shajib *et al.* [185] performed a new analysis using spatially resolved stellar kinematics of the lens galaxy RXJ1131–1231, obtained from Keck Cosmic Web Imager spectroscopy. This approach allows for a more flexible mass model that effectively breaks the MSD without relying on specific assumptions about the mass profile. By combining this new kinematic data with previously published time delay and lens models derived from Hubble Space Telescope imaging, they were able to robustly estimate H_0 while accounting for all uncertainties, including those related to the MSD.

The result of this improved analysis yields $H_0 = 77.1^{+7.3}_{-7.1} \text{ km s}^{-1} \text{ Mpc}^{-1}$ for a flat Λ CDM cosmology. While this new measurement has a larger uncertainty

Index	First Author (Year)	Measured H_0 (km/s/Mpc)	Method
1	Reese (2003) [124]	61 ± 18	SZ Effect
2	Kuo (2013) [176]	68 ± 9	Megamasers (MCP)
3	Gao (2015) [127]	66.0 ± 6.0	Megamasers (MCP)
4	Millon (2019) [131]	74.2 ± 1.6	Lensing TD TDCOSMO I.
5	Pesce (2020) [126]	73.9 ± 3.0	Megamasers (MCP+SH0ES)
6	Birrer (2020) [130]	67.4 ± 4	Lensing TD TDCOSMO + SLACS
7	Abbott (2021) [151]	68.0_{-6}^{+8}	47 GW sources from GWTC-3
8	Wu (2021) [177]	$64.67_{-4.66}^{+5.62}$	Fast Radio Bursts
9	Philcox (2022) [137]	64.8 ± 2.4	T_{eq} standard ruler
10	Zhang (2022) [178]	65.9 ± 3.0	Cosmic Chronometers + HII galaxies
11	Bulla (2022) [149]	69.6 ± 5.5	Gravitational Waves + Kilonovae
12	Moresco (2023) [140]	66.7 ± 5.3	Cosmic Chronometers
13	Liu (2023) [179]	$72.9_{-2.3}^{+2.0}$	Strong lensing + SnIa
14	Du (2023) [135]	$71.5_{-3.0}^{+4.4}$	Time-delay galaxy lenses + GRBs
15	Favale (2023) [180]	71.5 ± 3.1	Pantheon+ calibrated by Cosmic Chronometers
16	DESI (2023) [181]	$85.4_{-33.9}^{+29.1}$	Dark siren (GW190412 & DESI)
17	Palmese (2023) [182]	$75.46_{-5.39}^{+5.34}$	Standard Siren GW170817 + afterglow
18	Dominguez (2023) [153]	62.4 ± 4.0	Gamma ray attenuation
19	Sneppen (2023) [183]	67.0 ± 3.6	EPM + Kilonovae
20	Liu (2023) [184]	$59.1_{-3.5}^{+3.6}$	Cluster Lensed Quasar
21	TDCOSMO (2023) [185]	$77.1_{-7.1}^{+7.3}$	Lensing time delay + stellar kinematics
22	Kelly (2023) [186]	66.6 ± 3.8	Lensing TD SN Refsdal
23	Gao (2023) [187]	$65.5_{-5.4}^{+6.4}$	Fast Radio Bursts + SnIa
24	Alfradique (2023) [188]	$68.84_{-7.7}^{+15.5}$	2 new dark sirens (LIGO/Virgo/Delve)
25	Colaco (2023) [189]	67.22 ± 6.07	SZ + X-ray calibrated SnIa
26	Pogosian (2024) [157]	69.88 ± 0.93	BAO-DESI data (No Sound Horizon)
27	Pogosian (2024) [157]	67.37 ± 0.96	BAO-pre DESI data (No Sound Horizon)
28	Liu (2024) [190]	$70.0_{-4.9}^{+4.7}$	Cluster-lensed supernova (SN Refsdal)
29	Bom (2024) [191]	$69.9_{-12.0}^{+13.3}$	Gravitational Waves + Kilonovae
30	TDCOSMO (2024) [136]	65_{-14}^{+23}	Time-delay cosmography (WGD 2038-4008)
31	Grillo (2024) [192]	65.1 ± 3.5	Lensing TD HFF
32	Pascale (2024) [193]	$71.8_{-7.6}^{+9.8}$	Lensed SnIa (JWST)
33	Li (2024) [194]	$66.3_{-3.6}^{+3.8}$	Lensed SnIa Refsdal

TABLE II: Measurements of H_0 independent of the distance ladder and the sound horizon scale with corresponding first authors and methods.

than the previous result from Millon *et al.* [131], it represents a more robust estimate that accounts for the potential systematics introduced by simplified mass profile assumptions. This study demonstrates the importance of incorporating spatially resolved kinematics in time-delay cosmography to mitigate systematic uncertainties and provide a more reliable measurement of the Hubble constant.

5. Pesce (2020) [126]: Pesce et al. (2020) used data from the Megamaser Cosmology Project to derive a new constraint on the Hubble constant of $H_0 = 73.9 \pm 3.0$ km s⁻¹ Mpc⁻¹. This measurement is independent of distance ladders and the cosmic microwave background. The study combined updated distance measurements for six megamaser-hosting galaxies: UGC 3789, NGC 6264, NGC 6323, NGC 5765b, CGCG 074-064, and NGC 4258.

The authors applied an improved approach for fitting maser data, which incorporated “error floor” systematic uncertainties as model parameters. This allowed for marginalization over a previous source of systematic uncertainty and resulted in better distance estimates for four galaxies previously published by the project.

Assuming a fixed velocity uncertainty of 250 km s⁻¹ associated with peculiar motions, they derived their best H_0 value using only maser-based distance and velocity measurements, without any peculiar velocity corrections. Different approaches for correcting peculiar velocities did not modify H_0 by more than $\pm 1\sigma$, with the full range of best-fit Hubble constant values spanning 71.8–76.9 km s⁻¹ Mpc⁻¹. This study corroborates prior indications that the local value of H_0 exceeds the early-Universe value derived from cosmic microwave background measurements. The confidence level for this discrepancy varies from 95–99% for different treatments of the peculiar velocities.

6. Birrer (2020) [130]: In the continuation of leveraging strong lensing systems, Birrer et al. combined the TDCOSMO data set with additional constraints from the SLACS survey, leading to a measurement of $H_0 = 67.4 \pm 4$ km/s/Mpc. This work illustrates how adding external data on the lens galaxy’s environment and structure, specifically through extended stellar kinematics, can influence the mass profile estimation and thus the derived value of the Hubble constant.

7. Abbott (2021) [151]: This analysis presents a comprehensive measurement of the Hubble constant (H_0) using gravitational wave (GW) events from GWTC-3. The study employs two main approaches: a hierarchical inference method that jointly estimates cosmological parameters and black hole population properties, and a statistical galaxy catalog method using GLADE+ for redshift information. The hierarchical method, using 42 binary black hole events, yields $H_0 = 68_{-8}^{+12}$ km s⁻¹ Mpc⁻¹ when combined with GW170817. The galaxy catalog method, incorporating 47 GW events and assuming a fixed black hole population model, results in $H_0 = 68_{-6}^{+8}$ km s⁻¹ Mpc⁻¹. Both approaches show improvement over previous analyses, with the galaxy catalog method achieving a 42% improvement compared to GWTC-1 results. However, the authors critically note that the results are dominated by population model assumptions, particularly the mass distribution of black holes. The study highlights the importance of the excess of black holes around $35 M_\odot$ in constraining H_0 , but also emphasizes the potential systematic uncertainties introduced by these assumptions. The analysis demonstrates the growing precision of GW cosmology while underscoring the need for careful consideration of population models and systematic effects in future measurements.

8. Wu et al. (2021) [177]: This analysis employed a novel method using Fast Radio Bursts (FRBs) to measure the Hubble constant, independent of the cosmic distance ladder. This approach leverages the dispersion measure (DM) of FRBs, which is related to the electron column density along the line of sight and thus serves as a proxy for cosmological distance. The authors used a sample of 18 localized FRBs with known redshifts and carefully modeled the contributions to the DM from the Milky Way, host galaxies, and the intergalactic medium (IGM). By using the DM-redshift relation and accounting for the probability distributions of various DM components, they derived $H_0 = 64.67_{-4.66}^{+5.62}$ km s⁻¹ Mpc⁻¹. This method is particularly noteworthy as it requires no local distance calibrators and is independent of the cosmic distance ladder, potentially offering a new probe to address the Hubble tension. The authors also demonstrated that with a future sample of 100 localized FRBs, the precision of H_0 measurement could reach $\sim 2.6\%$, making FRBs a promising tool for cosmology.

9. Philcox (2022) [137]: Philcox et al. introduced a novel approach by using the T_{eq} standard ruler, independent of the sound horizon scale, deriving $H_0 = 64.8 \pm 2.4$ km/s/Mpc. This method utilizes the horizon scale at matter-radiation equality, offering a different sensitivity to early-universe physics compared to traditional r_s -based measurements, potentially providing insights into discrepancies observed in H_0 values from early and late universe observations.

10. Zhang (2022) [178]: Zhang and colleagues employed cosmic chronometers and HII galaxies, calibrated through a non-parametric Artificial Neural Network, to measure $H_0 = 65.9 \pm 3.0$ km/s/Mpc. This method lever-

ages the $L-\sigma$ relation of HII galaxies, combined with aging of cosmic chronometers, to offer an independent and model-agnostic approach to determining the Hubble constant, contributing to resolving the Hubble tension.

11. Bulla (2022) [149]: Utilizing multi-messenger observations from gravitational waves, gamma-ray bursts, and kilonovae associated with neutron star mergers, Bulla et al. reported $H_0 = 69.6 \pm 5.5$ km/s/Mpc (weighted mean of the measurements shown in Table 1 of [149] using a typical uncertainty from the Table). This technique harnesses data from different astrophysical events linked by the same originating source, providing a unique way to measure cosmic distances and H_0 without relying on traditional cosmic ladders.

12. Moresco (2023) [140]: Moresco utilized cosmic chronometers to measure H_0 , obtaining a value of 66.7 ± 5.3 km/s/Mpc. This method calculates the Hubble constant by directly determining the age difference between cosmic chronometers at different redshifts, thereby estimating the expansion rate of the Universe independently of traditional distance ladders. This approach provides a unique perspective by focusing on the change in the Universe's age over time to infer H_0 .

13. Liu (2023) [179]: This analysis presents a cosmological model-independent measurement of the Hubble constant H_0 using strong gravitational lensing time delays combined with Type Ia supernova data. The authors utilize four lensed quasar systems from the H0LiCOW collaboration, which provide time-delay distances and lens angular diameter distances. To avoid assuming a specific cosmological model, they reconstruct the distance-redshift relation from the Pantheon SN Ia sample using Gaussian process regression. By combining these unanchored distances with the lensing data, they simultaneously constrain H_0 and the post-Newtonian parameter γ_{PPN} . Their main result is $H_0 = 72.9_{-2.3}^{+2.0}$ km s⁻¹ Mpc⁻¹. The method is robust as it does not rely on a parametric cosmological model, potentially reducing biases. However, it still assumes spatial flatness and depends on the chosen mean function for the Gaussian process. The precision is comparable to model-dependent analyses, demonstrating the power of combining lensing time delays with standardizable candles to measure H_0 independently of the cosmic distance ladder or early universe physics.

14. Du (2023) [135]: This analysis presents a model-independent determination of the Hubble constant H_0 and spatial curvature $\Omega_{K,0}$ using time-delay galaxy lenses (TDGLs) combined with gamma-ray burst (GRB) distances. The authors employ the distance sum rule, assuming only the validity of the FLRW metric and geometrical optics. They use 7 TDGLs from H0LiCOW and STRIDES collaborations, along with 193 GRBs calibrated via the Amati relation. The method parameterizes distances using a fourth-order cosmographic expansion in y -redshift, including curvature. Combining TDGLs and GRBs yields $H_0 = 71.5_{-3.0}^{+4.4}$ km s⁻¹ Mpc⁻¹ and $\Omega_{K,0} = -0.07_{-0.06}^{+0.13}$. Assuming a flat universe im-

proves the constraint to $H_0 = 70.9^{+4.2}_{-2.9}$ km s⁻¹ Mpc⁻¹. The analysis is performed in a Bayesian framework using dynamic nested sampling. While the precision is not yet competitive with other probes, this method provides a novel, independent constraint on both H_0 and $\Omega_{K,0}$. The authors critically discuss potential systematic effects, including GRB standardization and the limited number of low-redshift GRBs. They also explore future prospects using simulated GRB samples, demonstrating potential for significant improvement in precision.

15. Favale (2023) [180]: This analysis employs cosmic chronometers (CCH), Type Ia supernovae (SNIa) from the Pantheon+ compilation, and baryon acoustic oscillation (BAO) data to perform a model-independent calibration of the cosmic distance ladder and measurement of the Hubble constant H_0 . The authors use Gaussian Process regression to reconstruct $H(z)$ from CCH data and $m(z)$ from SNIa data. They then combine these reconstructions with BAO data to jointly constrain the absolute magnitude of SNIa M , the sound horizon scale r_d , and the curvature parameter Ω_k . Using CCH+SNIa+BAO data (excluding SNIa in SH0ES host galaxies), they obtain $H_0 = 71.5 \pm 3.1$ km s⁻¹ Mpc⁻¹. The method is largely independent of early universe physics and the first rungs of the cosmic distance ladder, providing a valuable cross-check on more model-dependent approaches. However, the precision is still limited compared to other methods, and the result falls between the values preferred by Planck and SH0ES, unable to definitively resolve the Hubble tension. The authors also explore the impact of potentially overestimated CCH uncertainties and the inclusion of SH0ES host galaxy SNIa, demonstrating the robustness of their approach while highlighting areas for future improvement as more precise data become available.

16. DESI (2023) [181]: This analysis presents a measurement of the Hubble constant H_0 using the gravitational wave event GW190412 as a dark standard siren, combined with galaxy data from the Dark Energy Spectroscopic Instrument (DESI). The authors employ the statistical standard siren method, marginalizing over potential host galaxies from DESI's Bright Galaxy Sample. They find $H_0 = 85.4^{+29.1}_{-33.9}$ km s⁻¹ Mpc⁻¹ for GW190412 alone, and $H_0 = 77.96^{+18.4}_{-9.48}$ km s⁻¹ Mpc⁻¹ when combined with the bright siren GW170817. The analysis uses a flat Λ CDM cosmology with $\Omega_m = 0.3$ and a uniform prior on H_0 between 20 and 140 km s⁻¹ Mpc⁻¹. The method critically relies on the completeness and accuracy of the DESI spectroscopic sample, which offers significant improvements over previous photometric catalogs. The authors explore the impact of various large-scale structure weights and different data releases. While the precision is not yet competitive with other probes, this work demonstrates the potential of combining well-localized gravitational wave events with deep spectroscopic surveys. The multi-peaked posterior reflects redshift overdensities in the GW localization volume, highlighting the importance of accurate redshift information in dark siren

analyses.

17. Palmese (2023) [182]: This analysis presents an updated measurement of the Hubble constant H_0 using GW170817 and the latest observations of its electromagnetic counterpart afterglow. The authors employ a Bayesian framework that combines gravitational wave data, afterglow observations spanning 3.5 years across multiple wavelengths, and a careful treatment of the host galaxy's peculiar velocity. They use the JetFit package to constrain the viewing angle from afterglow data, which helps break the distance-inclination degeneracy in the GW data. The analysis yields $H_0 = 75.46^{+5.34}_{-5.39}$ km s⁻¹ Mpc⁻¹ (68% credible interval), a 7% precision measurement that improves significantly upon the original 14% precision from the first standard siren measurement. The authors critically examine various assumptions in their modeling, particularly the impact of the bulk Lorentz factor prior on the viewing angle and H_0 estimates. While the result is consistent within 1σ of the Cepheid-anchored supernova measurements and within 1.5σ of CMB measurements, the precision is not yet sufficient to resolve the Hubble tension. The study demonstrates the potential of long-term, multi-wavelength afterglow observations in improving standard siren measurements, but also highlights the need for careful consideration of modeling assumptions in future high-precision cosmological studies using this method.

18. Dominguez (2023) [153]: This analysis presents a measurement of the Hubble constant H_0 using γ -ray attenuation data combined with an extragalactic background light (EBL) model derived from galaxy observations. The authors obtain $H_0 = 65.1^{+6.0}_{-4.9}$ km s⁻¹ Mpc⁻¹ when simultaneously fitting H_0 and Ω_m , and $H_0 = 62.4^{+4.1}_{-3.9}$ km s⁻¹ Mpc⁻¹ when fixing $\Omega_m = 0.32$. The method uses optical depth measurements from Fermi-LAT and Imaging Atmospheric Cherenkov Telescopes, combined with an EBL model based on deep multiwavelength galaxy data from CANDELS. The analysis accounts for cosmological dependence in both the EBL model and the line-of-sight integral for optical depth. Uncertainties in the EBL model are propagated through Monte Carlo realizations. The results are consistent with Planck CMB measurements but in tension with local distance ladder measurements. The authors critically discuss potential systematic effects, including discrepancies between EBL models and γ -ray data at high redshifts, and explore the impact of restricting the analysis to low-redshift data. While the method provides an independent probe of H_0 , current uncertainties are too large to definitively resolve the Hubble tension.

19. Sneppen (2023) [183]: This analysis presents a measurement of the Hubble constant H_0 using the expanding photosphere method (EPM) applied to the kilonova AT2017gfo. The authors analyze early VLT/X-shooter spectra, modeling the continuum as a blackbody and the Sr II lines as P Cygni profiles. They find $H_0 = 67.0 \pm 3.6$ km s⁻¹ Mpc⁻¹ by combining constraints from the first two epochs. The method exploits the well-

defined explosion time from gravitational wave detection, the apparent sphericity of the ejecta, and the negligible electron scattering opacity in kilonova atmospheres. The dominant uncertainty comes from the host galaxy peculiar velocity, while systematic uncertainties related to dust extinction, flux calibration, and ejecta geometry contribute at the 1-2% level each. The authors critically examine potential systematics, including line blending, reverberation effects, and relativistic corrections. While demonstrating the potential of the method, they caution that their simple framework does not account for full 3D radiative transfer effects, and the result should be considered preliminary. They forecast that 5-10 similar events could constrain H_0 to 1% precision, potentially helping to resolve the Hubble tension.

20. Liu (2023) [184]: This analysis explores the measurement of the Hubble constant H_0 using time-delay cosmography with the cluster-lensed quasar system SDSS J1004+4112. The authors employ 16 different lens mass models to investigate the dependence of H_0 on model assumptions. By combining posteriors from all models with equal weighting, they obtain $H_0 = 67.5_{-8.9}^{+14.5}$ km s⁻¹ Mpc⁻¹. The study critically examines the impact of various modeling choices, including dark matter halo profiles, treatment of the brightest cluster galaxy, and multiple perturbations. They find that H_0 values decrease as model complexity increases, and that different halo profiles yield significantly different results. The authors also explore weighting schemes and additional constraints to improve the measurement. By selecting two models that best reproduce observed shapes of lensed galaxies, they obtain a tighter constraint of $H_0 = 59.1_{-3.5}^{+3.6}$ km s⁻¹ Mpc⁻¹. However, they caution that their analysis does not fully explore all possible mass model uncertainties. The study highlights the importance of including extended arc information in cluster lens modeling for obtaining accurate H_0 constraints, while also emphasizing the challenges in rigorously incorporating such information due to small-scale matter distributions affecting image positions.

21. TDCOSMO (2023) [185]: (see 3. above)

22. Kelly (2023) [186]: Kelly et al. employed time-delay strong lensing, specifically focusing on SN Refsdal, to measure $H_0 = 66.6 \pm 3.8$ km/s/Mpc. This method utilizes the time delays between multiple observed images of a single supernova event caused by gravitational lensing. The precision of the measurement benefits from the unique opportunity provided by observing multiple light curves of the same supernova, allowing for a detailed modeling of the lensing mass distribution and the overall geometry of the system.

23. Gao (2023) [187]: This analysis employs a cosmographic approach to measure the Hubble constant H_0 using Fast Radio Bursts (FRBs) and Type Ia supernovae (SnIa). The authors derive a Taylor expansion for the mean intergalactic medium dispersion measure ($\langle DM_{\text{IGM}}(z) \rangle$) of FRBs and combine it with uncalibrated SnIa data from the Pantheon sample to constrain cosmo-

graphic parameters. Using 18 localized FRBs and assuming a constant baryon fraction in the IGM, they obtain $H_0 = 65.5_{-5.4}^{+6.4}$ km s⁻¹ Mpc⁻¹ (68% C.L.). The method is largely independent of cosmological models but relies on assumptions about the IGM baryon fraction and FRB host galaxy properties. The authors critically examine the impact of these assumptions and parameter degeneracies on their results. They find that allowing for redshift evolution in the IGM baryon fraction shifts the H_0 estimate to $69.0_{-5.7}^{+6.7}$ km s⁻¹ Mpc⁻¹. While the precision is lower than some other recent FRB-based measurements, this approach provides a useful cross-check that is less dependent on early-universe physics. The authors also present forecasts suggesting that ~ 100 localized FRBs could improve the H_0 precision to $\sim 4.6\%$.

24. Alfradique (2023) [188]: This analysis presents a measurement of the Hubble constant H_0 using the dark siren method with two new gravitational wave (GW) events, GW190924-021846 and GW200202-154313, combined with previous results. The authors employ the DECam Local Volume Exploration Survey (DELVE) galaxy catalog to obtain photometric redshifts of potential host galaxies using a Mixture Density Network approach. They implement a Bayesian framework that marginalizes over possible host galaxies and incorporates photometric redshift uncertainties. The combination of these two new events with the bright siren GW170817 yields $H_0 = 68.84_{-7.74}^{+15.51}$ km s⁻¹ Mpc⁻¹, improving the precision by 7% compared to GW170817 alone. When combined with 8 previously analyzed dark sirens, they obtain $H_0 = 76.00_{-13.45}^{+17.64}$ km s⁻¹ Mpc⁻¹. The analysis critically examines the impact of photometric redshift bias and the use of full redshift probability distributions. While the precision is lower than some recent studies using larger GW samples, this approach is less sensitive to assumptions about the black hole mass distribution and demonstrates the potential of well-localized dark sirens for cosmological measurements. The authors note that future analyses will need to address additional systematic effects as the precision improves.

25. Colaco (2023) [189]: This analysis presents a measurement of the Hubble constant H_0 using a combination of galaxy cluster angular diameter distances and type Ia supernovae (SnIa) luminosity distances. The method employs a model-independent approach based on the cosmic distance duality relation, requiring only geometrical distances. The authors use 25 galaxy cluster measurements from De Filippis et al. (2005), modeled with an elliptical β -model, and the Pantheon SnIa sample. A Gaussian Process regression is applied to reconstruct the SnIa distance-redshift relation at galaxy cluster redshifts. The analysis yields $H_0 = 67.2 \pm 6.1$ km s⁻¹ Mpc⁻¹ (68% confidence level), with an uncertainty of about 9%. This result is consistent with both Planck CMB and local distance ladder measurements, though it does not resolve the Hubble tension. The authors critically discuss the impact of cluster modeling assumptions and combine statistical and systematic errors in quadrature. While the precision is

limited by current galaxy cluster measurements, this approach provides a promising avenue for future constraints as cluster data improve, offering an independent probe of H_0 that avoids potential biases from local distance calibration or specific cosmological model assumptions.

26-27. Pogosian (2024) [157]: This analysis presents a cosmological-model-independent measurement of the Hubble constant H_0 using the DESI Year 1 BAO data combined with the CMB acoustic scale θ_* and a Planck Λ CDM prior on $\Omega_m h^2$. The authors treat the sound horizon at baryon decoupling r_d as a free parameter, avoiding assumptions about recombination physics. Using CosmoMC, they find $H_0 = 69.88 \pm 0.93 \text{ km s}^{-1} \text{ Mpc}^{-1}$, which is $\sim 2\sigma$ higher than the Planck Λ CDM value. For comparison, they perform the same analysis with pre-DESI BAO data, obtaining $H_0 = 67.37 \pm 0.96 \text{ km s}^{-1} \text{ Mpc}^{-1}$. The difference stems from the larger $r_d h$ value measured by DESI. This method provides a valuable consistency test of the cosmological model at recombination, with no direct dependence on the sound horizon scale. It should be stressed however that the assumed prior on $\Omega_m h^2$ is model dependent assumes Λ CDM and would be violated in the context of EDE models which predict a higher value of $\Omega_m h^2$ [52]. The authors critically discuss the differences between DESI and pre-DESI results, noting that future DESI data covering larger volumes will help resolve discrepancies. While this approach does not fully resolve the Hubble tension, it offers important insights into potential modifications needed in the standard cosmological model around the epoch of recombination.

28. Liu (2024) [190]: This analysis presents a detailed study of the Hubble constant (H_0) measurement using the cluster-lensed supernova SN Refsdal in MACS J1149.5+2223. The authors employ 23 different lens mass models to thoroughly explore the dependence of H_0 on mass model assumptions. Using the software glafic, they construct parametric models with varying dark matter halo profiles, components, and multipole perturbations. By combining measurements from all models with equal weighting, they obtain $H_0 = 70.0^{+4.7}_{-4.9} \text{ km s}^{-1} \text{ Mpc}^{-1}$. A weighting scheme based on positional errors yields a slightly tighter constraint of $H_0 = 70.3 \pm 4.4 \text{ km s}^{-1} \text{ Mpc}^{-1}$. The analysis reveals that the H_0 measurement is relatively robust against different mass model assumptions, unlike previous studies on cluster-lensed quasars. The authors critically examine correlations between H_0 and various lensing properties, finding that steeper radial density profiles tend to yield larger H_0 values. They also demonstrate a clear correlation between H_0 and magnification factors, highlighting the potential of gravitationally lensed Type Ia supernovae for accurate H_0 measurements. While the precision is comparable to previous analyses of SN Refsdal, this study provides a comprehensive exploration of mass model dependencies and insights for future improvements in H_0 constraints from cluster lensing.

29. Bom (2024) [191]: This analysis presents a new measurement of the Hubble constant H_0 using the dark

standard siren method with 5 well-localized gravitational wave events from the LIGO/Virgo/KAGRA O4a observing run, combined with 10 events from previous runs. The authors employ the galaxy catalog method, using photometric redshifts derived from deep learning techniques applied to DESI Legacy Survey and DELVE data. They find $H_0 = 69.9^{+13.3}_{-12.0} \text{ km s}^{-1} \text{ Mpc}^{-1}$ (68% HDI) from 15 dark sirens alone, and $H_0 = 68.0^{+4.3}_{-3.8} \text{ km s}^{-1} \text{ Mpc}^{-1}$ when combined with the bright siren GW170817 and its electromagnetic counterpart. The analysis critically examines the impact of photometric redshift quality, catalog completeness, and selection effects. The authors use a Bayesian framework to marginalize over potential host galaxies and incorporate a detailed treatment of the gravitational wave selection function. While the precision is comparable to previous dark siren analyses, this work demonstrates the potential of combining multiple well-localized events with high-quality photometric redshifts. The authors discuss potential systematics and limitations, particularly related to BBH population assumptions and catalog depth. This approach provides an independent probe of H_0 that could help arbitrate the Hubble tension as more events are detected and analyzed.

30. TDCOSMO (2024) [136]: This analysis presents a measurement of the Hubble constant H_0 using time-delay cosmography applied to the quadruply imaged lensed quasar WGD 2038 4008. The authors combine new time-delay measurements from optical monitoring with existing lens models to constrain the time-delay distance $D_{\Delta t}$ and H_0 . They employ two independent lens modeling codes (GLEE and Lenstronomy) and consider both power-law and composite (stars+dark matter) mass profiles. The analysis incorporates the full time-delay covariance matrix and external convergence estimates. Assuming a flat Λ CDM cosmology with $\Omega_m = 0.3$, they find $H_0 = 65^{+23}_{-14} \text{ km s}^{-1} \text{ Mpc}^{-1}$. The large uncertainty is primarily due to the weak time-delay constraints, as the quasar exhibited low variability during the monitoring period. The analysis was performed blindly with respect to cosmological parameters to prevent experimenter bias. This is the first lens in the TDCOSMO sample to incorporate multiple lens models in the final inference and use the full time-delay covariance matrix. While the precision is insufficient to address the Hubble tension, this system will contribute to future joint analyses of multiple lenses to improve overall constraints on H_0 .

31. Grillo (2024) [192]: This analysis presents a measurement of the Hubble constant H_0 using strong gravitational lensing in the galaxy cluster MACS J1149.5+2223, including time delays of the multiply-imaged supernova Refsdal. The authors employ a parametric lens model constrained by 89 multiple images from 28 background sources and 4 measured time delays of SN Refsdal. In an open w CDM cosmology, they find $H_0 = 65.1^{+3.5}_{-3.4} \text{ km s}^{-1} \text{ Mpc}^{-1}$. The analysis is performed using the GLEE software, considering four cosmological models (flat and open Λ CDM and w CDM) and three lens model vari-

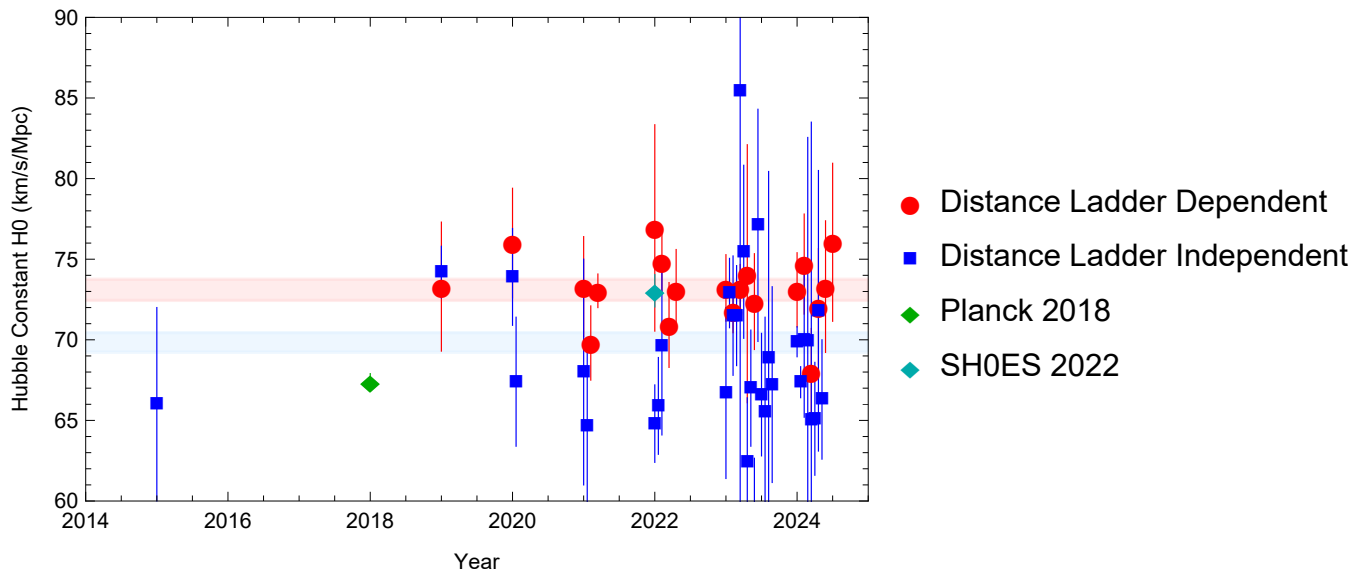


FIG. 1: The measurements of H_0 shown in Tables I (distance ladder dependent-red points) and II (one step distance ladder and sound horizon independent-blue points). The most precise distance ladder dependent measurement (SH0ES 2022[15]) and the most precise sound horizon dependent Planck 18[14] measurements are also shown as green points. The light red and light blue bands denote the combined constraints for distance ladder dependent and one step measurements respectively.

ants to assess systematic uncertainties. Remarkably, the H_0 measurement is robust across different cosmological models and lens parameterizations, with systematics estimated to be smaller than statistical errors. The precision achieved (6%) is competitive with other probes, and the method uniquely constrains multiple cosmological parameters simultaneously without external priors. The authors critically compare their results to other cosmological probes, demonstrating the complementarity and stability of their method. While based on a single lens system, this work showcases the potential of time-delay cosmography with galaxy clusters as a powerful and independent probe of cosmology.

32. Pascale (2024) [193]: This analysis presents the first precision measurement of the Hubble constant H_0 using a multiply-imaged Type Ia supernova, SN H0pe, discovered by JWST in the galaxy cluster PLCK G165.7+67.0. The authors employ a Bayesian approach combining photometric and spectroscopic time delay measurements with seven independent lens models. The standard candle nature of SN Ia allows for absolute magnification constraints, which are used to break degeneracies between lens models. Following strict blinding protocols, they obtain $H_0 = 71.8^{+9.8}_{-7.6}$ km s⁻¹ Mpc⁻¹. The analysis critically examines the impact of different lens modeling approaches, the correlation between predicted time delays and magnifications, and the effect of including weak lensing data. The authors discuss potential systematics, including the interpolation method for the unlensed SN Ia apparent magnitude and the thin-lens approximation. While the precision is limited by both lens

modeling and time delay measurement uncertainties, this work demonstrates the power of cluster-lensed SnIa for time-delay cosmography. The result is consistent with local universe measurements but in tension with early universe predictions at the $\sim 1.5\sigma$ level, providing new evidence in the context of the Hubble tension.

33. Li (2024) [194]: This analysis presents a cosmological-model-independent measurement of the Hubble constant H_0 using the gravitationally lensed supernova Refsdal in combination with the Pantheon+ supernova sample. The authors employ Gaussian process regression to reconstruct the expansion history from supernovae Ia data, which is then anchored by the time-delay distance of SN Refsdal. Using eight lens models for the cluster MACS J1149, they infer $H_0 = 64.2^{+4.4}_{-4.3}$ km s⁻¹ Mpc⁻¹, while using only the two models most consistent with observations yields $H_0 = 66.3^{+3.8}_{-3.6}$ km s⁻¹ Mpc⁻¹. These results are consistent with previous model-dependent analyses but avoid potential biases from assuming a specific cosmological model. The precision is comparable to model-dependent methods, demonstrating the power of this approach. The results are in tension with distance ladder measurements at the 1.8-2 σ level but agree well with Planck CMB data. The authors critically compare their findings to other time-delay cosmography results and discuss the impact of lens modeling uncertainties. While assuming spatial flatness, this method provides a valuable cross-check on H_0 measurements that is less sensitive to cosmological model assumptions.

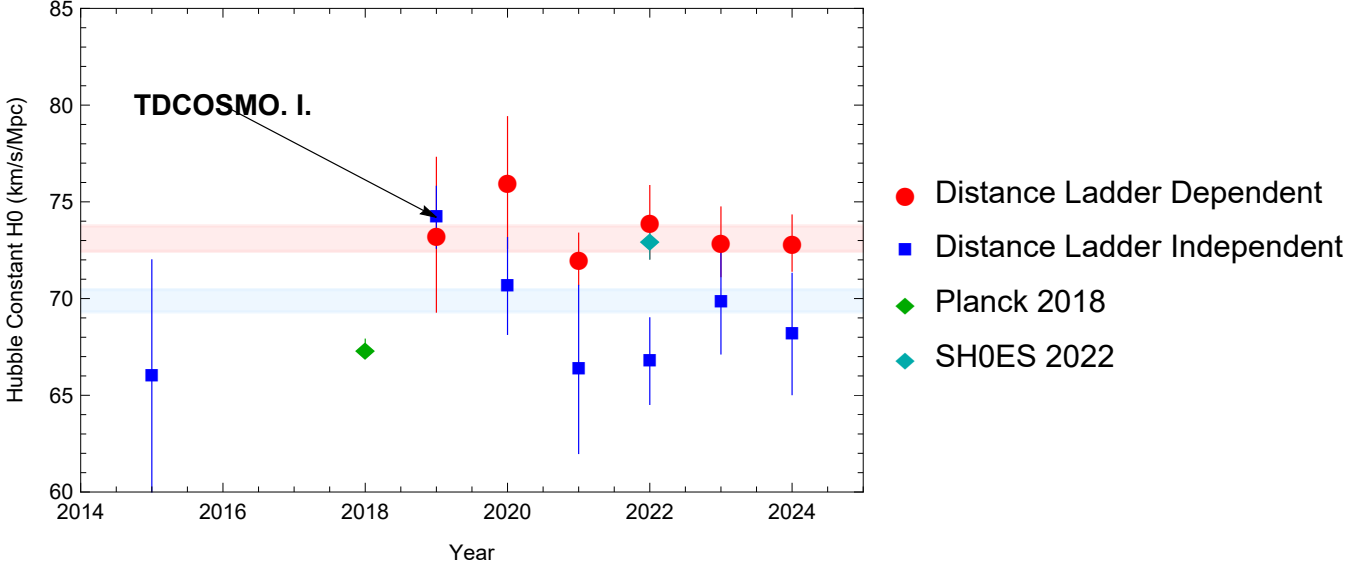


FIG. 2: Same as Fig. 1 but the measurements are binned by year. Notice that for most years the one step H_0 are consistent with the Planck 18 measurement of H_0 . The only one step measurement that is in significant tension with Planck 18[14] is the TDCOSMO. I. strong lensing time delay measurement[131] which has been shown to suffer from a systematic issue (related to the mass-sheet degeneracy (MSD)) by later TDCOSMO analyses[130, 185]. However, more recent TDCOSMO measurements are consistent with Planck 18 and other sound horizon based measurements (eg [130, 136]).

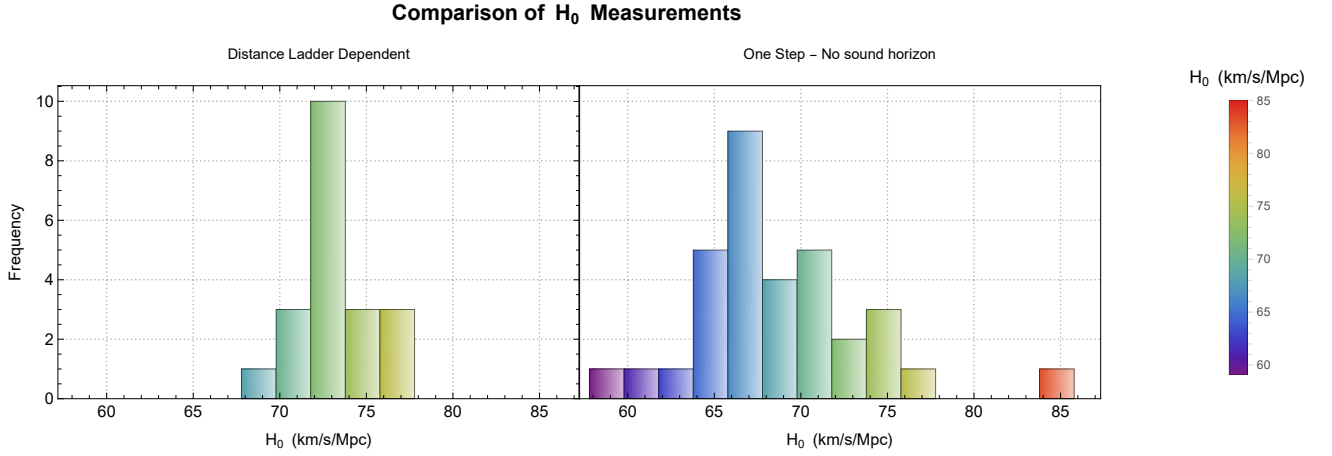


FIG. 3: Histogram comparison of H_0 measurements. Left: Distribution of Distance Ladder Dependent measurements. Right: Distribution of One Step - No sound horizon measurements. The color gradient represents the range of H_0 values from approximately 60 to 85 km/s/Mpc. This comparison highlights the frequency distribution of measurements for each method, allowing for a direct visual comparison of their respective ranges and central tendencies.

III.2. Results: One step methods vs distance ladder methods

In this section, we present a comprehensive statistical analysis of the Hubble constant (H_0) measurements, categorized into two distinct groups: distance ladder-dependent measurements and one-step measurements that are independent of both the distance ladder

and the sound horizon scale. Our analysis reveals significant differences between these two approaches, with important implications for the Hubble tension.

Figures 1 and 2 provide a visual representation of the H_0 measurements from both categories. In Figure 1, we observe a clear separation between the distance ladder-dependent measurements (red points) and the one-step measurements (blue points). The distance ladder mea-

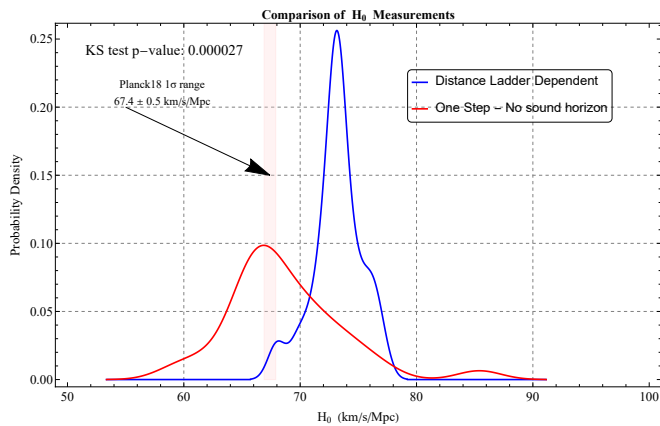


FIG. 4: Comparison of H_0 measurements using smooth histogram representations. The blue curve represents the Distance Ladder Dependent measurements, while the red curve shows the One Step - No sound horizon measurements. The vertical light red band indicates the Planck18 1σ range of 67.4 ± 0.5 km/s/Mpc. A Kolmogorov-Smirnov test between the two distributions yields a p-value of 0.000102, indicating a statistically significant difference between the two measurement methods.

measurements consistently yield higher H_0 values, clustering around 73 km/s/Mpc, while the one-step measurements tend to be lower, grouping closer to the Planck 18 value of 67.4 ± 0.5 km/s/Mpc.

Figure 2 presents the same data binned by year, offering insights into the temporal evolution of H_0 measurements. This visualization highlights a consistent trend over recent years: one-step measurements (blue points) consistently report lower H_0 values compared to distance ladder measurements (red points). Notably, most one-step measurements align well with the Planck 18 result, with the exception of the 2019 TDCOSMO.I strong lensing time delay measurement. This outlier has since been attributed to systematic issues related to the mass-sheet degeneracy (MSD), as demonstrated by subsequent TDCOSMO analyses.

The histogram comparison in Figure 3 further illustrates the distinct distributions of H_0 measurements between the two methods. The distance ladder-dependent measurements (left panel) show a distribution centered at higher H_0 values, while the one-step measurements (right panel) exhibit a distribution shifted towards lower values, more consistent with Planck 18 results.

Figure 4 presents a smooth histogram representation of the two measurement categories, providing a clear visualization of their distinct probability distributions. The blue curve (one-step measurements) shows a peak that aligns closely with the Planck 18 1σ range (indicated by the vertical light red band), while the red curve (distance ladder-dependent measurements) peaks at a notably higher H_0 value.

To combine the multiple measurements of H_0 from

both distance ladder dependent and independent methods, we employed a weighted average approach. This method assumes that all measurements are independent of each other. The procedure is as follows:

- 1. Weighted Mean Calculation:** Each H_0 measurement is weighted by the inverse square of its uncertainty, giving more weight to measurements with smaller uncertainties. The weighted mean H_0 is calculated as:

$$\overline{H_0} = \frac{\sum_i H_{0,i}/\sigma_i^2}{\sum_i 1/\sigma_i^2} \quad (3.3)$$

where $H_{0,i}$ is the i -th measurement and σ_i is its uncertainty.

- 2. Uncertainty Calculation:** The uncertainty of the weighted mean is estimated as the inverse square root of the sum of weights:

$$\sigma_{\overline{H_0}} = \frac{1}{\sqrt{\sum_i 1/\sigma_i^2}} \quad (3.4)$$

This method assumes that all measurements are independent of each other, allowing us to treat each measurement as providing separate information. However, it's important to note that in reality, some measurements might have correlations due to shared data or methodologies. The independence assumption, while commonly used for simplicity, may lead to an underestimation of the final uncertainty if significant correlations exist between measurements.

Our statistical analysis reveals significant differences between the two groups of H_0 measurements:

1. Weighted Means:

- Distance Ladder Dependent: $H_0 = 72.8 \pm 0.5$ km/s/Mpc
- One-step (Distance Ladder Independent): $H_0 = 69.0 \pm 0.5$ km/s/Mpc. This value decreases further to $H_0 = 68.3 \pm 0.5$ km/s/Mpc if two outliers are removed from the sample as discussed below.

These weighted means differ by approximately 3.75 km/s/Mpc, which is statistically significant given their respective uncertainties.

- 2. Distribution Comparison:** A Kolmogorov-Smirnov (KS) test comparing the two groups of measurements yields a p-value of 0.000102. This extremely low p-value indicates that the probability of these two distributions being drawn from the same underlying population is negligible. In other words, there is strong statistical evidence that the distance ladder-dependent and one-step measurements represent fundamentally different distributions of H_0 values.

The consistency of one-step measurements with sound horizon-based measurements like Planck 18 ($H_0 = 67.4 \pm 0.5$ km/s/Mpc) and standard BAO measurements is particularly noteworthy. This alignment suggests that the one-step methods, which are independent of both the distance ladder and sound horizon scale, corroborate the lower H_0 values inferred from early universe observations.

III.2.1. χ^2 analysis and robustness of results

To further assess the consistency and reliability of our findings, we conducted a comprehensive χ^2 analysis on various subsets of the distance ladder independent dataset. This analysis serves to evaluate the internal consistency of different measurement methods and identify potential sources of tension within the data.

We constructed and minimized the χ^2 statistic for each subset, defined as:

$$\chi^2 = \sum_i \frac{(H_{0,i} - H_{0,\text{best fit}})^2}{\sigma_i^2} \quad (3.5)$$

where $H_{0,i}$ are the individual measurements, σ_i their uncertainties, and $H_{0,\text{best fit}}$ the best-fit value that minimizes χ^2 .

Table III presents the results of this analysis for various subsets of the data:

Our analysis reveals that most subsamples are self-consistent and in agreement with each other, as evidenced by their reduced χ^2 values close to 1. However, we observe some tension in the full dataset (reduced $\chi^2 = 1.43$) and in two subsamples: Megamasers and Lensing All.

The tension in the full dataset and the in the above two subsamples can be attributed to two notable outliers: data points 3 and 4 of Table II, associated with TDCOSMO I lensing[131] and the Megamasers MCP+SH0ES [126] points respectively. The TDCOSMO I measurement (point 3) has been shown to suffer from systematic issues related to the mass-sheet degeneracy (MSD), as demonstrated by subsequent TDCOSMO analyses[130, 185]. When we exclude these two outliers (Full Data excl. 3,4), the reduced χ^2 (χ^2 per dof) improves significantly to 1.00585, indicating excellent consistency among the remaining data points. In addition, the consistency of the remaining one step-sound horizon free measurements with sound horizon based measurements improves further and the new best fit value of H_0 becomes $H_0 = 68.3 \pm 0.5$ km s⁻¹ Mpc⁻¹.

The GW+kilonovae subset combines measurements based on gravitational waves with measurements based on kilonovae. Even though this subset encompasses diverse methods, it shows good internal consistency (reduced $\chi^2 = 1.16106$) and yields a best-fit H_0 value of 66.3 ± 2.0 km s⁻¹ Mpc⁻¹, which is in close agreement with the Planck 18 result. This supports the potential of

gravitational wave standard sirens as a promising independent probe of H_0 .

The Lensing subset, after excluding the TDCOSMO I outlier, demonstrates improved consistency (reduced $\chi^2 = 0.892011$) and a best-fit H_0 of 69.7 ± 1.2 km s⁻¹ Mpc⁻¹, aligning more closely with other independent measurements.

Cosmic Chronometers and the revised Lensing subset both show excellent internal consistency (reduced $\chi^2 < 1$) and yield H_0 values that are in good agreement with the overall trend of one-step measurements.

The Megamasers subset, while showing some tension (reduced $\chi^2 = 1.38689$), is based on only two data points. The tension is apparently due to the outlier MCP+SH0ES datapoint[126] discussed above.

The outlier data: Here we discuss in some more detail the two outlier one-step H_0 measurements and point out potential sources of systematic errors in these measurements.

III.2.1.1. TDCOSMO.I measurement (2019) [131]
 $H_0 = 74.2 \pm 1.6$: The TDCOSMO I measurement (point 3 of Table II) suffers from systematic issues related to the mass-sheet degeneracy (MSD). This early analysis by [131] assumed simple parametric mass models (power-law or composite) for the lens galaxies, which implicitly break the MSD. However, these assumptions can potentially bias the H_0 measurement or underestimate the errors if the true mass profile deviates from these simple models.

Subsequent analyses, particularly [130] (TDCOSMO IV) and [185], have effectively replaced this measurement by addressing the MSD issue more rigorously. These later studies have much larger uncertainties because they relax the assumptions on the mass profile and instead use stellar kinematics to constrain the MSD. Ref. [130] (measurement 5 of Table II) used single-aperture stellar kinematics for the TDCOSMO sample, while [185] (measurement 19 of Table II) used spatially-resolved kinematics for RXJ1131–1231. By allowing more freedom in the mass model and constraining it with kinematic data, these analyses provide a more robust, albeit less precise, measurement of H_0 . The increased uncertainties reflect the additional degeneracies introduced when the mass profile is not assumed to follow a simple parametric form.

III.2.1.2. MCP-SH0ES measurement (2020) [126]
 $H_0 = 73.9 \pm 3.0$: This analysis attempts to estimate H_0 using 6 megamasers in galaxies with relatively low redshifts ($z \approx 0.002 - 0.034$), which are barely in the Hubble flow. Given these low redshifts, it is expected that peculiar velocities should lead to increased uncertainties in the H_0 measurement. However, the reported uncertainty of ± 3.0 km s⁻¹ Mpc⁻¹ seems surprisingly small given this effect. Notably, this measurement is in tension with previous megamaser-based H_0 determinations, which found significantly lower values (e.g., $H_0 = 66.0 \pm 6.0$ km s⁻¹ Mpc⁻¹ from Gao et al. 2016 [127] and $H_0 = 68 \pm 9$ km s⁻¹ Mpc⁻¹ from Kuo et al. 2013 [176]). The lack of any updated megamaser-based H_0 measurements since 2020

TABLE III: Analysis of Various Subsets of the One Step - Sound Horizon and Distance Ladder Independent Sample.

The data numbers correspond to Table II. Notice the dramatic improvement of the self consistency of the full sample (decrease of the reduced $\chi^2_{\text{red}} \equiv \chi^2/\text{dof}$) if the two outliers (TDCOSMO.I and MCP-SHOES) are removed. These outliers have been removed from most of the subsamples after row 2. If they were present the value of χ^2_{red} would have been significantly larger (see eg row 5 where TDCOSMO.I has been included).

Dataset	H_0 (km s ⁻¹ Mpc ⁻¹)	χ^2_{min}	χ^2_{red}	DoF	Data points
Full Sample	69.0 ± 0.5	43.69	1.37	32	All
Full Sample (excl. 4,5)	68.3 ± 0.5	28.51	0.95	30	All except outliers 4,5
Gravitational Waves (GW)	71.4 ± 3.1	1.18	0.24	5	7,11,16,17,24,29
Full Sample (excl. GW)	68.2 ± 0.5	26.31	1.10	24	All except 4,5,7,11,16,17,24,29
TD Lensing All	71.4 ± 1.0	12.00	1.33	9	4,6,13,14,21,22,28,31-33
Full Sample (excl. TD Lensing)	68.2 ± 0.6	23.46	1.07	22	All except 4-6,13,14,21,22,28,31-33
TD Lensing (no TDCOSMO I)	69.7 ± 1.2	7.14	0.89	8	6,13,14,21,22,28,31-33
Cosmic Chronometers	68.3 ± 2.0	1.80	0.90	2	10,12,15
Full Sample (excl. CC)	68.3 ± 0.5	26.71	0.99	27	All except 4,5,10,12,15
Megamasers	72.0 ± 2.6	1.60	0.80	2	2,3,5
Full Sample (excl. Megamasers)	68.3 ± 0.5	28.36	1.01	28	All except 2-5
Megamasers (excl. MCP-SHOES)	67.0 ± 5.0	0.03	0.03	1	2,3
Early Time (No Sound Horizon)	68.4 ± 0.6	5.93	2.97	2	9,26,27
Full Sample (excl. Early Time)	68.1 ± 0.9	22.50	0.83	27	All except 4,5,9,26,27

raises further questions about the robustness of this result. Other potential sources of systematics include the assumptions made in the disk modeling, particularly the treatment of warps and eccentricity, as well as possible biases in the selection of megamaser galaxies (6 chosen out of more than 15 known[195]). The reliance of the analysis on external galaxy flow models to correct for peculiar velocities introduces additional model-dependent uncertainties. Furthermore, the small sample size makes the measurement susceptible to cosmic variance effects.

These arguments along with the results of Table III support the robustness of our findings across various subsets of the distance ladder independent data. The consistency observed after removing known problematic outliers strengthens our conclusion that one-step methods tend to favor lower H_0 values, in better agreement with Planck 18 results, compared to distance ladder-dependent measurements.

III.2.1.3. The distance ladder sample: Correlations and over fitting Interestingly, the analysis of the full distance ladder dependent dataset yields a notably different result. With a best-fit H_0 of $72.7^{+0.5}_{-0.5}$ km s⁻¹ Mpc⁻¹, this dataset shows a clear preference for higher H_0 values compared to most of the independent subsets. However, the most striking feature is the unusually low reduced χ^2 value of 0.52.

A reduced χ^2 significantly below 1, as observed in the distance ladder dependent dataset, suggests that the model is "overfitting" the data. This could be due to several factors:

1. Overestimated uncertainties: If the reported uncertainties in the distance ladder measurements are consistently larger than the true uncertainties, it would lead to an artificially low χ^2 value.
2. Correlation between measurements: If there are un-

accounted correlations between different distance ladder measurements, it could lead to an underestimation of the true variance in the data, resulting in a lower χ^2 .

3. Publication bias: There might be a tendency to publish results that are in agreement with previous measurements, leading to an artificially low scatter in the published values.

This unusually low reduced χ^2 in the distance ladder dependent dataset contrasts sharply with the more typical values seen in the independent dataset subsets. It suggests that the uncertainties in the distance ladder measurements may be overestimated, or that there are significant correlations or dependencies among these measurements that are not being accounted for in the analysis.

III.2.1.4. Interpretation and the Road Ahead: This analysis highlights the importance of critically examining individual measurements and their potential systematic effects. It also demonstrates the value of using multiple independent methods to constrain H_0 , as this approach allows for the identification and mitigation of method-specific biases, systematics or new physics.

Given these results, the most probable interpretation is that the distance ladder measurements should be carefully reexamined. This reanalysis should focus on identifying potential systematics or local physics phenomena that may not have been adequately accounted for in previous distance ladder analyses. The consistent discrepancy between distance ladder methods and other independent techniques points to the likelihood of unresolved issues within the distance ladder methodology or assumptions.

The analysis presented here underscores the critical importance of diverse measurement techniques in cosmology. The agreement between one-step measurements and

sound horizon based estimates provided by CMB observations (Planck 18) suggests that the resolution to the Hubble tension may lie in refining our understanding of local distance ladder measurements rather than in revising our models of the early universe.

Future efforts should concentrate on:

1. Enhancing the accuracy and reducing systematic uncertainties in distance ladder methods.
2. Further developing and refining one-step measurement techniques.
3. Investigating potential local universe phenomena that could affect distance ladder measurements without impacting one-step or CMB-based methods.
4. Conducting cross-checks and joint analyses between different measurement techniques to identify and resolve discrepancies.

By pursuing these avenues, we can work towards a more coherent understanding of the universe's expansion rate and potentially resolve the long-standing Hubble tension.

IV. CONCLUSION-DISCUSSION-FUTURE PROSPECTS

This study presents a comprehensive analysis of Hubble constant (H_0) measurements, categorizing them into two distinct groups: distance ladder measurements and one-step measurements. The distance ladder approach, which relies on various calibrators and cosmic distance indicators, yielded an H_0 value of 72.8 ± 0.5 km/s/Mpc. In contrast, one-step measurements, which are independent of the CMB sound horizon scale and do not require a distance ladder, indicated a lower H_0 of 69.0 ± 0.5 km/s/Mpc. It's important to note that these uncertainties are likely underestimated, as the H_0 measurements were assumed to be independent, an assumption not fully realized in practice.

The discrepancy between these results suggests a significant shift in our understanding of the Hubble tension. Contrary to the prevailing view that the tension primarily exists between local measurements and early-time observations, this analysis indicates that the core of the tension lies between distance ladder measurements and all other methods. These other methods include local one-step measurements, early-time measurements independent of the sound horizon, and sound horizon-based measurements.

If this conjecture holds true, it implies that the origin of the Hubble tension may be rooted in misunderstood local physics affecting all distance ladder measurements similarly. This could manifest in two ways:

1. A fundamental change in physics that impacts the relationships among the distance ladder rungs[42, 44, 76, 196–201].
2. An unknown local systematic effect influencing all distance ladder calibrators in a similar manner[100, 202–208].

Thus, the present analysis offers a novel perspective on the Hubble tension, suggesting that the discrepancy may primarily lie between distance ladder measurements and other methods. This finding opens up several avenues for future research and potential extensions of our work:

1. **Probing Physics Changes in Distance Ladder Regimes:** A crucial extension would involve a comprehensive search for evidence of physics changes in astrophysical observations that overlap in redshift space with the rungs of the distance ladder, particularly the first two rungs[197, 209]. This could include:
 - Analyzing gravitational lensing data in the relevant redshift ranges for any anomalies.
 - Investigating galaxy rotation curves and galaxy cluster dynamics for potential deviations from expected behavior.
 - Examining the behavior of standard candles and standard sirens across different distance scales[44, 76, 209–211].
2. **Theoretical Model Construction:** Developing theoretical models that predict localized changes in physics, especially gravitational physics, could provide a framework for understanding potential discrepancies[200, 201, 212]. These models might include:
 - Modified gravity theories with scale-dependent effects [200, 201, 212, 213].
 - Models incorporating interactions between dark energy and standard model particles that become significant at specific scales.
 - Theories proposing variations in fundamental constants over cosmic time or distance.
3. **Reanalysis of Distance Ladder Datasets:** A critical extension would involve reanalyzing existing distance ladder datasets with additional degrees of freedom to test if the data supports more complex models. This could include:
 - Introducing new parameters in the Cepheid calibration that allow for a change in the Period-Luminosity (P-L) relation parameters at certain redshifts or distances[44, 76].
 - Exploring potential environmental dependencies of standard candle luminosities[100, 202–206].

- Investigating the possibility of a smooth transition in physical laws affecting distance measurements across different scales.
4. **Expansion of H_0 Measurement Compilations:** To improve statistical robustness, future work could aim to expand the compilation of H_0 measurements. This expansion could involve:
- Incorporating new measurements as they become available from ongoing and future surveys.
 - Reanalyzing older datasets with updated methodologies to potentially extract more precise H_0 estimates.
 - Actively seeking out and including H_0 measurements from diverse methodologies to ensure a comprehensive representation of measurement techniques.
5. **Detailed Correlation Analysis:** A more nuanced treatment of correlations among the measurements considered in this study could provide valuable insights. This extension would involve:
- Developing a comprehensive correlation matrix for all included H_0 measurements.
 - Performing a principal component analysis to identify the most significant independent factors contributing to the observed tensions.
 - Investigating how accounting for these correlations affects the statistical significance of the observed discrepancies between measurement methods.
6. **Systematic Error Investigation:** A detailed exploration of potential systematic errors specific to distance ladder measurements could help identify the source of the observed discrepancy. This could include:
- Reanalyzing the calibration of local distance indicators, such as Cepheids and RR Lyrae stars.
 - Investigating potential biases in supernova Ia standardization techniques.
- Examining the impact of cosmic variance on distance ladder H_0 measurements.
7. **Cross-Methodology Consistency Checks:** Developing new methods to cross-check results between different H_0 measurement techniques could help isolate potential issues. This might involve:
- Creating hybrid measurement techniques that combine aspects of distance ladder and one-step methods.
 - Designing observational tests that can discriminate between different proposed explanations for the Hubble tension.

By pursuing these extensions, we can hope to gain a deeper understanding of the nature of the Hubble tension and potentially resolve this significant cosmological puzzle. The resolution may lie in uncovering subtle systematic effects, or it may point towards exciting new physics beyond our current standard models. In either case, these investigations promise to advance our understanding of the universe’s expansion history and fundamental physics.

ACKNOWLEDGEMENTS

I thank Adam Riess for insightful comments and stimulating discussions which motivated the addition of the χ^2 analysis that identified the two outliers. This article is based upon work from COST Action CA21136 - Addressing observational tensions in cosmology with systematics and fundamental physics (CosmoVerse), supported by COST (European Cooperation in Science and Technology). This project was also supported by the Hellenic Foundation for Research and Innovation (H.F.R.I.), under the "First call for H.F.R.I. Research Projects to support Faculty members and Researchers and the procurement of high-cost research equipment Grant" (Project Number: 789).

Numerical Analysis Files: The numerical analysis files used in this work are publicly available through GitHub. These files can be accessed [through this link](#). We encourage interested readers to explore this repository for further details on our computational methods and to facilitate reproducibility of our results.

-
- [1] Leandros Perivolaropoulos and Foteini Skara, "Challenges for Λ CDM: An update," *New Astron. Rev.* **95**, 101659 (2022), [arXiv:2105.05208 \[astro-ph.CO\]](#).
- [2] Elcio Abdalla *et al.*, "Cosmology intertwined: A review of the particle physics, astrophysics, and cosmology associated with the cosmological tensions and anomalies," *JHEAp* **34**, 49–211 (2022), [arXiv:2203.06142 \[astro-ph.CO\]](#).
- [3] Eleonora Di Valentino, Olga Mena, Supriya Pan, Luca Visinelli, Weiqiang Yang, Alessandro Melchiorri, David F. Mota, Adam G. Riess, and Joseph Silk, "In the realm of the Hubble tension—a review of solutions," *Class. Quant. Grav.* **38**, 153001 (2021), [arXiv:2103.01183 \[astro-ph.CO\]](#).
- [4] Jose Luis Bernal, Licia Verde, and Adam G. Riess, "The trouble with H_0 ," *JCAP* **10**, 019 (2016), [arXiv:1607.05617 \[astro-ph.CO\]](#).

- [5] Jian-Ping Hu and Fa-Yin Wang, “Hubble Tension: The Evidence of New Physics,” *Universe* **9**, 94 (2023), [arXiv:2302.05709 \[astro-ph.CO\]](#).
- [6] George Efstathiou, “Challenges to the Lambda CDM Cosmology,” (2024) [arXiv:2406.12106 \[astro-ph.CO\]](#).
- [7] George Efstathiou, “To H_0 or not to H_0 ?” *Mon. Not. Roy. Astron. Soc.* **505**, 3866–3872 (2021), [arXiv:2103.08723 \[astro-ph.CO\]](#).
- [8] Ali Rida Khalife, Maryam Bahrami Zanjani, Silvia Galli, Sven Günther, Julien Lesgourgues, and Karim Benabed, “Review of Hubble tension solutions with new SH0ES and SPT-3G data,” *JCAP* **04**, 059 (2024), [arXiv:2312.09814 \[astro-ph.CO\]](#).
- [9] R. Brent Tully, “The Hubble Constant: A Historical Review,” (2023), [arXiv:2305.11950 \[astro-ph.CO\]](#).
- [10] Maria Dainotti, Biagio De Simone, Giovanni Montani, Tiziano Schiavone, and Gaetano Lambiase, “The Hubble constant tension: current status and future perspectives through new cosmological probes,” *PoS CORFU2022*, 235 (2023), [arXiv:2301.10572 \[astro-ph.CO\]](#).
- [11] Paul Shah, Pablo Lemos, and Ofer Lahav, “A buyer’s guide to the Hubble constant,” *Astron. Astrophys. Rev.* **29**, 9 (2021), [arXiv:2109.01161 \[astro-ph.CO\]](#).
- [12] Nils Schöneberg, Guillermo Franco Abellán, Andrea Pérez Sánchez, Samuel J. Witte, Vivian Poulin, and Julien Lesgourgues, “The H_0 Olympics: A fair ranking of proposed models,” *Phys. Rept.* **984**, 1–55 (2022), [arXiv:2107.10291 \[astro-ph.CO\]](#).
- [13] Dimitrios Bousis and Leandros Perivolaropoulos, “Hubble tension tomography: BAO vs SnIa distance tension,” (2024), [arXiv:2405.07039 \[astro-ph.CO\]](#).
- [14] N. Aghanim *et al.* (Planck), “Planck 2018 results. VI. Cosmological parameters,” *Astron. Astrophys.* **641**, A6 (2020), [Erratum: *Astron. Astrophys.* 652, C4 (2021)], [arXiv:1807.06209 \[astro-ph.CO\]](#).
- [15] Adam G. Riess *et al.*, “A Comprehensive Measurement of the Local Value of the Hubble Constant with 1 km/s Mpc Uncertainty from the Hubble Space Telescope and the SH0ES Team,” *Astrophys. J. Lett.* **934**, L7 (2022), [arXiv:2112.04510 \[astro-ph.CO\]](#).
- [16] Vivian Poulin, Tristan L. Smith, Tanvi Karwal, and Marc Kamionkowski, “Early Dark Energy Can Resolve The Hubble Tension,” *Phys. Rev. Lett.* **122**, 221301 (2019), [arXiv:1811.04083 \[astro-ph.CO\]](#).
- [17] Marc Kamionkowski and Adam G. Riess, “The Hubble Tension and Early Dark Energy,” *Ann. Rev. Nucl. Part. Sci.* **73**, 153–180 (2023), [arXiv:2211.04492 \[astro-ph.CO\]](#).
- [18] Théo Simon, Pierre Zhang, Vivian Poulin, and Tristan L. Smith, “Updated constraints from the effective field theory analysis of the BOSS power spectrum on early dark energy,” *Phys. Rev. D* **107**, 063505 (2023), [arXiv:2208.05930 \[astro-ph.CO\]](#).
- [19] Matteo Braglia, William T. Emond, Fabio Finelli, A. Emir Gumrukcuoglu, and Kazuya Koyama, “Unified framework for early dark energy from α -attractors,” *Phys. Rev. D* **102**, 083513 (2020), [arXiv:2005.14053 \[astro-ph.CO\]](#).
- [20] Florian Niedermann and Martin S. Sloth, “Resolving the Hubble tension with new early dark energy,” *Phys. Rev. D* **102**, 063527 (2020), [arXiv:2006.06686 \[astro-ph.CO\]](#).
- [21] Tristan L. Smith, Vivian Poulin, José Luis Bernal, Kimberly K. Boddy, Marc Kamionkowski, and Riccardo Murgia, “Early dark energy is not excluded by current large-scale structure data,” *Phys. Rev. D* **103**, 123542 (2021), [arXiv:2009.10740 \[astro-ph.CO\]](#).
- [22] K. Rezazadeh, A. Ashoorioon, and D. Grin, “Cascading Dark Energy,” (2022), [arXiv:2208.07631 \[astro-ph.CO\]](#).
- [23] Matteo Braglia, Mario Ballardini, Fabio Finelli, and Kazuya Koyama, “Early modified gravity in light of the H_0 tension and LSS data,” *Phys. Rev. D* **103**, 043528 (2021), [arXiv:2011.12934 \[astro-ph.CO\]](#).
- [24] Philippe Brax, Carsten van de Bruck, Sebastien Clesse, Anne-Christine Davis, and Gregory Sculthorpe, “Early Modified Gravity: Implications for Cosmology,” *Phys. Rev. D* **89**, 123507 (2014), [arXiv:1312.3361 \[astro-ph.CO\]](#).
- [25] Tal Adi and Ely D. Kovetz, “Can conformally coupled modified gravity solve the Hubble tension?” *Phys. Rev. D* **103**, 023530 (2021), [arXiv:2011.13853 \[astro-ph.CO\]](#).
- [26] Timothy Clifton, Pedro G. Ferreira, Antonio Padilla, and Constantinos Skordis, “Modified Gravity and Cosmology,” *Phys. Rept.* **513**, 1–189 (2012), [arXiv:1106.2476 \[astro-ph.CO\]](#).
- [27] Meng-Xiang Lin, Marco Raveri, and Wayne Hu, “Phenomenology of Modified Gravity at Recombination,” *Phys. Rev. D* **99**, 043514 (2019), [arXiv:1810.02333 \[astro-ph.CO\]](#).
- [28] Eleonora Di Valentino, Alessandro Melchiorri, and Joseph Silk, “Cosmological hints of modified gravity?” *Phys. Rev. D* **93**, 023513 (2016), [arXiv:1509.07501 \[astro-ph.CO\]](#).
- [29] Yashar Akrami *et al.* (CANTATA), *Modified Gravity and Cosmology: An Update by the CANTATA Network*, edited by Emmanuel N. Saridakis, Ruth Lazkoz, Vincenzo Salzano, Paulo Vargas Moniz, Salvatore Capozziello, Jose Beltrán Jiménez, Mariafelicia De Laurentis, and Gonzalo J. Olmo (Springer, 2021) [arXiv:2105.12582 \[gr-qc\]](#).
- [30] Massimo Rossi, Mario Ballardini, Matteo Braglia, Fabio Finelli, Daniela Paoletti, Alexei A. Starobinsky, and Caterina Umiltà, “Cosmological constraints on post-Newtonian parameters in effectively massless scalar-tensor theories of gravity,” *Phys. Rev. D* **100**, 103524 (2019), [arXiv:1906.10218 \[astro-ph.CO\]](#).
- [31] Matteo Braglia, Mario Ballardini, William T. Emond, Fabio Finelli, A. Emir Gumrukcuoglu, Kazuya Koyama, and Daniela Paoletti, “Larger value for H_0 by an evolving gravitational constant,” *Phys. Rev. D* **102**, 023529 (2020), [arXiv:2004.11161 \[astro-ph.CO\]](#).
- [32] Guillermo Franco Abellán, Matteo Braglia, Mario Ballardini, Fabio Finelli, and Vivian Poulin, “Probing early modification of gravity with Planck, ACT and SPT,” *JCAP* **12**, 017 (2023), [arXiv:2308.12345 \[astro-ph.CO\]](#).
- [33] Osamu Seto and Yo Toda, “Comparing early dark energy and extra radiation solutions to the Hubble tension with BBN,” *Phys. Rev. D* **103**, 123501 (2021), [arXiv:2101.03740 \[astro-ph.CO\]](#).
- [34] Jeremy Sakstein and Mark Trodden, “Early Dark Energy from Massive Neutrinos as a Natural Resolution of the Hubble Tension,” *Phys. Rev. Lett.* **124**, 161301 (2020), [arXiv:1911.11760 \[astro-ph.CO\]](#).
- [35] Sunny Vagnozzi, “New physics in light of the H_0 tension: An alternative view,” *Phys. Rev. D* **102**, 023518 (2020), [arXiv:1907.07569 \[astro-ph.CO\]](#).

- [36] Karsten Jedamzik, Levon Pogosian, and Gong-Bo Zhao, “Why reducing the cosmic sound horizon alone can not fully resolve the Hubble tension,” *Commun. in Phys.* **4**, 123 (2021), arXiv:2010.04158 [astro-ph.CO].
- [37] Sunny Vagnozzi, “Seven Hints That Early-Time New Physics Alone Is Not Sufficient to Solve the Hubble Tension,” *Universe* **9**, 393 (2023), arXiv:2308.16628 [astro-ph.CO].
- [38] Sunny Vagnozzi, “Consistency tests of Λ CDM from the early integrated Sachs-Wolfe effect: Implications for early-time new physics and the Hubble tension,” *Phys. Rev. D* **104**, 063524 (2021), arXiv:2105.10425 [astro-ph.CO].
- [39] J. Colin Hill, Evan McDonough, Michael W. Toomey, and Stephon Alexander, “Early dark energy does not restore cosmological concordance,” *Phys. Rev. D* **102**, 043507 (2020), arXiv:2003.07355 [astro-ph.CO].
- [40] Samuel Goldstein, J. Colin Hill, Vid Iršič, and Blake D. Sherwin, “Canonical Hubble-Tension-Resolving Early Dark Energy Cosmologies Are Inconsistent with the Lyman- α Forest,” *Phys. Rev. Lett.* **131**, 201001 (2023), arXiv:2303.00746 [astro-ph.CO].
- [41] Emanuele Fondi, Alessandro Melchiorri, and Luca Pagano, “No evidence for EDE from Planck data in extended scenarios,” *JHEAp* **39**, 14–20 (2023), arXiv:2203.12930 [astro-ph.CO].
- [42] Valerio Marra and Leandros Perivolaropoulos, “Rapid transition of G_{eff} at $z_t \simeq 0.01$ as a possible solution of the Hubble and growth tensions,” *Phys. Rev. D* **104**, L021303 (2021), arXiv:2102.06012 [astro-ph.CO].
- [43] George Alestas, Lavrentios Kazantzidis, and Leandros Perivolaropoulos, “ $w - M$ phantom transition at $z_t < 0.1$ as a resolution of the Hubble tension,” *Phys. Rev. D* **103**, 083517 (2021), arXiv:2012.13932 [astro-ph.CO].
- [44] Leandros Perivolaropoulos and Foteini Skara, “Hubble tension or a transition of the Cepheid SNIa calibrator parameters?” *Phys. Rev. D* **104**, 123511 (2021), arXiv:2109.04406 [astro-ph.CO].
- [45] Bao Wang, Martín López-Corredoira, and Jun-Jie Wei, “The Hubble Tension Survey: A Statistical Analysis of the 2012-2022 Measurements,” (2023), 10.1093/mnras/stad3724, arXiv:2311.18443 [astro-ph.CO].
- [46] Martín Lopez-Corredoira, “Hubble tensions: a historical statistical analysis,” *Mon. Not. Roy. Astron. Soc.* **517**, 5805–5809 (2022), arXiv:2210.07078 [astro-ph.CO].
- [47] Shulei Cao and Bharat Ratra, “ $H_0 = 69.8 \pm 1.3$ km s $^{-1}$ Mpc $^{-1}$, $\Omega_{\text{m}0} = 0.288 \pm 0.017$, and other constraints from lower-redshift, non-CMB, expansion-rate data,” *Phys. Rev. D* **107**, 103521 (2023), arXiv:2302.14203 [astro-ph.CO].
- [48] Licia Verde, Nils Schöneberg, and Héctor Gil-Marín, “A tale of many H_0 ,” (2023), arXiv:2311.13305 [astro-ph.CO].
- [49] Robert M. Wald, *General Relativity* (University of Chicago Press, Chicago, 1984).
- [50] Steven Weinberg, *Gravitation and Cosmology: Principles and Applications of the General Theory of Relativity* (John Wiley and Sons, New York, 1972) p. 688.
- [51] Daniel J. Eisenstein and Wayne Hu, “Baryonic features in the matter transfer function,” *Astrophys. J.* **496**, 605 (1998), arXiv:astro-ph/9709112.
- [52] Vivian Poulin, Tristan L. Smith, and Tanvi Karwal, “The Ups and Downs of Early Dark Energy solutions to the Hubble tension: A review of models, hints and constraints circa 2023,” *Phys. Dark Univ.* **42**, 101348 (2023), arXiv:2302.09032 [astro-ph.CO].
- [53] Prateek Agrawal, Francis-Yan Cyr-Racine, David Pinner, and Lisa Randall, “Rock ‘n’ roll solutions to the Hubble tension,” *Phys. Dark Univ.* **42**, 101347 (2023), arXiv:1904.01016 [astro-ph.CO].
- [54] Luke Hart and Jens Chluba, “Varying fundamental constants principal component analysis: additional hints about the Hubble tension,” *Mon. Not. Roy. Astron. Soc.* **510**, 2206–2227 (2022), arXiv:2107.12465 [astro-ph.CO].
- [55] Gabriel P. Lynch, Lloyd Knox, and Jens Chluba, “Reconstructing the recombination history by combining early and late cosmological probes,” (2024), arXiv:2404.05715 [astro-ph.CO].
- [56] Nanoom Lee, Yacine Ali-Haïmoud, Nils Schöneberg, and Vivian Poulin, “What It Takes to Solve the Hubble Tension through Modifications of Cosmological Recombination,” *Phys. Rev. Lett.* **130**, 161003 (2023), arXiv:2212.04494 [astro-ph.CO].
- [57] Levon Pogosian, Marco Raveri, Kazuya Koyama, Matteo Martinelli, Alessandra Silvestri, Gong-Bo Zhao, Jian Li, Simone Peirone, and Alex Zucca, “Imprints of cosmological tensions in reconstructed gravity,” *Nature Astron.* **6**, 1484–1490 (2022), arXiv:2107.12992 [astro-ph.CO].
- [58] G. Efstathiou, “CMB anisotropies and the determination of cosmological parameters,” *NATO Sci. Ser. C* **565**, 179–189 (2001), arXiv:astro-ph/0002249.
- [59] D. N. Spergel *et al.* (WMAP), “First year Wilkinson Microwave Anisotropy Probe (WMAP) observations: Determination of cosmological parameters,” *Astrophys. J. Suppl.* **148**, 175–194 (2003), arXiv:astro-ph/0302209.
- [60] Steve K. Choi *et al.* (ACT), “The Atacama Cosmology Telescope: a measurement of the Cosmic Microwave Background power spectra at 98 and 150 GHz,” *JCAP* **12**, 045 (2020), arXiv:2007.07289 [astro-ph.CO].
- [61] Daniel J. Eisenstein *et al.* (SDSS), “Detection of the Baryon Acoustic Peak in the Large-Scale Correlation Function of SDSS Luminous Red Galaxies,” *Astrophys. J.* **633**, 560–574 (2005), arXiv:astro-ph/0501171.
- [62] Éric Aubourg *et al.* (BOSS), “Cosmological implications of baryon acoustic oscillation measurements,” *Phys. Rev. D* **92**, 123516 (2015), arXiv:1411.1074 [astro-ph.CO].
- [63] Julian E. Bautista *et al.* (eBOSS), “The Completed SDSS-IV extended Baryon Oscillation Spectroscopic Survey: measurement of the BAO and growth rate of structure of the luminous red galaxy sample from the anisotropic correlation function between redshifts 0.6 and 1,” *Mon. Not. Roy. Astron. Soc.* **500**, 736–762 (2020), arXiv:2007.08993 [astro-ph.CO].
- [64] Arianna Favale, Adrià Gómez-Valent, and Marina Migliaccio, “2D vs. 3D BAO: quantification of their tension and test of the Etherington relation,” (2024), arXiv:2405.12142 [astro-ph.CO].
- [65] W. L. Freedman *et al.* (HST), “Final results from the Hubble Space Telescope key project to measure the Hubble constant,” *Astrophys. J.* **553**, 47–72 (2001), arXiv:astro-ph/0012376.
- [66] Adam G. Riess *et al.*, “A 2.4% Determination of the Local Value of the Hubble Constant,” *Astrophys. J.* **826**,

- 56 (2016), [arXiv:1604.01424 \[astro-ph.CO\]](#).
- [67] Wendy L. Freedman, Barry F. Madore, In Sung Jang, Taylor J. Hoyt, Abigail J. Lee, and Kayla A. Owens, “Status Report on the Chicago-Carnegie Hubble Program (CCHP): Three Independent Astrophysical Determinations of the Hubble Constant Using the James Webb Space Telescope,” (2024), [arXiv:2408.06153 \[astro-ph.CO\]](#).
- [68] M. W. Feast and R. M. Catchpole, “The Cepheid period-luminosity zero-point from HIPPARCOS trigonometrical parallaxes,” *Mon. Not. Roy. Astron. Soc.* **286**, L1–L5 (1997).
- [69] Barry F. Madore and Wendy L. Freedman, “The Cepheid distance scale,” *Publ. Astron. Soc. Pac.* **103**, 933–957 (1991).
- [70] Myung Gyoon Lee, Wendy L. Freedman, and Barry F. Madore, “The Tip of the Red Giant Branch as a Distance Indicator for Resolved Galaxies,” *Astrophys. J.* **417**, 553 (1993).
- [71] Luca Rizzi, R. Brent Tully, Dmitry Makarov, Lidia Makarova, Andrew E. Dolphin, Shoko Sakai, and Edward J. Shaya, “Tip of the Red Giant Branch Distances. 2. Zero-Point Calibration,” *Astrophys. J.* **661**, 815–829 (2007), [arXiv:astro-ph/0701518](#).
- [72] I. S. Glass and T. Lloyd Evans, “A period-luminosity relation for Mira variables in the Large Magellanic Cloud,” *Nature* **291**, 303 (1981).
- [73] M. W. Feast, I. S. Glass, P. A. Whitelock, and R. M. Catchpole, “A period-luminosity-colour relation for Mira variables,” *Mon. Not. Roy. Astron. Soc.* **241**, 375–392 (1989).
- [74] Barry F. Madore and Wendy L. Freedman, “Astrophysical Distance Scale: The AGB J-band Method. I. Calibration and a First Application,” *Astrophys. J.* **899**, 66 (2020), [arXiv:2005.10792 \[astro-ph.GA\]](#).
- [75] Henrietta S Leavitt and Edward C Pickering, “1777 variables in the magellanic clouds,” *Annals of Harvard College Observatory* **60**, 87–108 (1908).
- [76] Leandros Perivolaropoulos and Foteini Skara, “A Re-analysis of the Latest SH0ES Data for H_0 : Effects of New Degrees of Freedom on the Hubble Tension,” *Universe* **8**, 502 (2022), [arXiv:2208.11169 \[astro-ph.CO\]](#).
- [77] A. G. A. Brown *et al.* (Gaia), “Gaia Data Release 2: Summary of the contents and survey properties,” *Astron. Astrophys.* **616**, A1 (2018), [arXiv:1804.09365 \[astro-ph.GA\]](#).
- [78] G. S. Da Costa and T. E. Armandroff, “Standard globular cluster giant branches in the (MI,(V-I)0) plane,” *Astronomical Journal* **100**, 162–181 (1990).
- [79] W. Baade, “The Resolution of Messier 32, NGC 205, and the Central Region of the Andromeda Nebula,” *Astrophysical Journal* **100**, 137 (1944).
- [80] Myung Gyoon Lee, Wendy L. Freedman, and Barry F. Madore, “The Tip of the Red Giant Branch as a Distance Indicator for Resolved Galaxies,” *Astrophysical Journal* **417**, 553 (1993).
- [81] Wendy L. Freedman, Barry F. Madore, Taylor Hoyt, In Sung Jang, Rachael Beaton, Myung Gyoon Lee, Andrew Monson, Jill Neeley, and Jeffrey Rich, “Calibration of the Tip of the Red Giant Branch (TRGB),” (2020), [10.3847/1538-4357/ab7339](#), [arXiv:2002.01550 \[astro-ph.GA\]](#).
- [82] Siyang Li and Rachael L. Beaton, “The Tip of the Red Giant Branch Distance Ladder and the Hubble Constant,” (2024), [arXiv:2403.17048 \[astro-ph.CO\]](#).
- [83] In Sung Jang and Myung Gyoon Lee, “Improving the Tip of the Red Giant Branch Distance Scale: The Effect of Metallicity,” *Astrophysical Journal* **907**, 103 (2021).
- [84] Dmitry Makarov, Lidia Makarova, Luca Rizzi, R. Brent Tully, Andrew E. Dolphin, Shoko Sakai, and Edward J. Shaya, “Tip of the Red Giant Branch Distances. I. Optimization of a Maximum Likelihood Algorithm,” *Astronomical Journal* **132**, 2729–2742 (2006).
- [85] Aldo Serenelli, Achim Weiss, Santi Cassisi, Maurizio Salaris, and Adriano Pietrinferni, “The brightness of the red giant branch tip. Theoretical framework, a set of reference models, and predicted observables,” *Astronomy & Astrophysics* **606**, A33 (2017).
- [86] Patricia A. Whitelock, “Mira variables - Standard candles for the ages,” *Astrophysics and Space Science* **341**, 123–129 (2012).
- [87] Peter R. Wood, “The pulsation modes, masses and evolution of luminous red giants,” *Monthly Notices of the Royal Astronomical Society* **448**, 3829–3843 (2015).
- [88] B. P. Gerasimovič, “The Absolute Magnitudes of Long Period Variables,” *Proceedings of the National Academy of Sciences* **14**, 963–968 (1928).
- [89] R. F. Spine, “The Absolute Magnitudes of Long Period Variable Stars,” *Harvard Observatory Monographs* **7**, 189 (1948).
- [90] Patricia A. Whitelock, Michael W. Feast, and Floor Van Leeuwen, “Agb variables and the mira period-luminosity relation,” *Mon. Not. Roy. Astron. Soc.* **386**, 313–323 (2008), [arXiv:0801.4465 \[astro-ph\]](#).
- [91] Caroline D. Huang, “The Mira Distance Ladder,” (2024), [arXiv:2401.09581 \[astro-ph.CO\]](#).
- [92] Wenlong Yuan, Shiyuan He, Lucas M. Macri, James Long, and Jianhua Z. Huang, “The Infrared Properties of Mira Variables in the Large Magellanic Cloud,” *The Astronomical Journal* **153**, 170 (2017).
- [93] Matthew R. Templeton, Janet A. Mattei, and Lee Anne Willson, “Secular Evolution in Mira Variable Pulsations,” *The Astronomical Journal* **130**, 776–788 (2005).
- [94] Y. Ita, T. Tanabé, N. Matsunaga, Y. Nakajima, C. Nagashima, T. Nagayama, D. Kato, M. Kurita, T. Nagata, S. Sato, M. Tamura, H. Nakaya, and Y. Nakada, “Variable stars in the Magellanic Clouds - II. The data and infrared properties,” *Monthly Notices of the Royal Astronomical Society* **347**, 720–728 (2004).
- [95] Abigail J. Lee, Wendy L. Freedman, Barry F. Madore, In Sung Jang, Kayla A. Owens, and Taylor J. Hoyt, “The Chicago-Carnegie Hubble Program: The JWST J-region Asymptotic Giant Branch (JAGB) Extragalactic Distance Scale,” (2024), [arXiv:2408.03474 \[astro-ph.GA\]](#).
- [96] Amanda I. Karakas and John C. Lattanzio, “The Dawes Review 2: Nucleosynthesis and Stellar Yields of Low- and Intermediate-Mass Single Stars,” *Publications of the Astronomical Society of Australia* **31**, e030 (2014).
- [97] H. B. Richer and B. E. Westerland, “Carbon stars as standard candles,” *Astrophysical Journal* **248**, L49–L52 (1981).
- [98] Martin D. Weinberg and Sergei Nikolaev, “Stellar Populations in the Large Magellanic Cloud from 2MASS,” *Astrophysical Journal* **548**, 712–723 (2001).
- [99] Robert Tripp, “A Two-parameter luminosity correction for type Ia supernovae,” *Astron. Astrophys.* **331**, 815–820 (1998).

- [100] Radosław Wojtak and Jens Hjorth, “Intrinsic tension in the supernova sector of the local Hubble constant measurement and its implications,” *Mon. Not. Roy. Astron. Soc.* **515**, 2790–2799 (2022), arXiv:2206.08160 [astro-ph.CO].
- [101] Matt Visser, “Jerk, snap and the cosmological equation of state,” *Class. Quant. Grav.* **21**, 2603–2616 (2004), arXiv:gr-qc/0309109.
- [102] Celine Cattoen and Matt Visser, “Cosmography: Extracting the Hubble series from the supernova data,” *Gen. Rel. Grav.* **40**, 1311–1328 (2008), arXiv:gr-qc/0703122.
- [103] Adam G. Riess, Stefano Casertano, Wenlong Yuan, Lucas M. Macri, and Dan Scolnic, “Large Magellanic Cloud Cepheid Standards Provide a 1% Foundation for the Determination of the Hubble Constant and Stronger Evidence for Physics beyond Λ CDM,” *Astrophys. J.* **876**, 85 (2019), arXiv:1903.07603 [astro-ph.CO].
- [104] Wendy L. Freedman *et al.*, “The Carnegie-Chicago Hubble Program. VIII. An Independent Determination of the Hubble Constant Based on the Tip of the Red Giant Branch,” *Astrophys. J.* **882**, 34 (2019), arXiv:1907.05922 [astro-ph.CO].
- [105] Adam G. Riess, Stefano Casertano, Wenlong Yuan, J. Bradley Bowers, Lucas Macri, Joel C. Zinn, and Dan Scolnic, “Cosmic Distances Calibrated to 1% Precision with Gaia EDR3 Parallaxes and Hubble Space Telescope Photometry of 75 Milky Way Cepheids Confirm Tension with Λ CDM,” *Astrophys. J. Lett.* **908**, L6 (2021), arXiv:2012.08534 [astro-ph.CO].
- [106] David Camarena and Valerio Marra, “Local determination of the Hubble constant and the deceleration parameter,” *Phys. Rev. Res.* **2**, 013028 (2020), arXiv:1906.11814 [astro-ph.CO].
- [107] David Camarena and Valerio Marra, “A new method to build the (inverse) distance ladder,” *Mon. Not. Roy. Astron. Soc.* **504**, 5164–5171 (2021), arXiv:2101.08641 [astro-ph.CO].
- [108] D. M. Scolnic *et al.*, “The Complete Light-curve Sample of Spectroscopically Confirmed SNe Ia from Pan-STARRS1 and Cosmological Constraints from the Combined Pantheon Sample,” *Astrophys. J.* **859**, 101 (2018), arXiv:1710.00845 [astro-ph.CO].
- [109] Tamara M. Davis *et al.*, “The effect of peculiar velocities on supernova cosmology,” *Astrophys. J.* **741**, 67 (2011), arXiv:1012.2912 [astro-ph.CO].
- [110] Suhail Dhawan, Saurabh W. Jha, and Bruno Leibundgut, “Measuring the Hubble constant with Type Ia supernovae as near-infrared standard candles,” *Astron. Astrophys.* **609**, A72 (2018), arXiv:1707.00715 [astro-ph.CO].
- [111] Wendy L. Freedman, “Measurements of the Hubble Constant: Tensions in Perspective,” *Astrophys. J.* **919**, 16 (2021), arXiv:2106.15656 [astro-ph.CO].
- [112] John L. Tonry, Alan Dressler, John P. Blakeslee, Edward A. Ajhar, Andre B. Fletcher, Gerard A. Luppino, Mark R. Metzger, and Christopher B. Moore, “The sbf survey of galaxy distances. 4. Sbf magnitudes, colors, and distances,” *Astrophys. J.* **546**, 681–693 (2001), arXiv:astro-ph/0011223.
- [113] Ricardo Chávez, Roberto Terlevich, Elena Terlevich, Fabio Bresolin, Jorge Melnick, Manolis Plionis, and Spyros Basilakos, “The L - σ relation for massive bursts of star formation,” *Mon. Not. Roy. Astron. Soc.* **442**, 3565–3597 (2014), arXiv:1405.4010 [astro-ph.GA].
- [114] Balakrishna S. Haridasu, Paolo Salucci, and Gauri Sharma, “Radial Tully–Fisher relation and the local variance of Hubble parameter,” *Mon. Not. Roy. Astron. Soc.* **532**, 2234–2247 (2024), arXiv:2403.06859 [astro-ph.CO].
- [115] David G. Russell, “The Ks-band Tully–Fisher Relation - A Determination of the Hubble Parameter from 218 ScI Galaxies and 16 Galaxy Clusters,” *J. Astrophys. Astron.* **30**, 93 (2009), arXiv:0812.1288 [astro-ph].
- [116] Allan Sandage and G. A. Tammann, “The Distance to the Virgo Cluster from a Recalibrated Tully–Fisher Relation Based on HST Cepheids and a Demonstrated Teerikorpi Cluster Incompleteness Bias,” (2006), arXiv:astro-ph/0608677.
- [117] L. Verde, T. Treu, and A. G. Riess, “Tensions between the Early and the Late Universe,” *Nature Astron.* **3**, 891 (2019), arXiv:1907.10625 [astro-ph.CO].
- [118] John E. Carlstrom, Gilbert P. Holder, and Erik D. Reese, “Cosmology with the Sunyaev-Zel’dovich effect,” *Ann. Rev. Astron. Astrophys.* **40**, 643–680 (2002), arXiv:astro-ph/0208192.
- [119] Mark Birkinshaw, “The Sunyaev-Zel’dovich effect,” *Phys. Rept.* **310**, 97–195 (1999), arXiv:astro-ph/9808050.
- [120] P. A. R. Ade *et al.* (Planck), “Planck 2015 results. XXIV. Cosmology from Sunyaev-Zeldovich cluster counts,” *Astron. Astrophys.* **594**, A24 (2016), arXiv:1502.01597 [astro-ph.CO].
- [121] Matthew Hasselfield *et al.*, “The Atacama Cosmology Telescope: Sunyaev-Zel’dovich selected galaxy clusters at 148 GHz from three seasons of data,” *Astrophys. J. Suppl.* **209**, 17 (2013), arXiv:1301.0816 [astro-ph.CO].
- [122] S. Bocquet *et al.*, “Cluster Cosmology Constraints from the 2500 deg² SPT-SZ Survey: Inclusion of Weak Gravitational Lensing Data from Magellan and the Hubble Space Telescope,” *Astrophys. J.* **878**, 55 (2019), arXiv:1812.01679 [astro-ph.CO].
- [123] Laura Salvati, Marian Douspis, and Nabila Aghanim, “Constraints from thermal Sunyaev-Zeldovich cluster counts and power spectrum combined with CMB,” *Astron. Astrophys.* **614**, A13 (2018), arXiv:1708.00697 [astro-ph.CO].
- [124] Erik D. Reese, “Measuring the hubble constant with the sunyaev-zel’dovich effect,” in *Carnegie Observatories Centennial Symposium. 2. Measuring and Modeling the Universe* (2003) pp. 138–158, arXiv:astro-ph/0306073.
- [125] M. J. Reid, J. A. Braatz, J. J. Condon, K. Y. Lo, C. Y. Kuo, C. M. V. Impellizzeri, and C. Henkel, “The Megamaser Cosmology Project: IV. A Direct Measurement of the Hubble Constant from UGC 3789,” *Astrophys. J.* **767**, 154 (2013), arXiv:1207.7292 [astro-ph.CO].
- [126] D. W. Pesce *et al.*, “The Megamaser Cosmology Project. XIII. Combined Hubble constant constraints,” *Astrophys. J. Lett.* **891**, L1 (2020), arXiv:2001.09213 [astro-ph.CO].
- [127] F. Gao, J. A. Braatz, M. J. Reid, K. Y. Lo, J. J. Condon, C. Henkel, C. Y. Kuo, C. M. V. Impellizzeri, D. W. Pesce, and W. Zhao, “The Megamaser Cosmology Project VIII. A Geometric Distance to NGC 5765b,” *Astrophys. J.* **817**, 128 (2016), arXiv:1511.08311 [astro-ph.GA].
- [128] S. Birrer, M. Millon, D. Sluse, A. J. Shajib, F. Courbin, S. Erickson, L. V. E. Koopmans, S. H. Suyu, and

- T. Treu, “Time-Delay Cosmography: Measuring the Hubble Constant and Other Cosmological Parameters with Strong Gravitational Lensing,” *Space Sci. Rev.* **220**, 48 (2024), [arXiv:2210.10833 \[astro-ph.CO\]](#).
- [129] V. Bonvin *et al.* (H0LiCOW), “H0LiCOW – V. New COSMOGRAIL time delays of HE 0435–1223: H_0 to 3.8 per cent precision from strong lensing in a flat Λ CDM model,” *Mon. Not. Roy. Astron. Soc.* **465**, 4914–4930 (2017), [arXiv:1607.01790 \[astro-ph.CO\]](#).
- [130] S. Birrer *et al.*, “TDCOSMO - IV. Hierarchical time-delay cosmography – joint inference of the Hubble constant and galaxy density profiles,” *Astron. Astrophys.* **643**, A165 (2020), [arXiv:2007.02941 \[astro-ph.CO\]](#).
- [131] M. Millon *et al.*, “TDCOSMO. I. An exploration of systematic uncertainties in the inference of H_0 from time-delay cosmography,” *Astron. Astrophys.* **639**, A101 (2020), [arXiv:1912.08027 \[astro-ph.CO\]](#).
- [132] Gregory Dobler, Christopher Fassnacht, Tommaso Treu, Phillip J. Marshall, Kai Liao, Alireza Hojjati, Eric Linder, and Nicholas Rumbaugh, “Strong Lens Time Delay Challenge: I. Experimental Design,” *Astrophys. J.* **799**, 168 (2015), [arXiv:1310.4830 \[astro-ph.IM\]](#).
- [133] Eric J. Baxter and Blake D. Sherwin, “Determining the Hubble Constant without the Sound Horizon Scale: Measurements from CMB Lensing,” *Mon. Not. Roy. Astron. Soc.* **501**, 1823–1835 (2021), [arXiv:2007.04007 \[astro-ph.CO\]](#).
- [134] Kenneth C. Wong *et al.*, “H0LiCOW XIII. A 2.4% measurement of H_0 from lensed quasars: 5.3 σ tension between early and late-Universe probes,” *Mon. Not. Roy. Astron. Soc.* **498**, 1420–1439 (2020), [arXiv:1907.04869 \[astro-ph.CO\]](#).
- [135] Shen-Shi Du, Jun-Jie Wei, Zhi-Qiang You, Zu-Cheng Chen, Zong-Hong Zhu, and En-Wei Liang, “Model-independent determination of H_0 and Ω_K , 0 using time-delay galaxy lenses and gamma-ray bursts,” *Mon. Not. Roy. Astron. Soc.* **521**, 4963–4975 (2023), [arXiv:2302.13887 \[astro-ph.CO\]](#).
- [136] Kenneth C. Wong *et al.* (TDCOSMO), “TDCOSMO. XVI. Measurement of the Hubble Constant from the Lensed Quasar WGD 2038–4008,” (2024), [arXiv:2406.02683 \[astro-ph.CO\]](#).
- [137] Oliver H. E. Philcox, Gerrit S. Farren, Blake D. Sherwin, Eric J. Baxter, and Dillon J. Brout, “Determining the Hubble constant without the sound horizon: A 3.6% constraint on H_0 from galaxy surveys, CMB lensing, and supernovae,” *Phys. Rev. D* **106**, 063530 (2022), [arXiv:2204.02984 \[astro-ph.CO\]](#).
- [138] Samuel Brieden, Héctor Gil-Marín, and Licia Verde, “A tale of two (or more) h’s,” *JCAP* **04**, 023 (2023), [arXiv:2212.04522 \[astro-ph.CO\]](#).
- [139] Guido D’Amico, Leonardo Senatore, Pierre Zhang, and Henry Zheng, “The Hubble Tension in Light of the Full-Shape Analysis of Large-Scale Structure Data,” *JCAP* **05**, 072 (2021), [arXiv:2006.12420 \[astro-ph.CO\]](#).
- [140] Michele Moresco, “Addressing the Hubble tension with cosmic chronometers,” (2023), [arXiv:2307.09501 \[astro-ph.CO\]](#).
- [141] Adrià Gómez-Valent and Luca Amendola, “ H_0 from cosmic chronometers and Type Ia supernovae, with Gaussian Processes and the novel Weighted Polynomial Regression method,” *JCAP* **04**, 051 (2018), [arXiv:1802.01505 \[astro-ph.CO\]](#).
- [142] Michele Moresco, Raul Jimenez, Licia Verde, Andrea Cimatti, Lucia Pozzetti, Claudia Maraston, and Daniel Thomas, “Constraining the time evolution of dark energy, curvature and neutrino properties with cosmic chronometers,” *JCAP* **12**, 039 (2016), [arXiv:1604.00183 \[astro-ph.CO\]](#).
- [143] Michele Moresco, Lucia Pozzetti, Andrea Cimatti, Raul Jimenez, Claudia Maraston, Licia Verde, Daniel Thomas, Annalisa Citro, Rita Tojeiro, and David Wilkinson, “A 6% measurement of the Hubble parameter at $z \sim 0.45$: direct evidence of the epoch of cosmic re-acceleration,” *JCAP* **05**, 014 (2016), [arXiv:1601.01701 \[astro-ph.CO\]](#).
- [144] B. P. Abbott, R. Abbott, T. D. Abbott, F. Acernese, K. Ackley, C. Adams, T. Adams, P. Addesso, R. X. Adhikari, V. B. Adya, *et al.*, “A gravitational-wave standard siren measurement of the hubble constant,” *Nature* **551**, 85–88 (2017).
- [145] B. P. Abbott *et al.* (LIGO Scientific, Virgo, 1M2H, Dark Energy Camera GW-E, DES, DLT40, Las Cumbres Observatory, VINROUGE, MASTER), “A gravitational-wave standard siren measurement of the Hubble constant,” *Nature* **551**, 85–88 (2017), [arXiv:1710.05835 \[astro-ph.CO\]](#).
- [146] Kenta Hotokezaka, Ehud Nakar, Ore Gottlieb, Samaya Nissanke, Kento Masuda, Gregg Hallinan, Kunal P. Mooley, and Adam. T. Deller, “A Hubble constant measurement from superluminal motion of the jet in GW170817,” *Nature Astron.* **3**, 940–944 (2019), [arXiv:1806.10596 \[astro-ph.CO\]](#).
- [147] Hsin-Yu Chen, Maya Fishbach, and Daniel E. Holz, “A two per cent Hubble constant measurement from standard sirens within five years,” *Nature* **562**, 545–547 (2018), [arXiv:1712.06531 \[astro-ph.CO\]](#).
- [148] Shin’ichiro Ando *et al.*, “Colloquium: Multimessenger astronomy with gravitational waves and high-energy neutrinos,” *Rev. Mod. Phys.* **85**, 1401–1420 (2013), [arXiv:1203.5192 \[astro-ph.HE\]](#).
- [149] Mattia Bulla, Michael W. Coughlin, Suhail Dhawan, and Tim Dietrich, “Multi-Messenger Constraints on the Hubble Constant through Combination of Gravitational Waves, Gamma-Ray Bursts and Kilonovae from Neutron Star Mergers,” *Universe* **8**, 289 (2022), [arXiv:2205.09145 \[astro-ph.HE\]](#).
- [150] B. P. Abbott *et al.* (LIGO Scientific, Virgo), “GW170817: Observation of Gravitational Waves from a Binary Neutron Star Inspiral,” *Phys. Rev. Lett.* **119**, 161101 (2017), [arXiv:1710.05832 \[gr-qc\]](#).
- [151] R. Abbott *et al.* (LIGO Scientific, Virgo, KAGRA), “Constraints on the Cosmic Expansion History from GWTC–3,” *Astrophys. J.* **949**, 76 (2023), [arXiv:2111.03604 \[astro-ph.CO\]](#).
- [152] Alberto Domínguez, Radoslaw Wojtak, Justin Finke, Marco Ajello, Kari Helgason, Francisco Prada, Abhishek Desai, Vaidehi Paliya, Lea Marcotulli, and Dieter Hartmann, “A new measurement of the Hubble constant and matter content of the Universe using extragalactic background light γ -ray attenuation,” (2019), [10.3847/1538-4357/ab4a0e](#), [arXiv:1903.12097 \[astro-ph.CO\]](#).
- [153] A. Domínguez *et al.*, “A new derivation of the Hubble constant from γ -ray attenuation using improved optical depths for the Fermi and CTA era,” *Mon. Not. Roy. Astron. Soc.* **527**, 4632–4642 (2023), [arXiv:2306.09878](#)

- [astro-ph.HE].
- [154] Abhishek Desai, Kári Helgason, Marco Ajello, Vaidehi Paliya, Alberto Domínguez, Justin Finke, and Dieter H. Hartmann, “A GeV-TeV Measurement of the Extragalactic Background Light,” *Astrophys. J. Lett.* **874**, L7 (2019), arXiv:1903.03126 [astro-ph.HE].
- [155] A. Dominguez *et al.*, “Extragalactic background light inferred from AEGIS galaxy SED-type fractions,” *PoS TEXAS2010*, 228 (2010), arXiv:1103.4534 [astro-ph.CO].
- [156] Norman A. Grogin *et al.*, “CANDELS: The Cosmic Assembly Near-infrared Deep Extragalactic Legacy Survey,” *Astrophys. J. Suppl.* **197**, 35 (2011), arXiv:1105.3753 [astro-ph.CO].
- [157] Levon Pogosian, Gong-Bo Zhao, and Karsten Jedamzik, “A consistency test of the cosmological model at the epoch of recombination using DESI BAO and Planck measurements,” (2024), arXiv:2405.20306 [astro-ph.CO].
- [158] Tonghua Liu, Shuo Cao, and Jieci Wang, “A model-independent determination of the sound horizon using recent BAO measurements and strong lensing systems,” (2024), arXiv:2406.18298 [astro-ph.CO].
- [159] Adrià Gómez-Valent, “Measuring the sound horizon and absolute magnitude of SNIa by maximizing the consistency between low-redshift data sets,” *Phys. Rev. D* **105**, 043528 (2022), arXiv:2111.15450 [astro-ph.CO].
- [160] Caroline D. Huang, Adam G. Riess, Wenlong Yuan, Lucas M. Macri, Nadia L. Zakamska, Stefano Casertano, Patricia A. Whitelock, Samantha L. Hoffmann, Alexei V. Filippenko, and Daniel Scolnic, “Hubble Space Telescope Observations of Mira Variables in the Type Ia Supernova Host NGC 1559: An Alternative Candle to Measure the Hubble Constant,” (2019), 10.3847/1538-4357/ab5dbd, arXiv:1908.10883 [astro-ph.CO].
- [161] Ehsan Kourkchi, R. Brent Tully, Gagandeep S. Anand, Helene M. Courtois, Alexandra Dupuy, James D. Neill, Luca Rizzi, and Mark Seibert, “Cosmicflows-4: The Calibration of Optical and Infrared Tully–Fisher Relations,” *Astrophys. J.* **896**, 3 (2020), arXiv:2004.14499 [astro-ph.GA].
- [162] John P. Blakeslee, Joseph B. Jensen, Chung-Pei Ma, Peter A. Milne, and Jenny E. Greene, “The Hubble Constant from Infrared Surface Brightness Fluctuation Distances,” *Astrophys. J.* **911**, 65 (2021), arXiv:2101.02221 [astro-ph.CO].
- [163] Suhail Dhawan *et al.*, “A Uniform Type Ia Supernova Distance Ladder with the Zwicky Transient Facility: Absolute Calibration Based on the Tip of the Red Giant Branch Method,” *Astrophys. J.* **934**, 185 (2022), arXiv:2203.04241 [astro-ph.CO].
- [164] Suhail Dhawan, Stephen Thorp, Kaisey S. Mandel, Sam M. Ward, Gautham Narayan, Saurabh W. Jha, and Thaisen Chant, “A BayeSN distance ladder: H0 from a consistent modelling of Type Ia supernovae from the optical to the near-infrared,” *Mon. Not. Roy. Astron. Soc.* **524**, 235–244 (2023), arXiv:2211.07657 [astro-ph.CO].
- [165] W. D’Arcy Kenworthy, Adam G. Riess, Daniel Scolnic, Wenlong Yuan, José Luis Bernal, Dillon Brout, Stefano Casertano, David O. Jones, Lucas Macri, and Erik R. Peterson, “Measurements of the Hubble Constant with a Two-rung Distance Ladder: Two Out of Three Ain’t Bad,” *Astrophys. J.* **935**, 83 (2022), arXiv:2204.10866 [astro-ph.CO].
- [166] D. Scolnic, A. G. Riess, J. Wu, S. Li, G. S. Anand, R. Beaton, S. Casertano, R. I. Anderson, S. Dhawan, and X. Ke, “CATS: The Hubble Constant from Standardized TRGB and Type Ia Supernova Measurements,” *Astrophys. J. Lett.* **954**, L31 (2023), arXiv:2304.06693 [astro-ph.CO].
- [167] Syed A. Uddin *et al.*, “Carnegie Supernova Project I and II: Measurements of H_0 Using Cepheid, Tip of the Red Giant Branch, and Surface Brightness Fluctuation Distance Calibration to Type Ia Supernovae*,” *Astrophys. J.* **970**, 72 (2024), arXiv:2308.01875 [astro-ph.CO].
- [168] T. de Jaeger and L. Galbany, “The pursuit of the Hubble Constant using Type II Supernovae,” (2023), arXiv:2305.17243 [astro-ph.CO].
- [169] Caroline D. Huang *et al.*, “The Mira Distance to M101 and a 4% Measurement of H_0 ,” *Astrophys. J.* **963**, 83 (2024), arXiv:2312.08423 [astro-ph.CO].
- [170] Ricardo Chávez, Roberto Terlevich, Elena Terlevich, Ana González-Morán, David Fernández-Arenas, Fabio Bresolin, Manolis Plionis, Spyros Basilakos, Ricardo Amorín, and Mario Llerena, “Reconstructing Cosmic History: JWST-Extended Mapping of the Hubble Flow from $z \sim 0$ to $z \sim 7.5$ with HII Galaxies,” (2024), arXiv:2404.16261 [astro-ph.CO].
- [171] Siyang Li, Adam G. Riess, Stefano Casertano, Gagandeep S. Anand, Daniel M. Scolnic, Wenlong Yuan, Louise Breuval, and Caroline D. Huang, “Reconnaissance with JWST of the J-region Asymptotic Giant Branch in Distance Ladder Galaxies: From Irregular Luminosity Functions to Approximation of the Hubble Constant,” *Astrophys. J.* **966**, 20 (2024), arXiv:2401.04777 [astro-ph.CO].
- [172] Siyang Li, Gagandeep S. Anand, Adam G. Riess, Stefano Casertano, Wenlong Yuan, Louise Breuval, Lucas M. Macri, Daniel Scolnic, Rachael Beaton, and Richard I. Anderson, “Tip of the Red Giant Branch Distances with JWST. II. I-band Measurements in a Sample of Hosts of 10 SN Ia Match HST Cepheids,” (2024), arXiv:2408.00065 [astro-ph.CO].
- [173] Paula Boubel, Matthew Colless, Khaled Said, and Lister Staveley-Smith, “An improved Tully-Fisher estimate of H_0 ,” (2024), 10.1093/mnras/stae1925, arXiv:2408.03660 [astro-ph.CO].
- [174] Khaled Said *et al.*, “DESI Peculiar Velocity Survey – Fundamental Plane,” (2024), arXiv:2408.13842 [astro-ph.CO].
- [175] C. D. Huang *et al.*, “A near-infrared period-luminosity relation for miras in ngc 4258, an anchor for a new distance ladder,” *Astrophys. J.* **857**, 67 (2018), arXiv:1801.02711 [astro-ph.CO].
- [176] C. Y. Kuo, J. A. Braatz, M. J. Reid, K. Y. Lo, J. J. Condon, C. M. V. Impellizzeri, and C. Henkel, “The Megamaser Cosmology Project. V. An Angular-diameter Distance to NGC 6264 at 140 Mpc,” *Astrophys. J.* **767**, 155 (2013), arXiv:1207.7273 [astro-ph.CO].
- [177] Qin Wu, Guo-Qiang Zhang, and Fa-Yin Wang, “An 8 percent determination of the Hubble constant from localized fast radio bursts,” *Mon. Not. Roy. Astron. Soc.* **515**, L1–L5 (2022), [Erratum: *Mon. Not. Roy. Astron. Soc.* 531, L8 (2024)], arXiv:2108.00581 [astro-ph.CO].

- [178] Jian-Chen Zhang, Kang Jiao, Tingting Zhang, Tong-Jie Zhang, and Bo Yu, “A Reliable Calibration of H II Galaxies Hubble Diagram with Cosmic Chronometers and Artificial Neural Network,” *Astrophys. J.* **936**, 21 (2022), [arXiv:2208.03960 \[astro-ph.CO\]](#).
- [179] Tonghua Liu and Kai Liao, “Determining cosmological-model-independent H_0 and post-Newtonian parameter with time-delay lenses and supernovae,” *Mon. Not. Roy. Astron. Soc.* **528**, 1354–1359 (2024), [arXiv:2309.13608 \[astro-ph.CO\]](#).
- [180] Arianna Favale, Adrià Gómez-Valent, and Marina Migliaccio, “Cosmic chronometers to calibrate the ladders and measure the curvature of the Universe. A model-independent study,” *Mon. Not. Roy. Astron. Soc.* **523**, 3406–3422 (2023), [arXiv:2301.09591 \[astro-ph.CO\]](#).
- [181] W. Ballard *et al.* (DESI), “A Dark Siren Measurement of the Hubble Constant with the LIGO/Virgo Gravitational Wave Event GW190412 and DESI Galaxies,” *Res. Notes AAS* **7**, 250 (2023), [arXiv:2311.13062 \[astro-ph.CO\]](#).
- [182] A. Palmese, R. Kaur, A. Hajela, R. Margutti, A. McDowell, and A. MacFadyen, “Standard siren measurement of the Hubble constant using GW170817 and the latest observations of the electromagnetic counterpart afterglow,” *Phys. Rev. D* **109**, 063508 (2024), [arXiv:2305.19914 \[astro-ph.CO\]](#).
- [183] Albert Snepken, Darach Watson, Dovi Poznanski, Oliver Just, Andreas Bauswein, and Radosław Wojtak, “Measuring the Hubble constant with kilonovae using the expanding photosphere method,” *Astron. Astrophys.* **678**, A14 (2023), [arXiv:2306.12468 \[astro-ph.CO\]](#).
- [184] Yuting Liu, Masamune Oguri, and Shuo Cao, “Hubble constant from the cluster-lensed quasar system SDSS J1004+4112: Investigation of the lens model dependence,” *Phys. Rev. D* **108**, 083532 (2023), [arXiv:2307.14833 \[astro-ph.CO\]](#).
- [185] Anwar J. Shajib *et al.* (TDCOSMO), “TDCOSMO. XII. Improved Hubble constant measurement from lensing time delays using spatially resolved stellar kinematics of the lens galaxy,” *Astron. Astrophys.* **673**, A9 (2023), [arXiv:2301.02656 \[astro-ph.CO\]](#).
- [186] Patrick L. Kelly *et al.*, “Constraints on the Hubble constant from supernova Refsdal’s reappearance,” *Science* **380**, abh1322 (2023), [arXiv:2305.06367 \[astro-ph.CO\]](#).
- [187] Jiaze Gao, Zhihuan Zhou, Minghui Du, Rui Zou, Jianping Hu, and Lixin Xu, “A Measurement of Hubble Constant Using Cosmographic Approach from Fast Radio Bursts and SNe Ia,” (2023), [arXiv:2307.08285 \[astro-ph.CO\]](#).
- [188] V. Alfradique *et al.*, “A dark siren measurement of the Hubble constant using gravitational wave events from the first three LIGO/Virgo observing runs and DELVE,” *Mon. Not. Roy. Astron. Soc.* **528**, 3249–3259 (2024), [arXiv:2310.13695 \[astro-ph.CO\]](#).
- [189] L. R. Colaço, Marcelo Ferreira, R. F. L. Holanda, J. E. Gonzalez, and Rafael C. Nunes, “A Hubble constant estimate from galaxy cluster and type Ia SNe observations,” *JCAP* **05**, 098 (2024), [arXiv:2310.18711 \[astro-ph.CO\]](#).
- [190] Yuting Liu and Masamune Oguri, “Exploring the dependence of the Hubble constant from the cluster-lensed supernova SN Refsdal on mass model assumptions,” (2024), [arXiv:2402.13476 \[astro-ph.CO\]](#).
- [191] C. R. Bom, V. Alfradique, A. Palmese, G. Teixeira, L. Santana-Silva, A. Santos, and P. Darc, “A dark standard siren measurement of the Hubble constant following LIGO/Virgo/KAGRA O4a,” (2024), [arXiv:2404.16092 \[astro-ph.CO\]](#).
- [192] C. Grillo, L. Pagano, P. Rosati, and S. H. Suyu, “Cosmography with supernova Refsdal through time-delay cluster lensing: Independent measurements of the Hubble constant and geometry of the Universe,” *Astron. Astrophys.* **684**, L23 (2024), [arXiv:2401.10980 \[astro-ph.CO\]](#).
- [193] Massimo Pascale *et al.*, “SN H0pe: The First Measurement of H_0 from a Multiply-Imaged Type Ia Supernova, Discovered by JWST,” (2024), [arXiv:2403.18902 \[astro-ph.CO\]](#).
- [194] Xiaolei Li and Kai Liao, “Determining Cosmological-model-independent H_0 with Gravitationally Lensed Supernova Refsdal,” *Astrophys. J.* **966**, 121 (2024), [arXiv:2401.12052 \[astro-ph.CO\]](#).
- [195] F. Gao, J. A. Braatz, M. J. Reid, J. J. Condon, J. E. Greene, C. Henkel, C. M. V. Impellizzeri, K. Y. Lo, C. Y. Kuo, and D. W. Pesce, “THE MEGAMASER COSMOLOGY PROJECT. IX. BLACK HOLE MASSES FOR THREE MASER GALAXIES,” *The Astrophysical Journal* **834**, 52 (2017).
- [196] Ruchika, Leandros Perivolaropoulos, and Alessandro Melchiorri, “Effects of a local physics change on the SH0ES determination of H_0 ,” (2024), [arXiv:2408.03875 \[astro-ph.CO\]](#).
- [197] George Alestas, Ioannis Antoniou, and Leandros Perivolaropoulos, “Hints for a Gravitational Transition in Tully–Fisher Data,” *Universe* **7**, 366 (2021), [arXiv:2104.14481 \[astro-ph.CO\]](#).
- [198] Lu Huang, Shao-Jiang Wang, and Wang-Wei Yu, “No-go guide for the Hubble tension: late-time or local-scale new physics,” (2024), [arXiv:2401.14170 \[astro-ph.CO\]](#).
- [199] Yang Liu, Hongwei Yu, and Puxun Wu, “Alleviating the Hubble-constant tension and the growth tension via a transition of absolute magnitude favored by the Pantheon+ sample,” *Phys. Rev. D* **110**, L021304 (2024), [arXiv:2406.02956 \[astro-ph.CO\]](#).
- [200] Harry Desmond and Jeremy Sakstein, “Screened fifth forces lower the TRGB-calibrated Hubble constant too,” *Phys. Rev. D* **102**, 023007 (2020), [arXiv:2003.12876 \[astro-ph.CO\]](#).
- [201] Harry Desmond, Bhuvnesh Jain, and Jeremy Sakstein, “Local resolution of the Hubble tension: The impact of screened fifth forces on the cosmic distance ladder,” *Phys. Rev. D* **100**, 043537 (2019), [Erratum: *Phys.Rev.D* 101, 069904 (2020), Erratum: *Phys.Rev.D* 101, 129901 (2020)], [arXiv:1907.03778 \[astro-ph.CO\]](#).
- [202] Radosław Wojtak, Tamara M. Davis, and Jophiel Wiis, “Local gravitational redshifts can bias cosmological measurements,” *JCAP* **07**, 025 (2015), [arXiv:1504.00718 \[astro-ph.CO\]](#).
- [203] G. Efstathiou, “A Lockdown Perspective on the Hubble Tension (with comments from the SH0ES team),” (2020), [arXiv:2007.10716 \[astro-ph.CO\]](#).
- [204] S. Carneiro, C. Pigozzo, and J. S. Alcaniz, “Redshift systematics and the H_0 tension problem,” *Eur. Phys. J. Plus* **137**, 537 (2022).
- [205] Edvard Mortsell, Ariel Goobar, Joel Johansson, and Suhail Dhawan, “Sensitivity of the Hubble Constant Determination to Cepheid Calibration,” *Astrophys. J.*

- 933**, 212 (2022), [arXiv:2105.11461 \[astro-ph.CO\]](#).
- [206] Mohamed Rameez and Subir Sarkar, “Is there really a Hubble tension?” *Class. Quant. Grav.* **38**, 154005 (2021), [arXiv:1911.06456 \[astro-ph.CO\]](#).
- [207] Ioannis D. Gialamas, Gert Hütsi, Kristjan Kannike, Antonio Racioppi, Martti Raidal, Martin Vasar, and Hardi Veermäe, “Interpreting DESI 2024 BAO: late-time dynamical dark energy or a local effect?” (2024), [arXiv:2406.07533 \[astro-ph.CO\]](#).
- [208] Yun Chen, Suresh Kumar, Bharat Ratra, and Tengpeng Xu, “Effects of Type Ia Supernovae Absolute Magnitude Priors on the Hubble Constant Value,” *Astrophys. J. Lett.* **964**, L4 (2024), [arXiv:2401.13187 \[astro-ph.CO\]](#).
- [209] Evangelos Achilleas Paraskevas and Leandros Perivolaropoulos, “Effects of a Late Gravitational Transition on Gravitational Waves and Anticipated Constraints,” *Universe* **9**, 317 (2023), [arXiv:2307.00298 \[astro-ph.CO\]](#).
- [210] Adrià Gómez-Valent, Arianna Favale, Marina Migliaccio, and Anjan A. Sen, “Late-time phenomenology required to solve the H0 tension in view of the cosmic ladders and the anisotropic and angular BAO datasets,” *Phys. Rev. D* **109**, 023525 (2024), [arXiv:2309.07795 \[astro-ph.CO\]](#).
- [211] Maria Giovanna Dainotti, Giada Bargiacchi, Malgorzata Bogdan, Salvatore Capozziello, and Shigehiro Nagataki, “Reduced uncertainties up to 43% on the Hubble constant and the matter density with the SNe Ia with a new statistical analysis,” (2023), [arXiv:2303.06974 \[astro-ph.CO\]](#).
- [212] Leandros Perivolaropoulos and Foteini Skara, “Gravitational transitions via the explicitly broken symmetron screening mechanism,” *Phys. Rev. D* **106**, 043528 (2022), [arXiv:2203.10374 \[astro-ph.CO\]](#).
- [213] Marcus Högåås and Edvard Mörtzell, “Hubble tension and fifth forces,” *Phys. Rev. D* **108**, 124050 (2023), [arXiv:2309.01744 \[astro-ph.CO\]](#).